

Thermodynamics of Solution by Gas Liquid
Chromatography of Nonmesomorphic Solutes in the
Isotropic and Nematic Phases of Liquid Crystalline
Solvents

by

Ali Muhammad Al-Taqqiq

A Thesis Presented to the

FACULTY OF THE COLLEGE OF GRADUATE STUDIES
KING FAHD UNIVERSITY OF PETROLEUM & MINERALS
DHAHRAN, SAUDI ARABIA

In Partial Fulfillment of the
Requirements for the Degree of

MASTER OF SCIENCE

In

CHEMISTRY

June, 1996

INFORMATION TO USERS

This manuscript has been reproduced from the microfilm master. UMI films the text directly from the original or copy submitted. Thus, some thesis and dissertation copies are in typewriter face, while others may be from any type of computer printer.

The quality of this reproduction is dependent upon the quality of the copy submitted. Broken or indistinct print, colored or poor quality illustrations and photographs, print bleedthrough, substandard margins, and improper alignment can adversely affect reproduction.

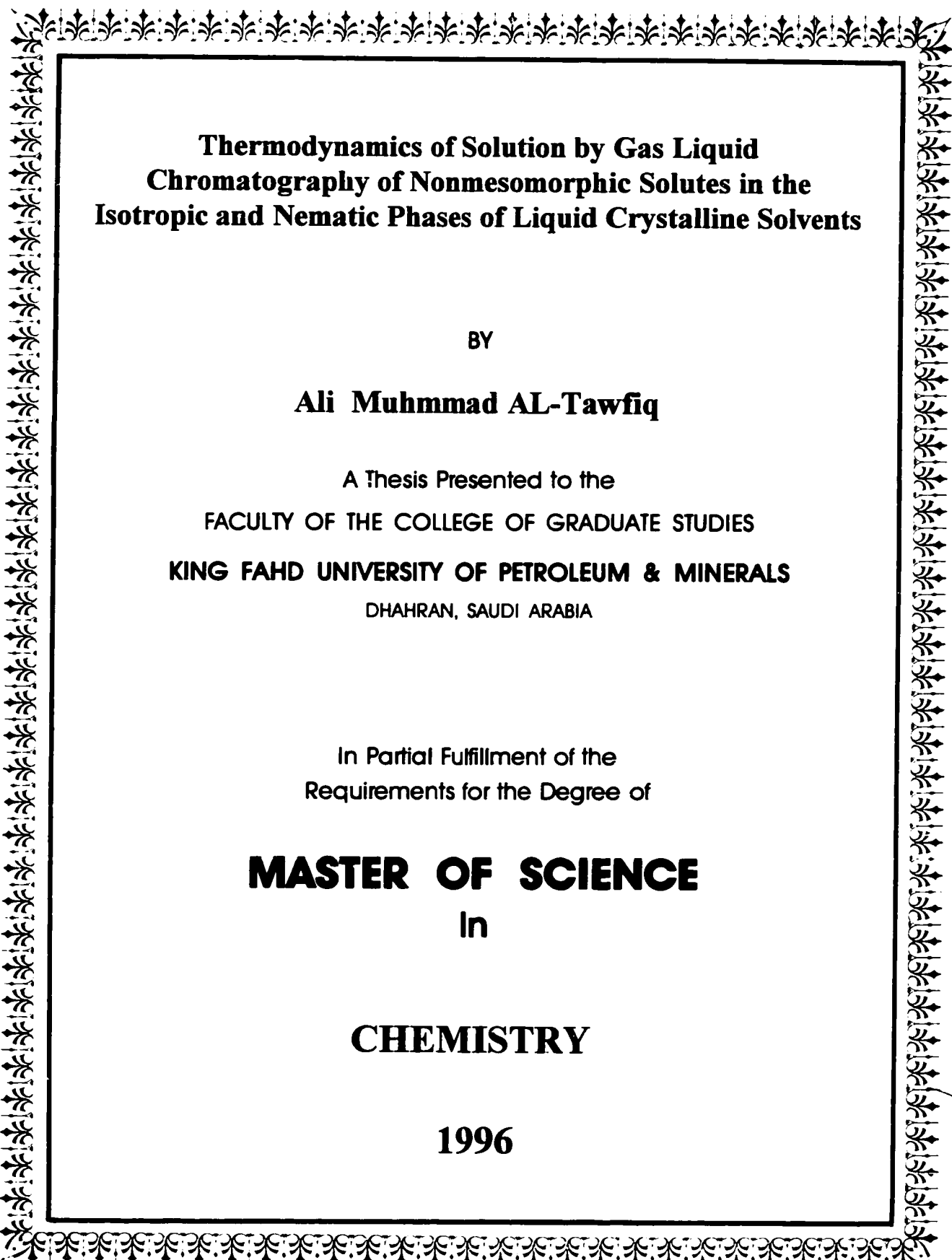
In the unlikely event that the author did not send UMI a complete manuscript and there are missing pages, these will be noted. Also, if unauthorized copyright material had to be removed, a note will indicate the deletion.

Oversize materials (e.g., maps, drawings, charts) are reproduced by sectioning the original, beginning at the upper left-hand corner and continuing from left to right in equal sections with small overlaps. Each original is also photographed in one exposure and is included in reduced form at the back of the book.

Photographs included in the original manuscript have been reproduced xerographically in this copy. Higher quality 6" x 9" black and white photographic prints are available for any photographs or illustrations appearing in this copy for an additional charge. Contact UMI directly to order.

UMI

A Bell & Howell Information Company
300 North Zeeb Road, Ann Arbor MI 48106-1346 USA
313/761-4700 800/521-0600



**Thermodynamics of Solution by Gas Liquid
Chromatography of Nonmesomorphic Solutes in the
Isotropic and Nematic Phases of Liquid Crystalline Solvents**

BY

Ali Muhammad AL-Tawfiq

A Thesis Presented to the
FACULTY OF THE COLLEGE OF GRADUATE STUDIES
KING FAHD UNIVERSITY OF PETROLEUM & MINERALS
DHAHRAN, SAUDI ARABIA

In Partial Fulfillment of the
Requirements for the Degree of

MASTER OF SCIENCE

In

CHEMISTRY

1996

UMI Number: 1388274

UMI Microform 1388274
Copyright 1998, by UMI Company. All rights reserved.

**This microform edition is protected against unauthorized
copying under Title 17, United States Code.**

UMI
300 North Zeeb Road
Ann Arbor, MI 48103

**THERMODYNAMICS OF SOLUTION BY GAS LIQUID
CHROMATOGRAPHY OF NONMESOMORPHIC SOLUTES
IN THE ISOTROPIC AND NEMATIC PHASES OF LIQUID
CRYSTALLINE SOLVENTS**

BY

ALI MUHMMAD AL-TAWFIQ

A thesis Presented to the

FACULTY OF THE COLLEGE OF GRADUATE STUDIES

**KING FAHD UNIVERSITY OF PETROLEUM AND MINERALS
DHAHRAN 31261, SAUDI ARABIA**

In Partial Fulfillment of the

Requirements for the Degree of

**MASTER OF SCIENCE
IN
CHEMISTRY**

JUNE, 1996

**KING FAHD UNIVERSITY OF PETROLEUM AND MINERALS
DHAHRAN 31261, SAUDI ARABIA**

COLLEGE OF GRADUATE STUDIES

This thesis, written by

Ali Muhammad AL-Tawfiq

under the direction of his Thesis Advisor and approved by his Thesis Committee,
has been presented and accepted by the Dean of College of Graduate Studies, in
partial fulfillment of the requirements for the degree of

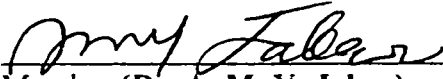
MASTER OF SCIENCE IN CHEMISTRY

Thesis Committee

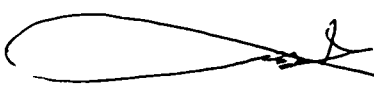

Thesis Advisor (Dr. Ghassan A. Oweimreen)



Member (Prof. Uwe K. A. Klein)


Member (Dr. H. Perzanowski)


Member (Dr. A. M. Y. Jaber)


Member (Dr. M. A. Morsy)


Dr. Abdulrahman A. Al-Arfaj
Chairman, Department of Chemistry


Dr. Ala H. Al-Rabeh
Dean, College of Graduate Studies

Date : 1/7/96



TO MY PARENTS

ACKNOWLEDGMENT

Praise be to Allah, the cherisher and sustainer of the world, who gave me the ability to accomplish this research.

Acknowledgment is due to King Fahd University of Petroleum and Minerals for facilitating all instruments needed for this research.

I am gratefully indebted to my thesis advisor Dr. Ghassan Oweimreen for his guidance, suggestions and continuous encouragement, and valuable discussions throughout this work. I also thank my thesis committee members, Prof. Uwe K. A. Klein, Dr. H. Perzanowski, Dr. A. Jaber, and Dr. M. A. Morsy for their comments, and suggestions. A special thank is due to Dr. M. A. Morsy for his help in the ESR study and in the ab initio calculations. I am also grateful to Dr. Abdulrhman Al-Arfaj the Chemistry Department Chairman for his assistance in facilitating my work

Thanks are also due to Mr. Javaid H. Khan for his assistance in the DSC study.

TABLE OF CONTENTS

LIST OF TABLES	x
LIST OF FIGURES.....	xiii
ABSTRACT (IN ENGLISH).....	xxiii
ABSTRACT (IN ARABIC)	xxiv
CHAPTER 1 INTRODUCTION.....	1
CHAPTER 2 DIFFERENTIAL SCANNING CALORIMETRY.....	13
2.1 Introduction.....	14
2.2 Theory.....	15
2.3 Experimental.....	18
2.3.1 Experimental Set Up.....	18
2.3.2 An Indium Sample Calibration.....	19
2.3.3 DSC Runs on Bulk Liquid Crystal Samples.....	20

2.4 DSC Runs on Liquid Crystals Coated on	
Chromosorb W.....	25
2.5 Odd-Even Effect.....	31
CHAPTER 3 ELECTRON PARAMAGNETIC RESONANCE...	36
3.1 Introduction.....	37
3.2 Theoretical Background.....	39
3.3 Experimental and Procedure	48
3.3.1 Sample Preparation.....	48
3.3.2 ESR Setup	49
3.3.3 Spectra Recording and Data	
Collection.....	49
3.3.4 Results and Discussion.....	50
CHAPTER 4 THE GLC EXPERIMENT.....	68
4.1 Introduction.....	69
4.2 Experimental	73

4.2.1	Chemicals	73
4.2.2	Preparation of Columns	77
4.2.3	Apparatus and Procedure	78
CHAPTER 5	GLC RESULTS	80
5.1	Specific Retention Volume	81
5.2	Solute Activity Coefficients	83
5.3	Partial Molar Excess Enthalpies and Entropies.....	85
5.4	Partial Molar Enthalpies and Entropies of Solution.....	86
5.5	Odd-Even Effect.....	111
CHAPTER 6	INTERPRETATION OF GLC DATA	116
6.1	Chow and Martire Statistical Model	117
6.2	Discussion.....	127
6.2.1	General Comparison	127
6.2.2	Odd-even effect	131

CHAPTER 7 SUMMARY AND CONCLUSIONS.....	134
APPENDIX A	140
APPENDIX B	163
APPENDIX C	186
REFERENCES.....	200

LIST OF TABLES

Table		Page
1.1	Characteristics of Types of Order in Smectic and Crystalline Solids	4
2.1	Melting Points, Clearing Points and the Changes in Enthalpy and Entropy at these Transitions.....	29
3.1	Isotropic-to-Nematic Temperatures (T_{NI}), Hyperfine Splitting a_{iso} in the Isotropic Phase and g-Factor at the Onset of the Isotropic-to-Nematic Transitions for PD-Tempone in the p-Cyanophenyl-p-n-alkkylbenzoate Liquid Crystal Solvents.....	51
3.2	Amorphous Solidification Transition Temperatures for the Series of Liquid Crystals Studied.....	59

3.3	3-21G Optimized Structural Parameters of p-Cyanophenyl-p-ethylbenzoate.....	63
4.1	Comparison of GLC and Static Specific Retention Volumes, V_g° , for n-Hexane in a Hexadecane Solvent.....	71
4.2	Some Physical Properties of the Ethyl, n-Propyl, n-Butyl, n-Pentyl, n-Hexyl, and n-Heptyl Members of p-Cyano-p-n-alkylbenzoate Homologous Series of Liquid Crystals.....	75
4.3	Melting Points and Molar Masses of the Solutes Studied.....	76
5.1	Thermodynamic Data for Solutes in the Isotropic Phase of p-Cyanophenyl-p ethylbenzoate.....	100
5.2	Thermodynamic Data for Solutes in the Isotropic Phase of p-Cyanophenyl-p-n-propylbenzoate.....	101
5.3	Thermodynamic Data for Solutes in the Nematic Phase of p-Cyanophenyl-p-n-propylbenzoate.....	102

	Thermodynamic Data for Solutes in the Isotropic	
5.4	Phase of p-Cyanophenyl-p-n-butylbenzoate.....	103
	Thermodynamic Data for Solutes in the Nematic	
5.5	Phase of p-Cyanophenyl-p-n-butylbenzoate.....	104
	Thermodynamic Data for Solutes in the Isotropic	
5.6	Phase of p-Cyanophenyl-p-n-pentylbenzoate.....	105
	Thermodynamic Data for Solutes in the Nematic	
5.7	Phase of p-Cyanophenyl-p-n-pentylbenzoate.....	106
	Thermodynamic Data for Solutes in the Isotropic	
5.8	Phase of p-Cyanophenyl-p-n-hexylbenzoate.....	107
	Thermodynamic Data for Solutes in the Nematic	
5.9	Phase of p-Cyanophenyl-p-n-hexylbenzoate.....	108
	Thermodynamic Data for Solutes in the Isotropic	
5.10	Phase of p-Cyanophenyl-p-n-heptylbenzoate.....	109
	Thermodynamic Data for Solutes in the Nematic	
5.11	Phase of p-Cyanophenyl-p-n-heptylbenzoate.....	110

LIST OF FIGURES

Figure		Page
1.1	Arrangements of Molecules in (a) a Smectic A Liquid Crystal (b) a Nematic Liquid Crystal and (c) a Cholesteric Liquid Crystal.....	7
2.1	Heating Thermogram for p-Cyanophenyl-p-n-propylbenzoate.....	21
2.2	Cooling Thermogram for p-Cyanophenyl-p-n-propylbenzoate.....	22
2.3	Heating and Cooling (Inset) Thermograms for p-Cyanophenyl-p-n-heptylbenzoate.....	23
2.4	DSC Thermograms for p-Cyanophenyl-p-n-propylbenzoate (a) Heating beyond the Crystal-to-Nematic Transition then Cooling (Inset) to	

	Below the Isotropic-to-Nematic transition. (b) Heating the Sample in (a) Prior to its Solidification beyond Nematic-to-Isotropic Transition on Heating and below Isotropic-to-Nematic Transition on Cooling (Inset). (c) Heating Thermogram after Allowing the Sample to Solidify.....	26
2.5	Heating Thermograms for (a) a Bulk Sample and (b) a Sample Coated on a Support for p-Cyanophenyl-p-n-propylbenzoate.....	28
2.6	The Variation of the temperature of Melting (●) and Clearing (■) with the Number of Carbon Atoms on the Alkyl Tail of the p-Cyanophenyl-p-n-alkylbenzoate.....	34
2.7	The Variation in (a) ΔH_m and (b) ΔH_{IN} , the Enthalpy Changes on Melting and Clearing	

	Respectively, with the Number of Carbon Atoms on the Alkyl Tail of p-Cyanophenyl-p-n-alkylbenzoate.....	35
3.1	The Hyperfine Splitting a Versus Temperature for PD-Tempone in p-Cyanophenyl-p-n-Butylbenzoate. T_{NI} is the Isotropic-to-Nematic Transition. The dashed Vertical Line is the Boundary between a Supercooled Phase Where Nematic Characteristics Persist and a Proposed Amorphous Solid Phase. The symbol (●) denotes a Cooling Cycle whereas the Symbol (■) Denotes a Heating Cycle.....	53
3.2	g-Factor Versus Temperature for PD-Tempone in p-Cyanophenyl Butylbenzoate. T_{NI} is the Isotropic-to-Nematic Transition. The Dashed Vertical Line is the Boundary between a Supercooled Phase where Nematic Characteristic	

	Persists and a Proposed Amorphous Solid Phase.	
	The Symbol (●) Denotes a Cooling Cycle whereas the Symbol (■) Denotes a Heating Cycle.....	54
3.3	ESR Spectra for PDT in (a) the Isotropic Phase (67.5 °C), (b) the Two Phase Region (42.0 °C) and (c) the Nematic Phase (40 °C) of p- Cyanophenyl-p-n-butylbenzoate.....	56
3.4	The Optimized Molecular Structure for p- Cyanophenyl-p-n-ethylbenzoate as Obtained from STO-3G basis set ab initio Calculations (a) the Symbol Labeled Structure and (b) the Number Labeled Structure.....	62
3.5	The Potential Energy Diagram for p- Cyanophenyl-p-ethylbenzoate Obtained from STO-3G basis set ab initio Calculations by	

	Variation of the Dihedral Angle between the Planes of the Cyanophenyl and Benzoate Portions of the Molecule at the Ester Oxygen (number 13 in Figure 3.4).....	66
5.1	ln γ^{∞}_2 Versus $10^3/T$ for n-Alkanes in the Isotropic and Phases of p-Cyanophenyl-p-ethylbenzoate. The Numbering of the Solutes Follows that Given in Table 4.3.....	87
5.2	ln γ^{∞}_2 Versus $10^3/T$ for Benzene (5),c-1,4-Hexadiene (6) and 1-Hexene in the Isotropic Phase of p-Cyanophenyl-p-ethylbenzoate.....	88
5.3	ln γ^{∞}_2 Versus $10^3/T$ for n-Alkanes in the Isotropic and Nematic Phases of p-Cyanophenyl-p-n-propylbenzoate. The Numbering of the Solutes Follows that Given in Table 4.3. The Dashed	

	Vertical Line is Located at the Isotropic-to-Nematic Transition Temperature.....	89
5.4	ln γ^∞_2 Versus $10^3/T$ for Benzene (5),c-1,4-Hexadiene (6) and 1-Hexene in the Isotropic Phase of p-Cyanophenyl-p-n-propylbenzoate. The Dashed Vertical Line is Located at the Isotropic-to-Nematic Transition Temperature.....	90
5.5	ln γ^∞_2 Versus $10^3/T$ for n-Alkanes in the Isotropic and Nematic Phases of p-Cyanophenyl-p-n-butylbenzoate. The Numbering of the Solutes Follows that Given in Table 4.3. The Dashed Vertical Line is Located at the Isotropic-to-Nematic Transition Temperature.....	91
5.6	ln γ^∞_2 Versus $10^3/T$ for Benzene (5),c-1,4-Hexadiene (6) and 1-Hexene in the Isotropic Phases of p-Cyanophenyl-p-n-butylbenzoate. The	

	Dashed Vertical Line is Located at the Isotropic-to-Nematic Transition Temperature.....	92
5.7	ln γ_2^∞ Versus $10^3/T$ for n-Alkanes in the Isotropic and Nematic Phases of p-Cyanophenyl-p-n-pentylbenzoate. The Numbering of the Solutes Follows that Given in Table 4.3. The Dashed Vertical Line is Located at the Isotropic-to-Nematic Transition Temperature.....	93
5.8	ln γ_2^∞ Versus $10^3/T$ for Benzene (5),c-1,4-Hexadiene (6) and 1-Hexene in the Isotropic Phase of p-Cyanophenyl-p-n-pentylbenzoate. The Dashed Vertical Line is Located at the Isotropic-to-Nematic Transition Temperature.....	94
5.9	ln γ_2^∞ Versus $10^3/T$ for n-Alkanes in the Isotropic and Nematic Phases of p-Cyanophenyl-p-n-hexylbenzoate. The Numbering of the Solutes	

	Follows that Given in Table 4.3. The Dashed Vertical Line is Located at the Isotropic-to-Nematic Transition Temperature.....	95
5.10	$\ln \gamma_2^\infty$ Versus $10^3/T$ for Benzene (5),c-1,4-Hexadiene (6) and 1-Hexene in the Isotropic and Nematic Phases of p-Cyanophenyl-p-n-hexylbenzoate. The Dashed Vertical Line is Located at the Isotropic-to-Nematic Transition Temperature.....	96
5.11	$\ln \gamma_2^\infty$ Versus $10^3/T$ for n-Alkanes in the Isotropic and Nematic Phases of p-Cyanophenyl-p-n-heptylbenzoate. The Numbering of the Solutes Follows that Given in Table 4.3. The Dashed Vertical Line is Located at the Isotropic-to-Nematic Transition Temperature.....	97

5.12	ln γ_2^∞ Versus $10^3/T$ for Benzene (5),c-1,4-Hexadiene (6) and 1-Hexene (7) in the Isotropic Phase of p-Cyanophenyl-p-n-heptylbenzoate. The Dashed Vertical Line is Located at the Isotropic-to-Nematic Transition Temperature.....	98
5.13	Reduced Activity Coefficients for n-Alkanes (Solutes 1-4) vs. n (the Number of Carbon Atoms on the Tails of the Liquid Crystals in (a) the Isotropic Phase and (b) the Nematic Phase.....	113
5.14	Reduced Activity Coefficients for Solutes (5-10) vs. n (the Number of Carbon Atoms on the Alkyl Tails) of the Liquid Crystals in (a) the Isotropic Phase and (b) the Nematic Phase.....	114
5.15	Reduced Activity Coefficients for n-Hexane, 1-Hexene, c-1,4-Hexadiene, and Benzene (Solutes	

1, 5-7) vs. n (the Number of Carbon Atoms on
the Tail of the Liquid Crystal) in (a) the Isotropic
Phase, and (b) the nematic Phase..... 115

THESIS ABSTRACT

Name : Ali Muhmmad AL-Tawfiq
Title : Thermodynamics of Solution by Gas Liquid
Chromatography of Nonmesomorphic Solutes in the
Isotropic and Nematic Phases of Liquid Crystalline Solvents
Major : Chemistry
Date : June, 1996

Differential scanning calorimetric (DSC) and electron spin resonance (ESR) studies are carried out over wide temperature ranges to investigate the nature of the transitions that the ethyl, n-propyl, n-butyl, n-pentyl, n-hexyl and n-heptyl members of the p-cyanophenyl-p-n-alkylbenzoate series of liquid crystals undergo. The DSC results for these liquid crystals, in bulk or when coated on chromosorb W, show that they can be satisfactorily used as stationary phases in a gas liquid chromatography (GLC) experiment that investigates the thermodynamics of solution of nonmesomorphic solutes in them. The ESR measurements reveal structural changes in the liquid crystal molecules during their transitions. Ab initio STO-3G calculations on the p-cyanophenyl-p-ethylbenzoate molecule shed light on the nature of these structural changes. The thermodynamic data from GLC were satisfactorily interpreted on the basis of an infinite dilution statistical thermodynamic model. They also rationalize the properties of these solutions on the basis of both solute and solvent structures. An odd-even effect for transition temperatures and enthalpies with respect to the number of the carbon atoms on the tail of the liquid crystal molecule was opposite to an odd-even effect observed for infinite dilution activity coefficient extrapolated from nematic and isotropic phases to a hypothetical common nematic-to-isotropic transition temperature. These effects were also rationalized on the basis of solute and solvent structures respectively. Finally the practical use of the combined DSC and GLC results to investigate the effect of solute structure on nematic phase stability is briefly discussed.

خلاصة الرسالة

اسم مقدم الرسالة : علي محمد علي آل توفيق

عنوان الرسالة : دراسة الديناميكية الحرارية للمذابات ذات الطور الموحد الصفات في الطور النيमतوجيني والطور الموحد الصفات في البلورات السائلة بواسطة كروماتوغرافيا الغاز السائل.

التخصص : كيمياء

التاريخ : يونيو 1996

تم دراسة البلورات السائلة إيثيل، بروبييل، بيوتيل، بنتيل، هكسيل و هبتيل باراسايانو فينيل بارا بنزوات الألكان العادي التابعة لسلسلة ذات صيغة عامة لمعرفة طبيعة تحولها من طور إلى آخر عند تغيير درجة حرارتها بواسطة جهاز "قياس الحرارة بالمسح التفاضلي"، "جهاز الطنين الإلكتروني المغناطيسي" وجهاز "كروماتوغرافيا الغاز". وقد أثبتت التجارب الجراة على هذه المركبات في حالتها السائلة وكذلك عندما تكون مطلية على السطح الداعم في جهاز كروماتوغرافيا الغاز أن درجات حرارة التحول من طور إلى آخر وكذلك كمية حرارة التحول في الحالتين متقاربة جداً مما يدعم إمكانية استخدام هذه المركبات كأطوار ثابتة في الدراسة المتعلقة بكروماتوغرافيا الغاز. أما نتائج دراسة الطنين المغناطيسي فقد أوضحت بإمكانية تغيير بنائي في هذه المركبات عند تحولها من طور إلى آخر. ولدراسة التغيير البنائي تم دراسة مركب الإيثيل من هذه المجموعة وفقاً لنموذج رياضي أيدت نتائجه حدوث هذه التغيرات. أما بالنسبة للنتائج الديناميكية الحرارية للمحاليل فقد فُسرَت وفقاً لنموذج إحصائي لديناميكية حرارة المحاليل الخاصة بالمذابات ذات التراكيز اللانهائية التخفيف في مثل هذه البلورات والتي تعتمد في تفسيرها على خواص كل من المذاب والمذيب. وعند دراسة حرارة التحول وكمية حرارة التحول وجد أنهما يظهران تأثيراً فردياً-زوجياً بالنسبة لعدد ذرات الكربون المتصلة بذيل البلورات. هذه الظاهرة مضادة للتأثير الفردي-الزوجي الذي تسلكه معاملات نشاط المذابات ذات التركيز اللانهائية التخفيف في المحاليل والمستقرة من طور النيमतوجين والطور الموحد الصفات بإعادة تعريف درجة حرارة تحول الطور نظرياً لدرجة حرارة موحدة لجميع البلورات السائلة التي تمت دراستها. هذه الظاهرة فُسرَت أيضاً على ضوء صفات كل من المذاب والمذيب. أخيراً بُنيت الإستخدامات العملية لنتائج كروماتوغرافيا الغاز وربطها بكمية الحرارة المتاحة لتقصي مدى استقرار أطوار هذه البلورات بإضافة المذابات إليها.

CHAPTER 1

INTRODUCTION

CHAPTER 1

INTRODUCTION

The three common states of matter (gas, liquid and solid) are different because the molecules in each state possess different amounts of order. Liquid crystals, which are also called crystalline liquids, mesophases, or mesomorphic phases, possess an intermediate ordering relative to that for the liquid state and the crystalline state. To describe the progression from the completely disordered isotropic phases through the mesomorphic phases, three types of orders are used [1-4]. The first is the orientation order in which molecules have the same preferential orientation analogous to the spin orientational order of ferromagnetic materials. The second type is referred to as bond orientational order which in the absence of a lattice is the essential property defining hexactic phases. The third type of order is the positional order of an indefinite lattice of the type that defines the 230

space groups of conventional crystals. These types of orders are summarized in Table 1.1

Table 1.1: Characteristics of Types of Order in Smectic and Crystalline Solids.

Phase	Molecular	Bond	Positional Order	
	Orientalional	Orientalional		
	Order	Order		
Smectic-A	S.R.O ^a	S.R.O	S.R.O	S.R.O
Smectic-C	L.R.O ^a	L.R.O	S.R.O	S.R.O
Hexactic-B	L.R.O	L.R.O	Q.L.R.O ^a	S.R.O
Smectic-F	L.R.O	L.R.O	Q.L.R.O	S.R.O
Smectic-I	L.R.O	L.R.O	Q.L.R.O	S.R.O
Crystalline-B	L.R.O	L.R.O	L.R.O	L.R.O
Crystalline-G	L.R.O	L.R.O	L.R.O	L.R.O
Crystalline-J	L.R.O	L.R.O	L.R.O	L.R.O
Crystalline-E	L.R.O	L.R.O	L.R.O	L.R.O
Crystalline-H	L.R.O	L.R.O	L.R.O	L.R.O
Crystalline-K	L.R.O	L.R.O	L.R.O	L.R.O

^a The terms L.R.O and S.R.O refer to “long range” and “short range” order respectively and Q.L.R.O refers to “quasi long range order”.

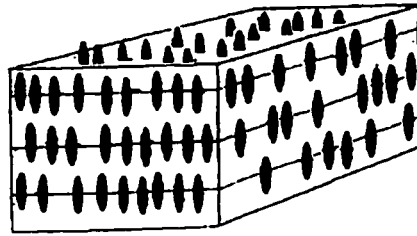
Mesomorphic phases fall into three main groups [5]; smectic, nematic and cholesteric. The smectic phase (Figure 1.1 (a)) is similar to a crystalline solid. In addition to the overall orientational order of the individual molecules, the smectic phases are layered structures exhibiting a two-dimensional positional order. The term smectic comes from the Greek 'σμηγμα' which means soap, because at first such liquid crystals were observed on ammonium and alkali soaps.

In the nematic phase (Figure 1.1(b)) the molecules have only long range orientational order. On heating to the isotropic phases this long range order disappears. The isotropic phase of liquid crystals at a temperature close to their nematic-to-isotropic transition possesses some short range orientational order. Upon the application of electrical or magnetic fields, ordinary nematic liquid crystals may be aligned.

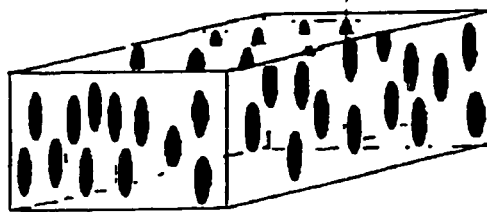
Cholesteric liquid crystals (Figure 1.1(c)) are composed of nematic layers oriented in different directions and are usually associated with

chiral compounds. These directions are related to each other and give a rise to a helical structure.

(a)



(b)



(c)

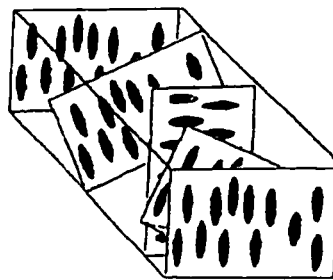


Figure 1.1 Arrangements of Molecules in (a) a Smectic A Liquid Crystal
(b) a Nematic Liquid Crystal and (c) a Cholesteric Liquid
Crystal.

Molecules that give rise to liquid crystalline properties are generally elongated with rigid cores and flexible tails and may be small simple molecules or large polymeric molecules. Molecules that exhibit liquid crystalline properties on heating are said to be thermotropic liquid crystals. Molecules that exhibit liquid crystal characteristics upon dissolution in a solvent (usually water) are called lyotropic liquid crystals and are not considered in this study.

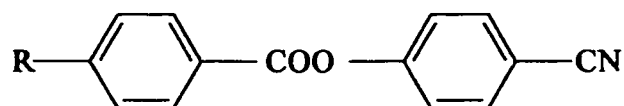
There have been three major prerequisites for the establishment of the growing success of the liquid crystal displays (LCD) technology since the early 1970s. Namely, the discovery of electro-optical field-effects on which today's LCDs are based, the successful search for liquid crystal materials with suitable properties, and the development of the technological tools which are required for manufacturing LCDs. The versatility of liquid crystals allow their use not only as direct view displays, but also as light modulators in large area projection systems. Most of today's commercial LCDs are based on the twisted nematic

or on super twisted nematic effects, that is , they all comprise nematic liquid crystals [6].

In this study thermodynamic data obtained by Gas Liquid Chromatography (GLC) are reported for n-hexane, 1-hexene, cyclohexane, c-1,4- hexadiene, benzene, 2-methyl pentane (all nonmesomorphic solutes of varying structures and containing six carbon atoms) and other nonmesomorphic solutes in the isotropic and nematic phases of the ethyl, n-propyl, n-butyl, n-pentyl, n-hexyl, and n-heptyl members of the p-cyanophenyl p-n-alkylbenzoate homologous series (see structure below). Such data combined with results from DSC measurements provide information [29] on the effect of a solute impurity on the nematic-to-isotropic transition and the creation of two phase region. This information is important to researchers using nematogens in LCDs and who intentionally add impurities to them to modify their viscosity and conductivity.

The first four members of the series are monotropic and show an isotropic-to-nematic phase transition on cooling their isotropic phase.

The n-hexyl and n-heptyl p-cyanophenyl-p-n-alkylbenzoate show a crystal to nematic transition on both heating and cooling.



R= ethyl, propyl, butyl, pentyl, hexyl, or heptyl

The term 'monotropic' refers to a single substance which exists in different forms (e.g. white and red phosphorous) only one of which (red phosphorous in this case) is stable and the change from the unstable to the stable form is irreversible [7]. For example N,N'-Terphthalalylidenebis (4-n-butylaniline) (TBBA) shows in addition to the transitions on heating (crystal to smectic B, Smectic B to smectic C, smectic C to Smectic A, smectic A to nematic, and nematic to isotropic) two transitions (smectic 4 and smectic 5) appear only on cooling. These transitions are 'monotropic'.

Liquid crystals previously used in gas chromatographic studies had completely rigid cores. Examples include, among others, the p-n-alkyl-p'-cyanobiphenyls (RCB) and the p-(n-alkyloxy)-p'-cyanobiphenyls (ROCB). The liquid crystals used in this study have an ester group connecting the two benzene rings thereby introducing some degree of flexibility. Such flexibility may be the reason why results from this study do not correlate well with those studies on RCB and ROCB.

In addition to the GLC study, Electron Spin Resonance (ESR) studies were conducted in the isotropic and nematic phases of the p-cyanophenyl-p-n-alkylbenzoate homologous series of liquid crystals. Also, Differential Scanning Calorimetry (DSC) experiments were conducted to determine the isotropic-to-nematic transition temperatures (T_{NI}), enthalpy changes (ΔH_{NI}), and, hence, entropy changes (ΔS_{NI}) both for bulk samples and for samples coated on chromosorb W which was our GLC support. The results show that

the coating of the liquid crystals on chromosorb W affects their transition temperatures and molecular ordering only very slightly.

CHAPTER 2

DIFFERENTIAL

SCANNING

CALORIMETRY

CHAPTER 2

DIFFERENTIAL SCANNING CALORIMETRY

2.1 Introduction

Differential Scanning Calorimetry (DSC) is a heat flow recording technique which was first developed by Watson in 1964 to determine transition temperatures and enthalpy changes. The sample under study and a reference material are maintained at the same temperature by supplying the proper electrical energy to them while they are heated or cooled at a linear rate. The thermogram obtained is a record of a heat flow (dh/dt), in mcal/sec, as a function of temperature. An upward peak results from an endothermic transition involving absorption of heat, while a downward peak results from an exothermic transition. The heat involved is obtained by comparing

the area under the peak of a reference sample of known mass and enthalpy of transition with that for the tested sample.

DSC studies were carried out on the ethyl, n-propyl, n-butyl, n-pentyl, n-hexyl, and n-heptyl members of the p-cyanophenyl p-n-alkylbenzoate homologous series of liquid crystals. Runs were carried out on bulk samples of these liquid crystals as well as on samples when these liquid crystals formed a layer of 'stationary phase' on a 60/80 mesh chromosorb W (AW-DMCS treated) support. The runs of liquid crystals on chromosorb W were carried out to determine if their liquid crystals properties are changed upon coating them on the support.

2.2 Theory

The peak area of a first order transition in DSC represents the heat that is involved in that transition. The first order transition is a transition accompanied by changes of enthalpy and volume in which

the slopes of the chemical potential plotted against either pressure or temperature are different on either side of the transition. In a DSC experiment, the heat capacity C_p of a substance is the slope of the enthalpy with respect to temperature. At a first order phase transition, ΔH changes by a finite amount for an infinitesimal change of temperature [8]. At the transition, the slope of ΔH and therefore the heat capacity are finite since heat drives the transition rather than raises the temperature.

The heat is calculated from the following equation:

$$\Delta H_f = \frac{K.R.A}{W.S} \quad (2.1)$$

where:

ΔH_f = heat of transition in calories/gram

K = calibrated instrument constant

R = range sensitivity in mcal/sec. in.

A = peak area in square inches

W = sample weight in milligrams

S = recorder chart speed in in/sec.

If the above equation is written for both the sample and the calibration standard (Indium), rearranging to solve for K, and setting the two equations equal to each other, since the instrumental constant (K) is the same in both cases, equation (2.2) is obtained

$$\Delta H_{sam} = \Delta H_{ind} \cdot \frac{W_{ind}}{W_{sam}} \cdot \frac{A_{sam}}{A_{ind}} \cdot \frac{R_{sam}}{R_{ind}} \cdot \frac{S_{ind}}{S_{sam}} \quad (2.2)$$

where ΔH , W, A, R, and S are the heat of transition, weight, area, range, and chart speed, respectively. The numbers with respect to Indium can be combined into a constant K' , so that:

$$\Delta H_{sam} = \frac{K' \cdot R \cdot A}{W \cdot S} \quad (2.3)$$

The peak area is usually determined by extrapolating the baseline under the peak.

2.3 Experimental

2.3.1 Experimental Set Up

As mentioned earlier, the main feature of the DSC experiment is to maintain the sample and the reference at same temperature. The instrument thus is provided with two thermocouple isolated from the sample and reference cells' walls to provide greater sensitivity. These thermocouples consist of a sheet of negative Platinel II type thermocouple alloy coupled to a positive Platinel II alloy. Flat shallow containers are employed for the sample and reference materials. These thermocouples are used to measure the temperature of the sample and reference cells and are used for the furnace programmer for limit switch, and temperature readout [9].

2.3.2 An Indium Sample Calibration

An Indium sample was used for calibrating the instrument (Perkin Elmer DSC-4) for both heating and cooling cycles. A fresh Indium sample was accurately weighed and encapsulated in a stainless steel sample cup (~ 5 mg). It was then placed in the left hand side DSC cup. The Indium was then heated at a rate of 2°C/min (which is the rate used in all DSC runs) from 75°C to 175°C while being purged with argon gas at a pressure of 20 psi. In the heating cycle the instrumental error was 1.68 °C and this value was subtracted from all the transition temperatures obtained from heating cycles. There was no detectable instrumental error in the cooling cycle.

2.3.3 DSC Runs on Bulk Liquid Crystal Samples

The ethyl, n-propyl, n-butyl, and n-pentyl members of the cyanophenyl p-n-alkylbenzoate homologous series of liquid crystals are monotropic and show nematic phases only upon cooling their isotropic phases. Their heating and cooling thermograms (Figures 2.1 and 2.2 for n-propyl member are shown as a representative examples) show only a crystal-to-isotropic transition on heating and only an isotropic-to-nematic transition on cooling. No freezing temperature was observed as far down as 36 °C which is the lower limit for the instrument except for the n-propyl member (Figure 2.2) which solidified at 44.1 °C . The n-hexyl and n-heptyl members of the above mentioned series are conventional nematogens. Their thermograms (Figure 2.3 for the n-heptyl member is shown as a representative example) show a crystal-to-nematic transition and a nematic-to-isotropic transition on heating but only an isotropic-to-nematic transition on cooling, again down to 36 °C which is the temperature limit of the instrument.

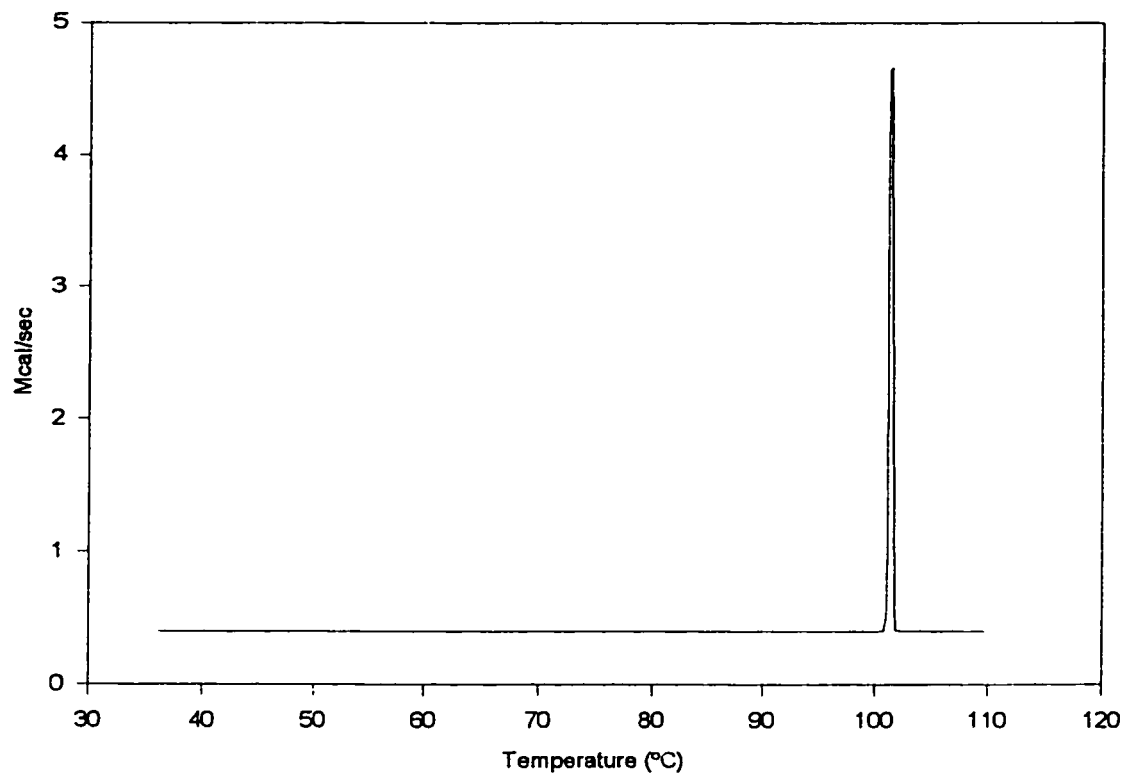


Figure 2.1 : Heating Thermogram for p-Cyanophenyl-p-n-propylbenzoate.

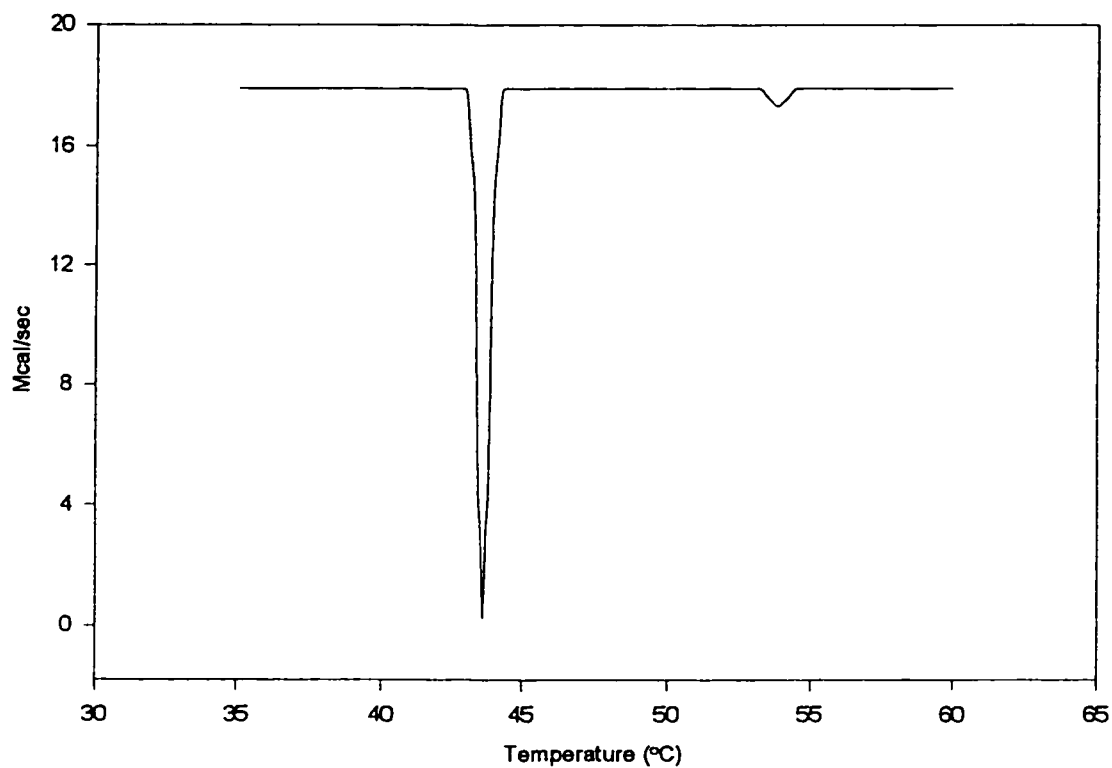


Figure 2.2: Cooling Thermogram for p-Cyanophenyl p-n propylbenzoate.

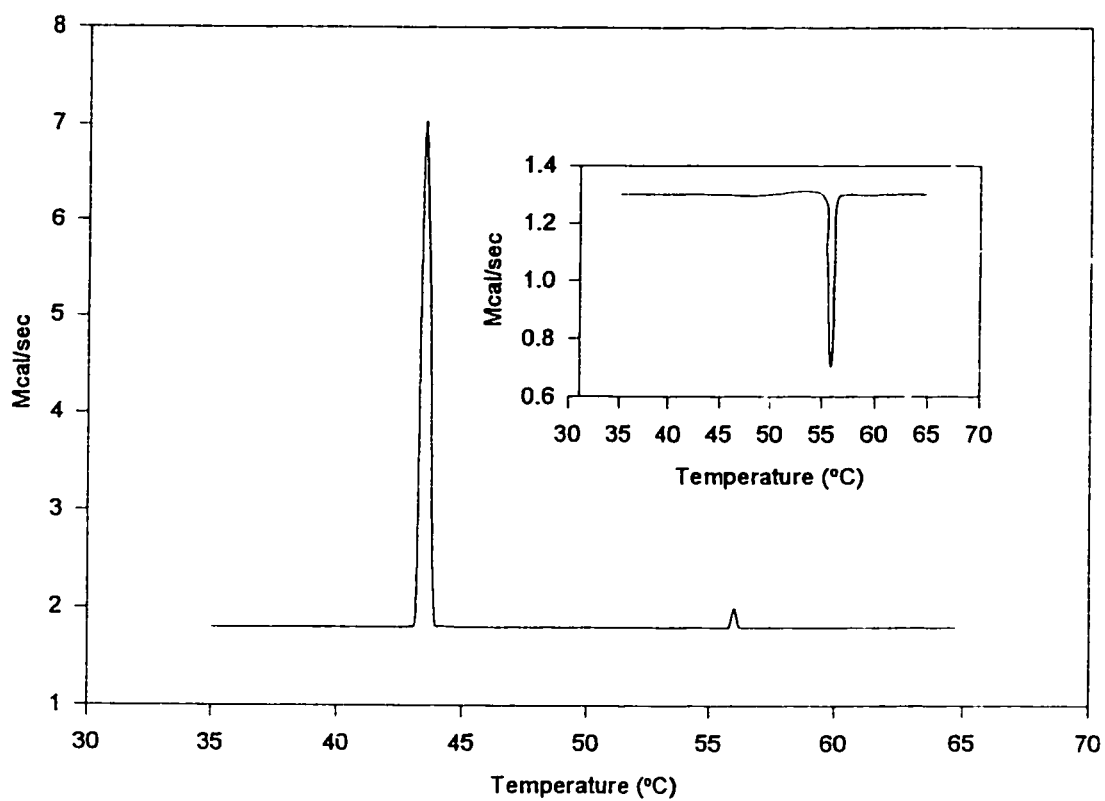


Figure 2.3 : Heating and Cooling (Inset) Thermograms for p-Cyanophenyl-p-n-heptylbenzoate..

We were interested in finding out if a nematic phase obtained by cooling the isotropic phase of a monotropic liquid crystal state exhibits, on reheating a nematic-to-isotropic transition. In other words we desired to examine the conditions for the reversibility of the nematic-to-isotropic transition once a nematic phase had been reached. Using the n-propyl and n-butyl members of the series (in Figure 2.4 the thermograms for the n-propyl member of the series is given as an example), the above mentioned test was carried out and we have found that as long as our material is not cooled enough to solidify (Figure 2.4 (b)) we can repeatedly obtain a nematic-to-isotropic transition on heating and an isotropic-to-nematic transition on cooling. Figure (2.4 (c)) shows that the nematic-to-isotropic transition on heating cannot be obtained once solidification occurs.

2.4 DSC Runs on Liquid Crystals Coated on Chromosorb W

As the above mentioned liquid crystals were also used as stationary phases in the GLC study (see chapter 4) it was necessary to check if their transition temperatures change once they are coated on the support used; namely chromosorb W. For this purpose heating and cooling thermograms were obtained for all the packing of the GLC columns used by us (which contained ~ 8 % of the liquid crystal on a chromosorb W support).

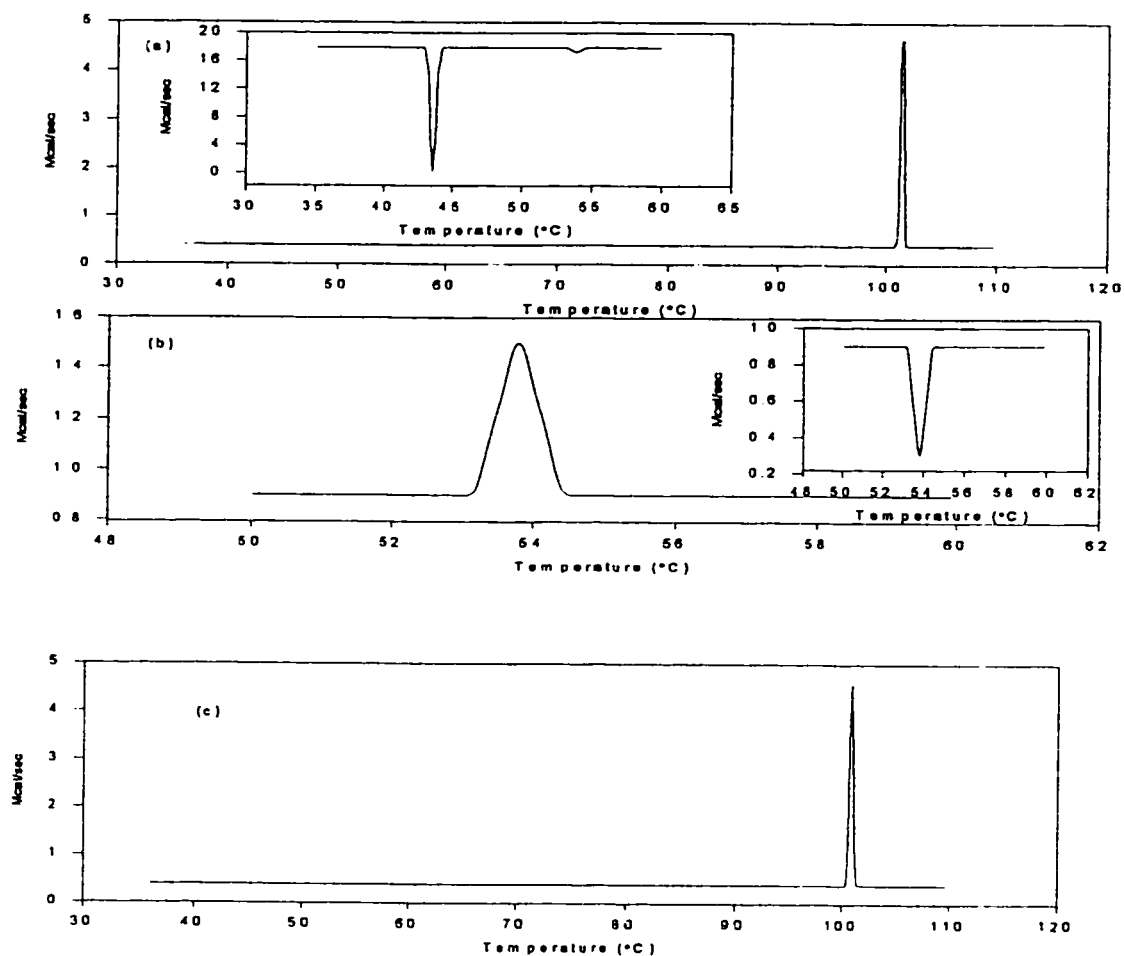


Figure 2.4 : DSC Thermograms for p-Cyanophenyl-p-n-propylbenzoate
 (a) Heating beyond the Crystal-to-Nematic Transition then Cooling
 (Inset) to Below the Isotropic-to-Nematic transition. (b) Heating the
 Sample in (a) Prior to its Solidification beyond Nematic-to-Isotropic
 Transition on Heating and below Isotropic-to-Nematic Transition on
 Cooling (Inset). (c) Heating Thermogram after Allowing the Sample
 to Solidify.

Good DSC results were obtained for all the systems used except for the ethyl member of the liquid crystal series which did not show an isotropic-to-nematic transition. This behavior was also exhibited by another packing containing 12 % of this liquid crystal. This liquid crystal also gave poor GLC results in the nematic phase. Thus except for the ethyl member of the series our DSC runs assured us that the isotropic-to-nematic transition temperature of the bulk samples and samples coated as stationary phases are the same (see Figure 2.5 and Table 2.1).

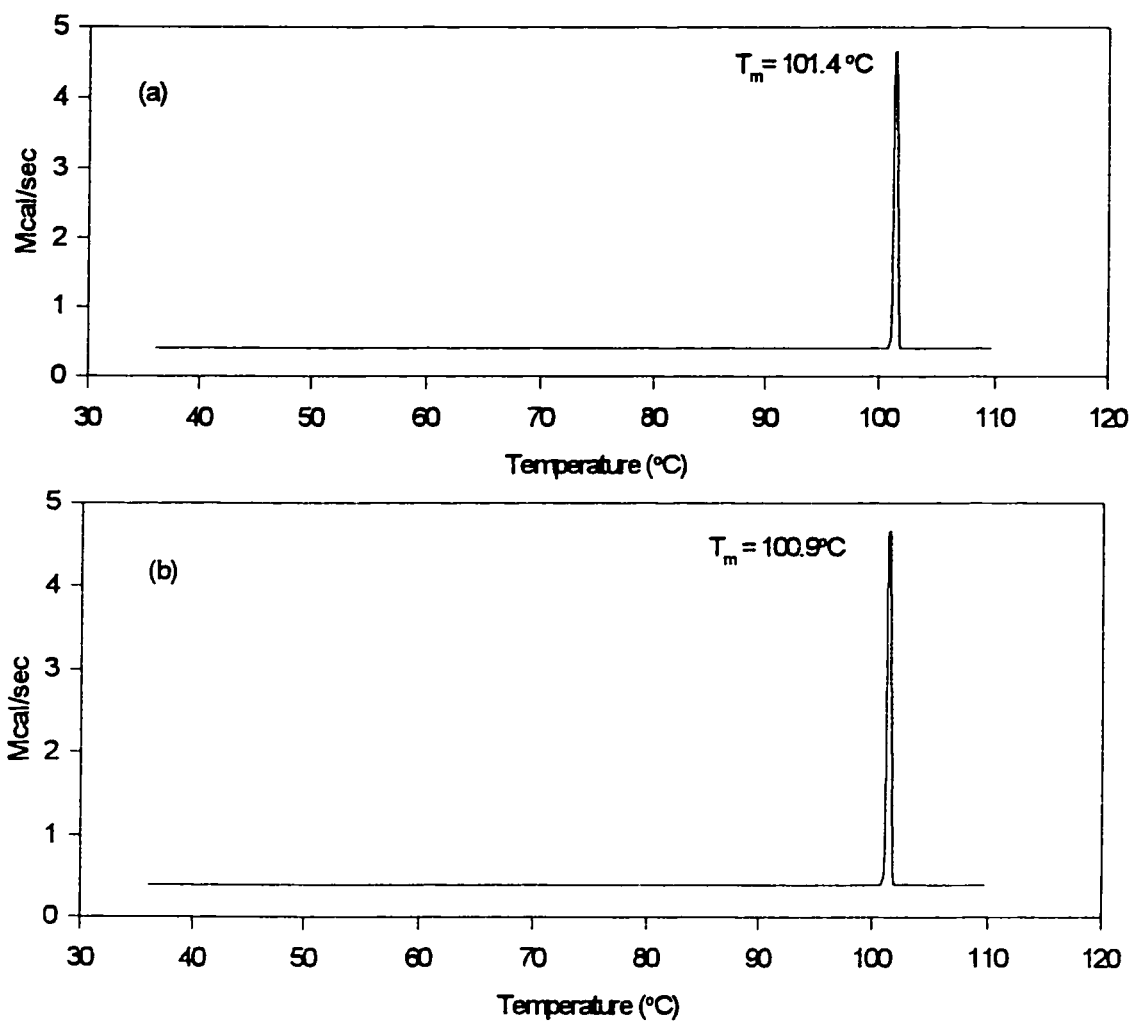


Figure 2.5: Heating Thermograms for (a) a Bulk and (b) a Sample Coated on a Support for p-Cyanophenyl-p-n-propylbenzoate.

Table 2.1 : Melting Points, Clearing Points and the Changes in Enthalpy and Entropy at these Transitions.

Liquid Crystal [#]	M.P.* (°C)	ΔH_m (kJmol ⁻¹)	$\Delta S_m/R$ kJ mol ⁻¹ K ⁻¹	C.P.* (°C)	ΔH_c (kJmol ⁻¹)	$\Delta S_m/R$ kJ mol ⁻¹ K ⁻¹
Ethyl	74.80	23.26	8.0405
	42.82	-0.2839	-0.1081
	76.11	24.04	8.2790

Propyl	101.43	30.52	9.8113
	53.83	-0.5994	-0.2205
	33.83	10.8780
	100.91	53.87	-0.6229	-0.2291
Butyl	66.17	26.89	9.5317
	42.63	-0.4441	-0.1692
	65.86	26.76	9.4943
	42.64	-0.4091	-0.1558

Table 2.1(continued) : Melting Points, Clearing Points and the Changes in Enthalpy and Entropy at these Transitions.

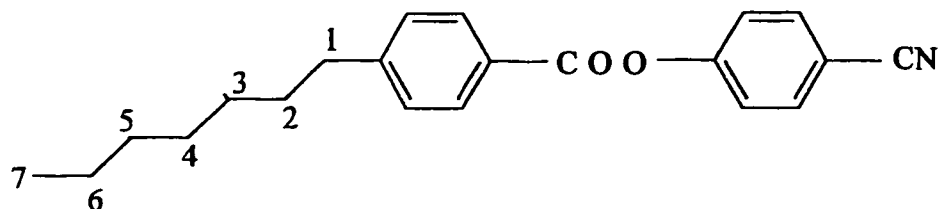
Pentyl	59.46	29.69	10.7366
	57.46	-0.7733	-0.2813
	62.63	15.24	5.4591
	57.29	-0.8791	-0.3200
Hexyl	44.28	34.39	13.0309	47.35	0.4759	0.1786
	48.48	-0.6173	-0.23308
	43.94	34.75	13.1814	47.22	0.4501	0.1690
	48.46	-0.6018	-0.2790
Heptyl	43.47	33.26	12.6350	56.01	0.8338	0.3047
	57.23	-0.8338	-0.3182
	42.97	31.83	12.1109	55.90	0.8069	0.2494
	57.24	-0.8069	-0.4063

* M.P. and C.P. stand for the melting and clearing temperatures respectively.

For each liquid crystal the first and the second line represent heating and cooling cycles for bulk samples while the third and the fourth lines represent heating and cooling cycles for samples coated on a support.

2.5 Odd-Even Effect

Like other earlier DSC studies on liquid crystals [11,61-63] our measurements on the p-Cyanophenyl-p-n-alkylbenzoate liquid crystals show an 'odd-even' effect in the values of the transition temperatures and enthalpy changes on melting and at the isotropic-to-nematic phase changes (see Figures 2.6 and 2.7). Earlier researchers [10] explained this effect using the following argument. The most energetically favored conformation for an alkyl chain is the fully extended, all trans or zigzag conformation and solid n-alkane chains are constrained exclusively in all trans arrangement that is necessary for efficient packing in a crystal. In the liquid state the carbon chain is free to adopt a variety of conformations depending on the temperature and the chain length. In the intermediate nematic phase a residual constraint tends to make an overwhelming number of conformations all trans ones.



If this is the case then as the figure below shows the introduction of an odd carbon atom along the alkyl tail increases the polarizability along the molecular axis more than the introduction of an even carbon atom thus for liquid crystals with tails having odd carbon numbers intermolecular forces are higher and in turn transition temperatures and enthalpy changes are higher. This odd even effect has been encountered in a variety of liquid crystals with biphenyl cores or similar structures having cores with two rings separated by an intermediate unit (an ester in our case). A model of these systems [11] seems to favor a structure where planes of the benzene rings are at an angle of about 30° to each other. As will discussed in the ESR chapter (chapter 3) ab initio calculations show that for our system the most stable state is one when the rings are at an angle of about 46.38° .

The GLC results also indicate the effect that the liquid crystal tail length has on the activity coefficients of a dissolved solute at infinite dilution. The γ_2^∞ values show an odd-even effect with respect to the number of carbon atoms on the alkyl tail of the liquid crystal solvents. The lower the infinite dilution solute activity coefficient values γ_2^∞ , obtained in solutions of liquid crystals with even tails (see Figures 5.13 and 5.14) reflect lower solvent-solvent compatibilities which give rise to higher solute-solvent compatibilities.

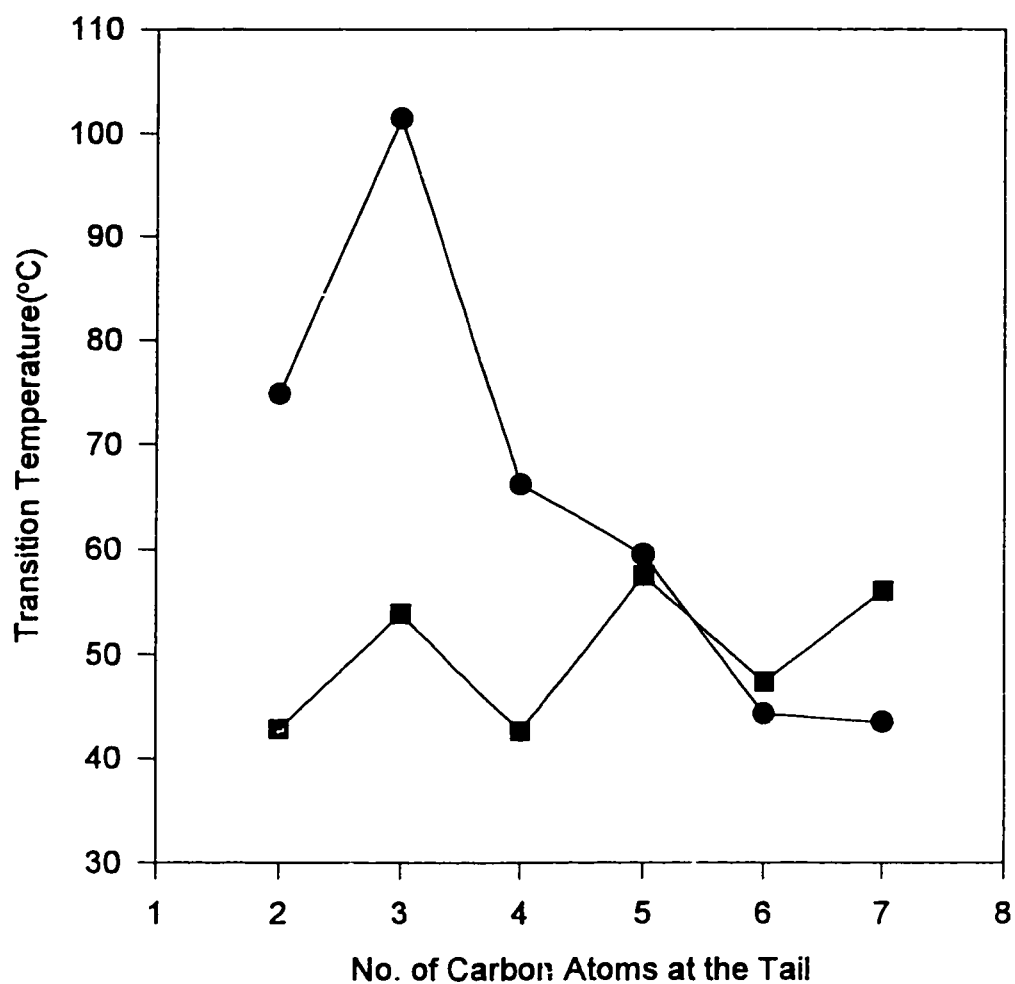


Figure 2.6 : The Variation of the Temperature of Melting (●) and Clearing (■) with the Number of Carbon Atoms on the Alkyl Tail of the p-Cyanophenyl-p-n-alkylbenzoate.

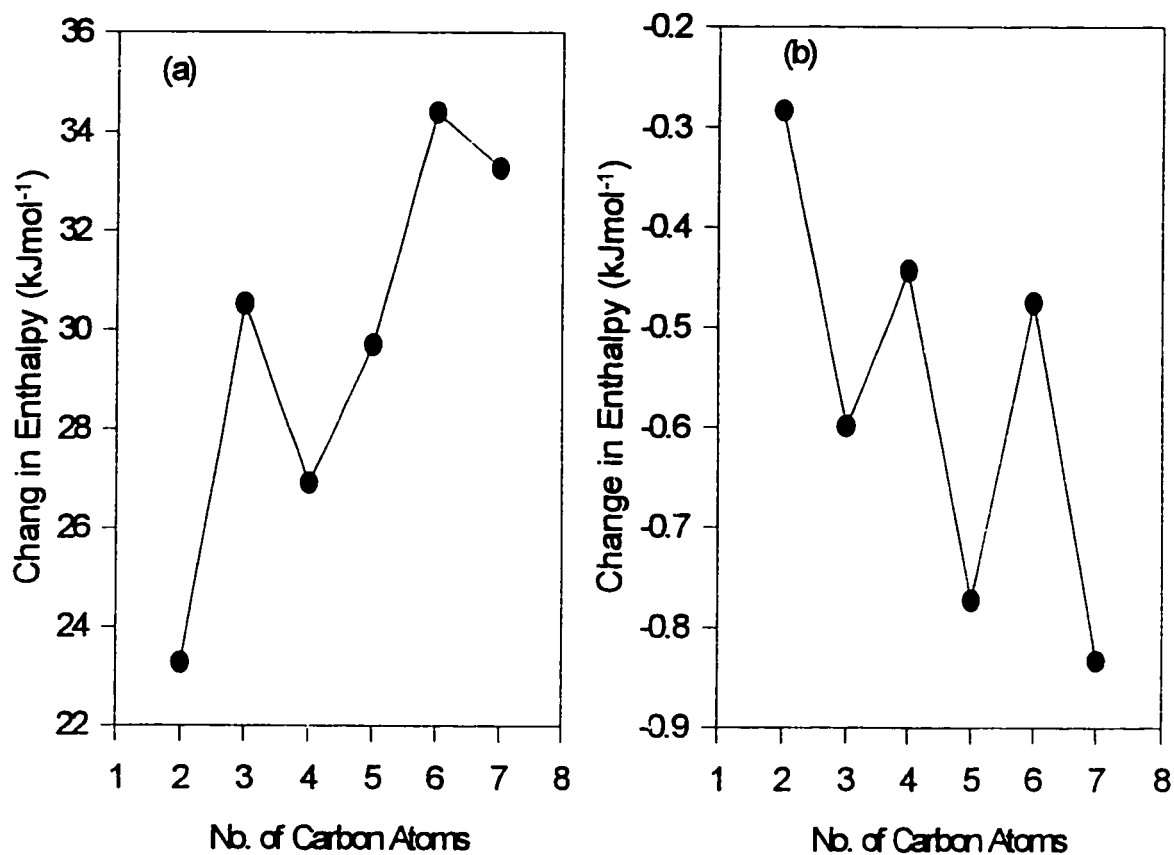


Figure 2.7 : The Variation in (a) in ΔH_m and (b) ΔH_N , the Enthalpy Changes on Melting and Clearing Respectively with the number of Carbon Atoms on the Alkyl Tail of p-Cyanophenyl-p-n-alkylbenzoate.

CHAPTER 3
ELECTRON
PARAMAGNETIC
RESONANCE

CHAPTER 3

ELECTRON PARAMAGNETIC RESONANCE

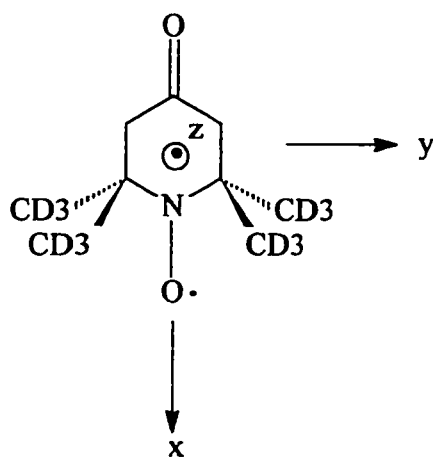
3.1 Introduction

To investigate diamagnetic mesophases, either spin labels or spin probes are needed. In general the probe used must meet some basic requirements[5]. These are :

1. The probe must be chemically stable and with known magnetic parameters (g and a tensors).
2. The probe must be shaped so as to be as sensitive as possible to the finest details of the surroundings without perturbing them.

3. The probe must be able to “transmit” via the ESR phenomenon data to the investigator.

Recently, several studies of the dynamics of nitroxide free radical probes in oriented systems such as nematic liquid crystals and lyotropic liquid crystals have been reported [12-20]. In our study the probe used was predeuterated-2,2,6,6-tetramethyl-4-piperidone-N-oxide (PD-Tempon) having the following structure :



Our study was designed to determine the isotropic-to-nematic transition temperatures and the ordering behavior in the three phases of the p-cyanophenyl-p-n-alkylbenzoate series of liquid crystals.

3.2 Theoretical Background

In a magnetic field B , the energy levels of an unpaired electron spin are described by [8]

$$E_{m_s} = g_e \mu_B m_s B \quad m_s = \pm 1/2 \quad (3.1)$$

The energy of an electron with a spin of $+1/2$ increases and the energy of an electron with a spin of $-1/2$ decreases as the field increases, and the separation of the levels is :

$$\Delta E = E_\alpha - E_\beta = g_e \mu_B B \quad (3.2)$$

The resonance condition is therefore :

$$h\nu = g_e \mu_B B \quad (3.3)$$

and when this condition is fulfilled strong absorption of radiation occurs.

The ESR experiment is thus the study of molecules containing unpaired electrons by observing the magnetic field at which they come into resonance with monochromatic radiation. The radiation used falls in the microwave region of the electromagnetic spectrum. In ESR, the spin magnetic moment interacts with the local magnetic field. The resonance condition is written as

$$h\nu = g\mu_B B \quad (3.4)$$

where $g = (1-\sigma) g_e$

The deviation from $g_e = 2.0023$ depends on the ability of the applied field to induce local electron currents in the radical, and therefore gives information about the electronic structure.

In ESR spectra, splitting of individual resonance lines into components occurs. The source of splitting is the magnetic field

arising from nuclear magnetic moments (I) within the radical. For example, an N^{14} nucleus ($I=1$) in a radical is a source of magnetic field and adds or subtracts from the applied field. The total field is thus

$$B_{\text{loc}} = B + a m_I \quad m_I = -1, 0, 1 \quad (3.5)$$

where a is the hyperfine coupling constant. The spectrum observed is a three lines spectrum.

The resolved component A_{zz} of the total tensor is written as :

$$A_{zz} = a + \sum_{\alpha, \beta} I_{z\alpha} I_{z\beta} A'_{\alpha\beta} \quad (3.6)$$

where $A'_{\alpha\beta}$ is an anisotropic tensor whose trace is zero, and α and β are the Cartesian axes set in the molecule.

When the spin probe is dissolved in a solvent, molecular reorientation will cause the direction cosines to fluctuate in time. If the molecular motion is fast, then the observed hyperfine splitting would be obtained by taking a time ensemble average of equation (3.6). The anisotropy in a hyperfine interaction is typically 100 MHz and so the rotational correlation time would need to be smaller than 10^{-8} s, to obtain the fast exchange limit. The correlation time in the mesophases of many nematogens is normally less than 10^{-8} s, although this is not the case for most cholesteric liquid crystals. The average $\overline{A_{zz}}$ is normally denoted by \overline{a} and so we have :

$$\overline{a} = a + \sum_{\alpha,\beta} \overline{I_{z\alpha} I_{z\beta}} A'_{\alpha\beta} \quad (3.7)$$

The quantities $\overline{I_{z\alpha} I_{z\beta}}$ could be used to describe the orientational order of the spin probe in the mesophases. The order parameter **S** is used to describe the pure mesophase. A matrix **S** with a diagonal element is defined as :

$$S_{\alpha\alpha} = \frac{\overline{(3I_{z\alpha}I_{z\beta} - 1)}}{2} \quad (3.8)$$

The off diagonal element by analogy is defined as :

$$S_{\alpha\beta} = \frac{\overline{3I_{z\alpha}I_{z\beta}}}{2} \quad (3.9)$$

These two expressions may be combined using kronecker delta to give an element defined as:

$$S_{\alpha\alpha} = \frac{\overline{(3I_{z\alpha}I_{z\beta} - \delta_{\alpha\beta})}}{2} \quad (3.10)$$

This definition may be incorporated into equation (3.7) for \bar{a} and remembering that the anisotropic hyperfine tensor is traceless, the following equation is defined:

$$\bar{a} = a + \frac{2}{3} \sum_{\alpha\beta} S_{\alpha\beta} A'_{\alpha\beta} \quad (3.11)$$

The quantity S is known as the ordering matrix and was originally introduced by Saupe to describe the extent of solute alignment in a liquid crystal [52]. A three by three matrix is used to describe this alignment but some of these elements are related. For example $l_{z\alpha}l_{z\beta}$ and $l_{z\beta}l_{z\alpha}$ are identical and the ordering matrix is thus symmetric:

$$S_{\alpha\beta} = S_{\beta\alpha} \quad (3.12)$$

As a result, the trace of the matrix is zero; Since from the direction cosines:

$$l_{z\alpha}^2 + l_{z\beta}^2 + l_{z\gamma}^2 = 1 \quad (3.13)$$

The largest number of independent elements for S is therefore five and this number can be further reduced. The ordering matrix can be diagonalized and this limits the number of independent components

to two. If the molecule is cylindrically symmetric, then the principal coordinate system contains the symmetry axis and any pair axes orthogonal to it. The elements of the ordering matrix for these two axes must be identical and equal to minus one half of the element for the symmetry axis :

$$S_{bb} = S_{cc} = -\left(\frac{1}{2}\right)S_{aa} \quad (3.14)$$

The ordering matrix is completely defined by the element S_{aa} which is the only element employed for liquid crystals. Some properties of the S matrix are like to those of the anisotropic hyperfine tensors. Accordingly the elements of the matrices change in the same way on transforming from one coordinate to another

$$S'_{ab} = \sum_{\alpha,\beta} l_{a\alpha} l_{b\beta} S_{\alpha\beta} \quad (3.15)$$

A variety of other functions have been used to describe the orientational order, but all of them are related to the ordering matrix and are not discussed here. In the isotropic phase of the nematogens,

the ordering matrix and the order parameter vanish and hyperfine spacing takes its scalar value a . On lowering the temperature below the isotropic-to-nematic transitions, the hyperfine spacing changes by an amount equal to :

$$\bar{a} - a = 2/3 \sum_{\alpha,\beta} S_{\alpha\beta} A'_{\alpha\beta} \quad (3.16)$$

because S is no longer equal to zero. To determine S , it is necessary to know the magnitude of the anisotropic hyperfine tensor. Unlike the nuclear dipole interactions, the hyperfine tensors can not be calculated accurately, but it can be extracted from the solid state electron resonance spectrum of the spin probe. However, there is still insufficient information to determine S and in fact the ordering matrix can be obtained from the hyperfine shift only if the spin probe is cylindrically symmetric. With this condition Equation (3.16) is reduced to:

$$\bar{a} - a = \sum_{\alpha,\beta} S_{\alpha\beta} A'_{\alpha\beta} \quad (3.17)$$

where A'_{11} is the component of the anisotropic hyperfine tensor along
 l. When the principal coordinate system is known from the molecular
 symmetry, equation (3.16) becomes :

$$\bar{a} - a = S_{11}A'_{11} + \frac{1}{3}(S_{22} - S_{33})(A'_{22} - A'_{33}) \quad (3.18)$$

If the two independent components of \mathbf{S} are to be determined, another
 experimental quantity is needed. It is the change in the g-factor on
 passing from the isotropic to the nematic phase. The g-factor is
 related to the principal components of the ordering matrix by the
 following expression :

$$\bar{g} - g = S_{11}g'_{11} + \frac{1}{3}(S_{22} - S_{33})(g'_{22} - g'_{33}) \quad (3.19)$$

where $g'_{\alpha\beta}$ is the anisotropic g tensor. Provided that g and the
 hyperfine tensors are not cylindrically symmetric about a common
 axis, equation (3.18) and equation (3.19) may be solved to give the
 principal components of \mathbf{S} .

3.3 Experimental and Procedure

3.3.1 Sample Preparation

The probe was obtained from Molecular probes and used without any further purification. The liquid crystals used in GLC studies and DSC studies are used here except for the propyl member of the series since at its high melting point the probe becomes inactive. The ESR sample was prepared by introducing the probe into the melted liquid crystal. The probed solution was transferred into the ESR Pyrex tube (3-mm i.d., 5-mm o.d.) adapted to 9 mm o. d. at the open end. The dimensions of the sample holder were chosen so that unhindered flow of circulating fluid is attained. For melting and controlling temperature of the sample, an RCS-20D refrigerating circulator and bath in which Ultra-Thermal SK Frigor (dimethylpolysiloxane) from Lauda was used as a circulating fluid. The temperature of the ESR samples was maintained to within ± 0.02 °C.

3.3.2 ESR Setup

The ESR- 200D-SRC series spectrometer was used to obtain the ESR spectra. The magnetic field sweep was calibrated with a Bruker-ER 035M NMR gaussmeter with an accuracy of 2 mG. The frequency used was measured with a Model 5342A Hewlett-Packard frequency counter. The cavity used along with the 9-GH microwave bridge is ER-4102-ST.

3.3.3 Spectra Recording and Data Collection

The sample was introduced into the sample holder which is fixed inside the microwave cavity. Temperature was changed as needed through the temperature control previously described. Near the isotropic-to-nematic transition temperatures small increments or decrements were applied to accurately determine these transition temperatures.

3.3.4 Results and Discussion

The isotropic to nematic transition temperatures obtained from ESR, shown in Table 3.1, are in agreement with the DSC study and with those quoted by the manufacturer [37]. ESR and DSC measurements show that these transition temperatures are reversible within the isotropic-nematic region; after the appearance of the nematic phase on cooling and as long as solidification does not occur. The hyperfine splitting a_{iso} for PD-Tempone in the liquid crystals studied are also shown in Table 3.1. For all the liquid crystals studied the values of a_{iso} in the isotropic phase are constant at about 14.7 ± 0.03 . Morsy et. al [20] showed that PDT is more free to reflect the part of the solvent molecule that contributes most to its liquid crystalline characteristics, and on average is close to the alkyl tail which is unaffected by temperature and a_{iso} remains constant up to the isotropic-to-nematic transition.

Table 3.1: Isotropic-to-Nematic Transition Temperatures (T_N), Hyperfine Splitting $a_{\text{h.o.}}$ in the Isotropic Phase and g-Factors at the Onset of the Isotropic-to-Nematic Transitions for PD-Tempone in the p-Cyanophenyl-p-n-alkylbenzoate Liquid Crystal Solvents.

Liquid Crystal	T_N ($^{\circ}\text{C}$)			$a_{\text{h.o.}}$ (G)	g_{NI}
	(reported)*	(DSC)	(ESR)		
p-Cyanophenyl p-ethylbenzoate	42.6	42.8	41.5	14.76	2.00615
p-Cyanophenyl-p-n-propylbenzoate	53.2	53.8
p-Cyanophenyl-p-n-butylbenzoate	42.3	42.6	42.0	14.72	2.00605
p-Cyanophenyl-p-n-pentylbenzoate	56.5	57.4	56.6	14.78	2.00615
p-Cyanophenyl-p-n-hexylbenzoate	48.0	47.4	47.8	14.76	2.00592
p-Cyanophenyl-p-n-heptylbenzoate	56.5	56.0	56.4	14.76	2.00577

* Reported transition temperatures quoted by the manufacturer [37] and were measured using a polarizing microscope method.

The isotropic-to-nematic transition as shown in Figures 3.1 and 3.2 for p-cyanophenyl-p-n-butylbenzoate is obtained by cooling and is characterized by a discontinuity with a large change in both the a value, and the g -factor. ESR representative spectra for PDT in the isotropic phase, in the two phase region and in the nematic phase of p-cyanophenyl p-n-butylbenzoate is shown in Figure 3.3. These spectra, as expected, are characterized by a high a value in the isotropic phase relative to that in the nematic phase. On further cooling a values characteristics of the nematic phase continued to decrease until a temperature is reached (dashed vertical line in Figure 3.1) when a sudden increase in a occurred. Beyond this point a solid amorphous phase is postulated. This transition does not show any doublets like those observed in the isotropic-to-nematic transitions. This phenomena is similar to that previously reported for 6CB by Morsy et al [20] and was attributed to a large degree of non planarity of the benzene rings of the biphenyl cores of the liquid crystal molecule.

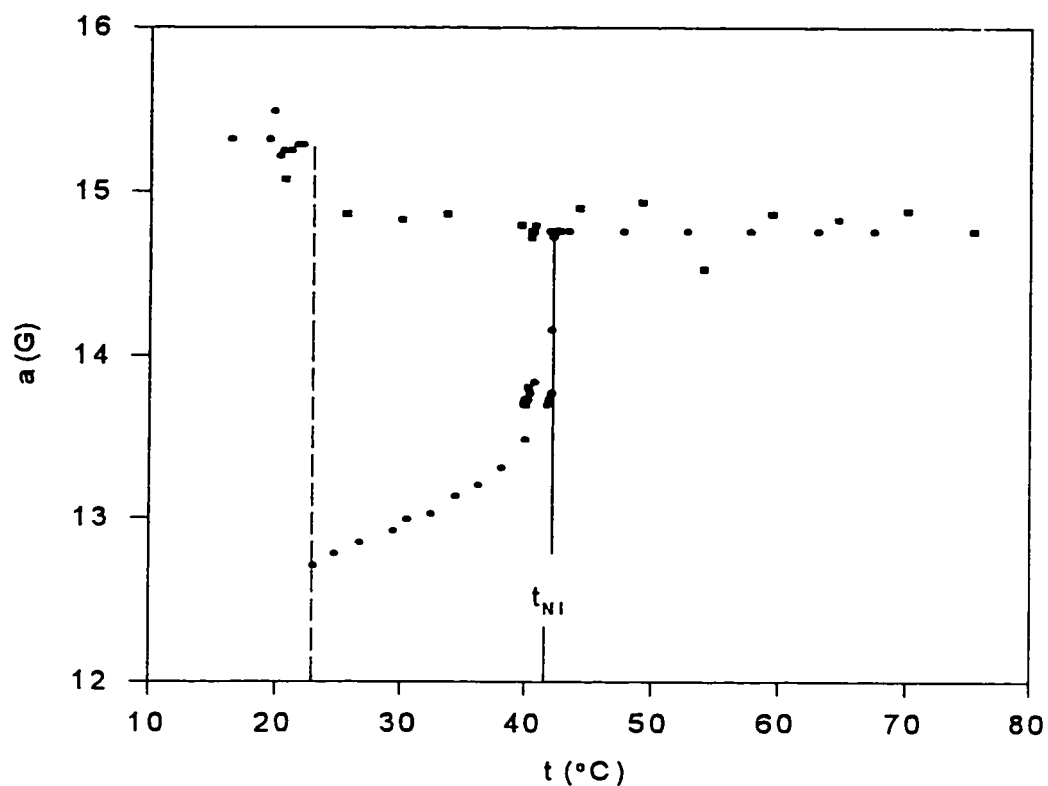


Figure 3.1: The Hyperfine Splitting a Versus Temperature for PD-Tempone in p-Cyanophenyl-p-n-Butylbenzoate. T_{NI} is the Isotropic-to-Nematic Transition. The dashed Vertical Line is the Boundary between a Supercooled Phase where Nematic Characteristics Persist and a Proposed Amorphous Solid Phase is Proposed. The symbol (\bullet) denotes a Cooling Cycle whereas the Symbol (\blacksquare) Denotes a Heating Cycle.

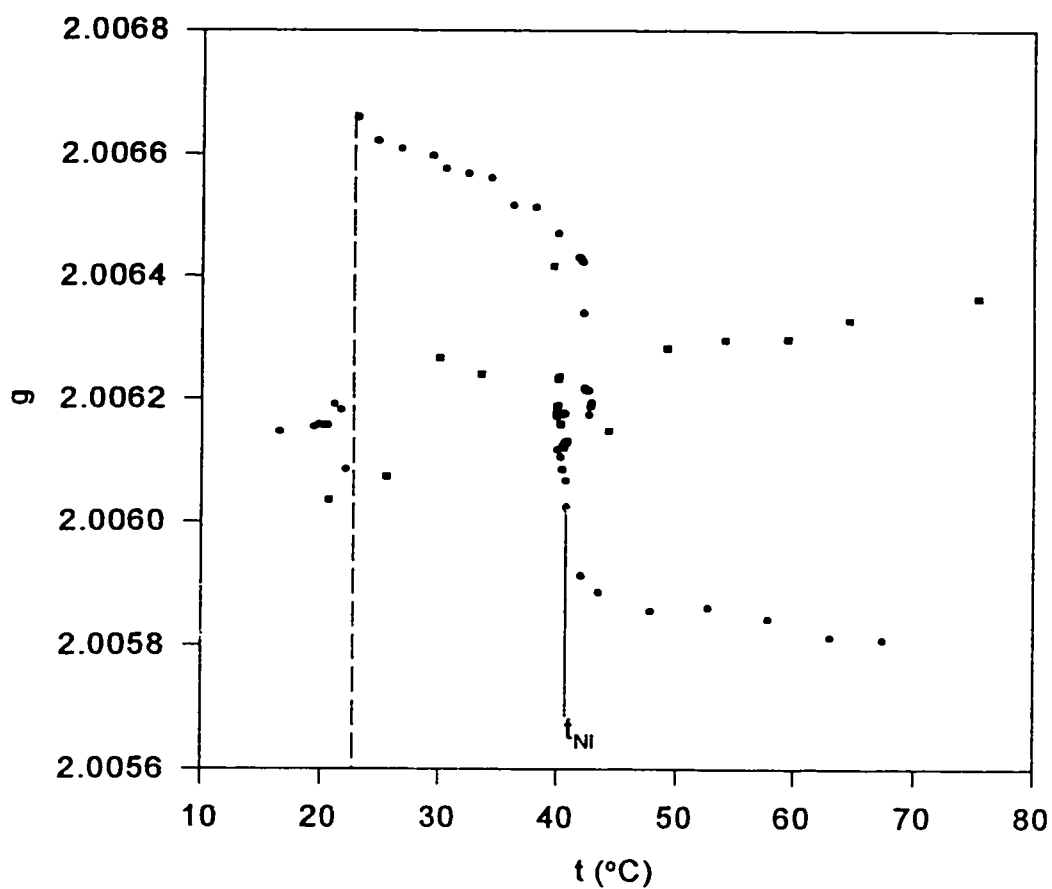


Figure 3.2 : g -Factor Versus Temperature for PD-Tempone in p -Cyanophenyl- p - n -butylbenzoate. T_{NI} is the Isotropic-to-Nematic Transition. The Dashed Vertical Line is the Boundary between a Supercooled Phase where Nematic Characteristic Persists and a Proposed Amorphous Solid Phase. The Symbol (●) Denotes a Cooling Cycle whereas the Symbol (■) Denotes a Heating Cycle.

Table 3.1 also shows that as the alkyl tail length increases the g-factor value for the probe at the onset of the isotropic-to-nematic transition decreases. This decrease in the direction of the spin of the free electron ($g = 2.00232$) suggests a decrease in the spin density around the oxygen atom of the probe due to increase in the solvent-probe interaction which in turn is attributed to an increasing degree of planarity between the phenyl groups of the solvent molecules. In the light of this finding our g values suggest that the degree of planarity among the phenyl groups of the liquid crystals studied by us increases as we go down from the ethyl to the heptyl members of the homologous series of liquid crystal studied.

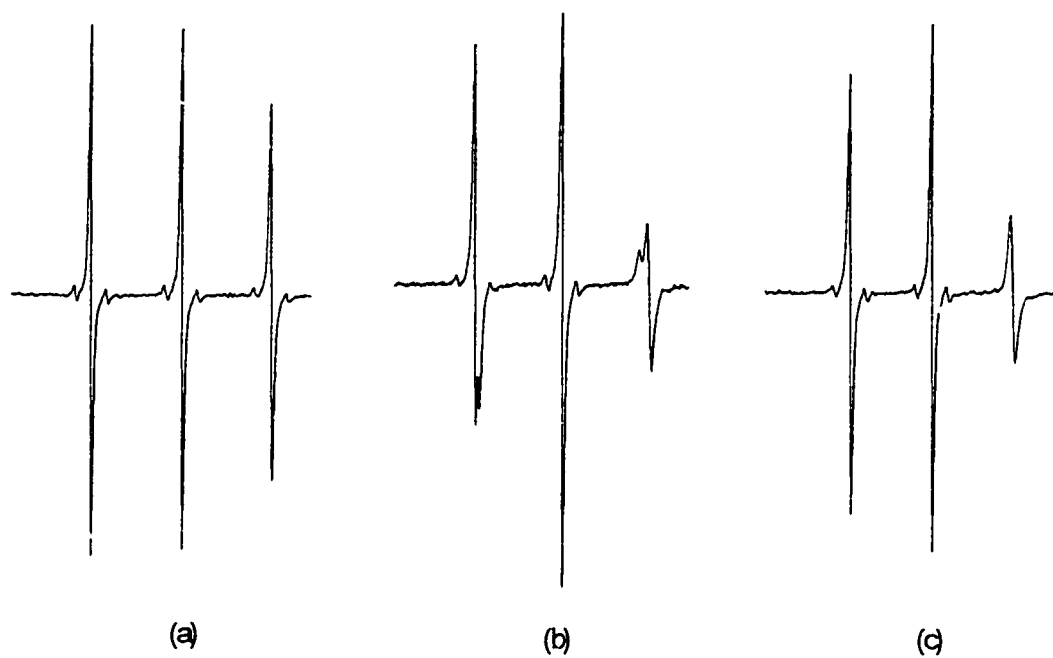


Figure 3.3 : ESR Spectra for PDT in (a) the Isotropic Phase (67.5 °C), (b) the Two Phase Region (42.0 °C), And (c) the Nematic Phase (40.0 °C) of p-Cyanophenyl-p-n-butylbenzoate.

The ethyl, n-propyl, n-butyl, n-pentyl members of p-cyanophenyl-p-n-alkylbenzoate series of liquid crystals exhibit a monotropic behavior that has been described in chapters 1 and 2. This behavior is also evident in the results of the ESR study. Since in the ESR experimental setup temperatures lower than those achieved by the DSC instrument may be reached (our temperature limit in the DSC instrument) we were able to go well below 36 °C. A seemingly strange behavior occurred at low enough temperatures are listed in Table 3.2. The ESR experiment could not be done for the p-cyanophenyl-p-n-propylbenzoate because it has a very high melting point that renders the probe inactive and for this reason no result is given for it in Table 3.2. This is unfortunate because this is the only liquid crystal that exhibited a solidification temperature during cooling in the DSC experiment at 44.1 °C (see Figure 2.2). At these temperatures the a value increased and the g value decreased to values comparable to the ones they had at the onset of the isotropic-to-nematic transition. It is established that an increase in a value reflects a decrease in order [10] and this behavior is interpreted as a

transition from a 'supercooled' or 'frozen nematic' to a disordered solid 'amorphous' solid. Such An order-disorder transition may be attributed to constraints on the molecules in the ordered structure.

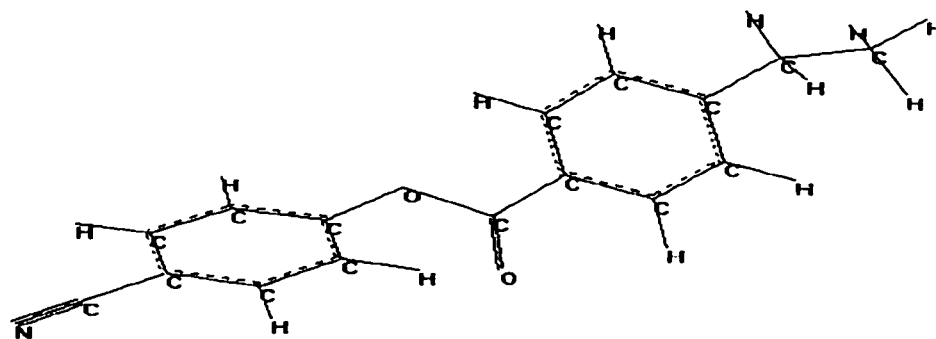
Table 3.2 : Amorphous Solidification Transition Temperatures for the Series of Liquid Crystals Studied.

Liquid Crystal	Amorphous
	Solidification Temperature (°C)
p-Cyanophenyl-p-ethylbenzoate	35.2
p-Cyanophenyl-p-n-butylbenzoate	22.9
p-Cyanophenyl-p-n-pentylbenzoate	24.2
p-Cyanophenyl-p-n-hexylbenzoate	18.5
p-Cyanophenyl-p-n-heptylbenzoate	23.1

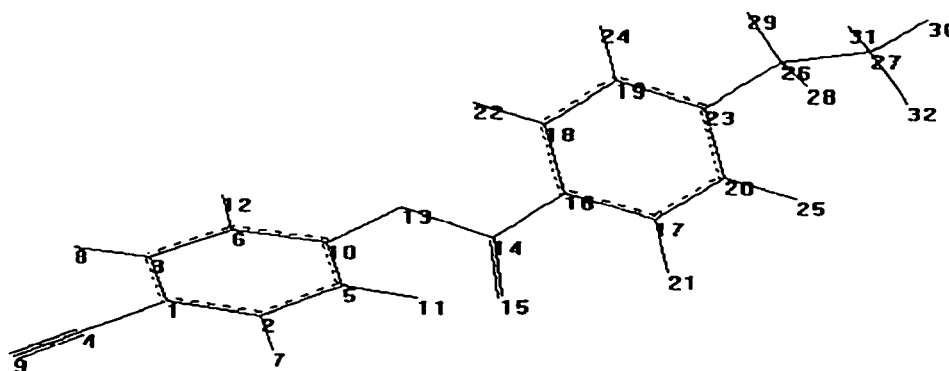
To investigate the probable cause of such disordering molecular modeling was done [65] to determine the most stable conformer(s) for the liquid crystals using the p-cyanophenyl-p-ethylbenzoate as our basic unit. The fully optimized molecular structure and structure parameters done using STO-3G basis set level [54] are given in Figure 3.4 and Table 3.3. The fully optimized structure shows that in this molecule, the cyanophenyl portion and the benzoate portion are individually planar with a dihedral angle of 46.38° between them at their linkage point at the ester oxygen. The potential energy diagram in Figure 3.5 was evaluated by fixing all the structure parameters and varying this dihedral angle in steps of 10° between -180° and $+180^\circ$. The two minima observed at -40.4° and $+46.4^\circ$ are for two very similar stable molecular geometries. Each of these geometries may be obtained by reflecting the cyano portion of the molecule in a mirror containing the plane of the benzoate portion in its plane.

It seems that at short to moderate alkyl tail an appreciable departure from planarity (dihedral angle between the cyanophenyl and benzoate portions) is not conducive to a stable nematic phase. Thus on heating

the solid liquid crystal (with a dihedral angle about 30°) changes directly to the isotropic phase where the 30° dihedral angle probably increases up to that of the most stable structure predicted by us, i.e., 46.4° .



(a)



(b)

Figure 3.4 : The Optimized Molecular Structure for p-Cyanophenyl-p-ethylbenzoate as Obtained from STO-3G Basis Set ab initio Calculations (a) the Symbols Labeled Structure and (b) the Numbers Labeled Structure.

Table 3.3 : 3-21G Optimized Structural Parameters of p-cyanophenyl-p ethylbenzoate.

Bond Lengths		Bond Angles		degree	Dihedral Angles	degree
r(C ₂ -C ₁)	1.402					
r(C ₃ -C ₁)	1.404	∠(C ₃ -C ₁ -C ₂)		120.2		
r(C ₄ -C ₁)	1.421	∠(C ₄ -C ₁ -C ₂)		119.9	τ(C ₄ -C ₁ -C ₂ -C ₃)	179.9
r(C ₅ -C ₂)	1.393	∠(C ₅ -C ₂ -C ₁)		120.1	τ(C ₅ -C ₂ -C ₁ -C ₃)	0.32
r(C ₆ -C ₃)	1.390	∠(C ₆ -C ₃ -C ₁)		120.1	τ(C ₆ -C ₃ -C ₁ -C ₂)	0.04
r(H ₇ -C ₂)	1.101	∠(H ₇ -C ₂ -C ₁)		120.0	τ(H ₇ -C ₂ -C ₁ -C ₅)	180.0
r(H ₈ -C ₃)	1.101	∠(H ₈ -C ₃ -C ₁)		120.0	τ(H ₈ -C ₃ -C ₁ -C ₆)	179.7
r(N ₉ -C ₄)	1.635	∠(N ₉ -C ₄ -C ₁)		179.9	τ(N ₉ -C ₄ -C ₁ -C ₂)	108.1
r(C ₁₀ -C ₅)	1.400	∠(C ₁₀ -C ₅ -C ₂)		119.0	τ(C ₁₀ -C ₅ -C ₂ -C ₁)	-0.22
r(H ₁₁ -C ₅)	1.100	∠(H ₁₁ -C ₅ -C ₂)		120.6	τ(H ₁₁ -C ₅ -C ₂ -C ₁₀)	-178.7
r(H ₁₂ -C ₆)	1.100	∠(H ₁₂ -C ₆ -C ₃)		121.0	τ(H ₁₂ -C ₆ -C ₃ -C ₁)	-179.9
r(O ₁₃ -C ₁₄)	1.391	∠(O ₁₃ -C ₁₄ -C ₅)		123.0	τ(O ₁₃ -C ₁₄ -C ₅ -C ₂)	174.4
r(C ₁₄ -C ₁₃)	1.384	∠(C ₁₄ -C ₁₃ -C ₁₀)		120.0	τ(C ₁₄ -C ₁₃ -C ₁₀ -C ₅)	46.4

Table 3.3 3-21G Optimized Structural Parameters of p-Cyanophenyl
(Continued) :
p-ethylbenzoate.

$r(\text{C}_{15}\text{-C}_{14})$	1.230	$\angle(\text{C}_{15}\text{-C}_{14}\text{-C}_{13})$	118.7	$\tau(\text{C}_{15}\text{-C}_{14}\text{-C}_{13}\text{-C}_{10})$	1.00
$r(\text{C}_{16}\text{-C}_{14})$	1.468	$\angle(\text{C}_{16}\text{-C}_{14}\text{-C}_{13})$	112.9	$\tau(\text{C}_{16}\text{-C}_{14}\text{-C}_{13}\text{-C}_{15})$	179.7
$r(\text{C}_{17}\text{-C}_{16})$	1.403	$\angle(\text{C}_{17}\text{-C}_{16}\text{-C}_{14})$	118.2	$\tau(\text{C}_{17}\text{-C}_{16}\text{-C}_{14}\text{-C}_{13})$	-176.4
$r(\text{C}_{18}\text{-C}_{16})$	1.400	$\angle(\text{C}_{18}\text{-C}_{16}\text{-C}_{14})$	121.8	$\tau(\text{C}_{18}\text{-C}_{16}\text{-C}_{14}\text{-C}_{17})$	-179.9
$r(\text{C}_{19}\text{-C}_{18})$	1.393	$\angle(\text{C}_{19}\text{-C}_{18}\text{-C}_{16})$	119.9	$\tau(\text{C}_{19}\text{-C}_{18}\text{-C}_{16}\text{-C}_{14})$	179.9
$r(\text{C}_{20}\text{-C}_{17})$	1.391	$\angle(\text{C}_{20}\text{-C}_{17}\text{-C}_{16})$	119.8	$\tau(\text{C}_{20}\text{-C}_{17}\text{-C}_{16}\text{-C}_{14})$	-179.9
$r(\text{H}_{21}\text{-C}_{17})$	1.102	$\angle(\text{H}_{21}\text{-C}_{17}\text{-C}_{16})$	119.4	$\tau(\text{H}_{21}\text{-C}_{17}\text{-C}_{16}\text{-C}_{20})$	-180.0
$r(\text{H}_{22}\text{-C}_{18})$	1.400	$\angle(\text{H}_{22}\text{-C}_{18}\text{-C}_{16})$	119.8	$\tau(\text{H}_{22}\text{-C}_{18}\text{-C}_{16}\text{-C}_{19})$	-180.0
$r(\text{H}_{23}\text{-C}_{19})$	1.400	$\angle(\text{H}_{23}\text{-C}_{19}\text{-C}_{18})$	120.5	$\tau(\text{H}_{23}\text{-C}_{19}\text{-C}_{18}\text{-C}_{16})$	0.02
$r(\text{H}_{24}\text{-C}_{19})$	1.101	$\angle(\text{H}_{24}\text{-C}_{19}\text{-C}_{18})$	119.6	$\tau(\text{H}_{24}\text{-C}_{19}\text{-C}_{18}\text{-C}_{23})$	180.0
$r(\text{H}_{25}\text{-C}_{20})$	1.101	$\angle(\text{H}_{25}\text{-C}_{20}\text{-C}_{17})$	119.8	$\tau(\text{H}_{25}\text{-C}_{20}\text{-C}_{17}\text{-C}_{16})$	-180.0
$r(\text{C}_{26}\text{-C}_{23})$	1.489	$\angle(\text{C}_{26}\text{-C}_{23}\text{-C}_{27})$	120.6	$\tau(\text{C}_{26}\text{-C}_{23}\text{-C}_{27}\text{-C}_{18})$	179.6
$r(\text{C}_{27}\text{-C}_{26})$	1.510	$\angle(\text{C}_{27}\text{-C}_{26}\text{-C}_{23})$	112.0	$\tau(\text{C}_{27}\text{-C}_{26}\text{-C}_{23}\text{-C}_{19})$	109.3
$r(\text{H}_{28}\text{-C}_{26})$	1.124	$\angle(\text{H}_{28}\text{-C}_{26}\text{-C}_{23})$	108.9	$\tau(\text{H}_{28}\text{-C}_{26}\text{-C}_{23}\text{-C}_{27})$	121.1

Table 3.3 3-21G Optimized Structural Parameters of p-Cyanophenyl
 (Continued) : p-ethylbenzoate.

$r(\text{H}_{29}-\text{C}_{26})$	1.231	$\angle(\text{H}_{29}-\text{C}_{26}-\text{C}_{23})$	109.9	$\tau(\text{H}_{29}-\text{C}_{26}-\text{C}_{23}-\text{C}_{27})$	-121.8
$r(\text{H}_{30}-\text{C}_{27})$	1.117	$\angle(\text{H}_{30}-\text{C}_{27}-\text{C}_{26})$	109.9	$\tau(\text{H}_{30}-\text{C}_{27}-\text{C}_{26}-\text{C}_{23})$	178.3
$r(\text{H}_{31}-\text{C}_{27})$	1.117	$\angle(\text{H}_{31}-\text{C}_{27}-\text{C}_{26})$	110.7	$\tau(\text{H}_{31}-\text{C}_{27}-\text{C}_{26}-\text{C}_{30})$	119.9
$r(\text{H}_{32}-\text{C}_{27})$	1.117	$\angle(\text{H}_{32}-\text{C}_{27}-\text{C}_{26})$	110.6	$\tau(\text{H}_{32}-\text{C}_{27}-\text{C}_{26}-\text{C}_{30})$	-119.9

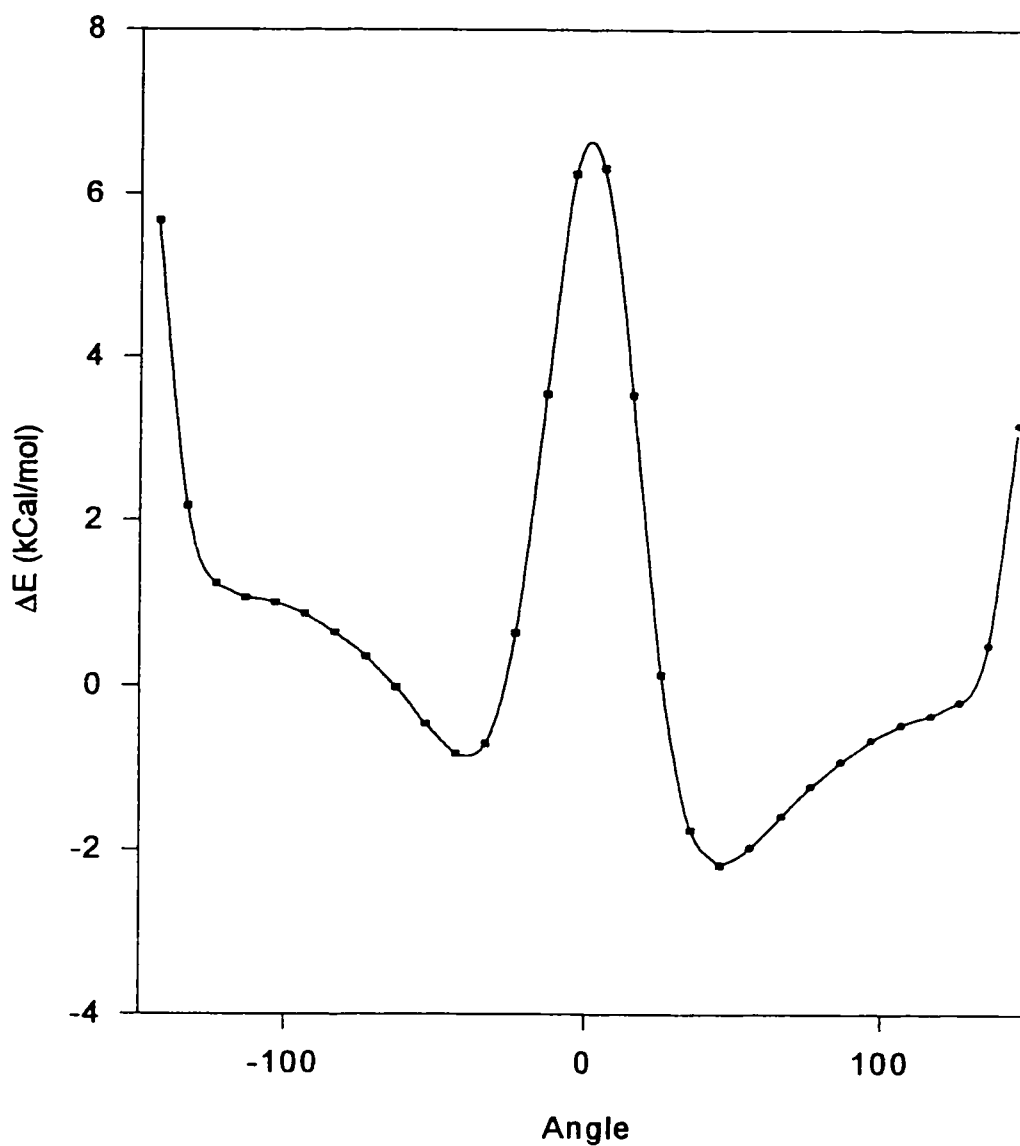


Figure 3.5 : The Potential Energy Diagram for p-Cyanophenyl-p ethylbenzoate Obtained from STO-3G basis set ab initio Calculations by Variation of the Dihedral Angle between the Planes of the Cyanophenyl and the benzoate portions of the Molecule at the Ester Oxygen (number 13 in Figure 3.4)

Experiment shows that a nematic phase appears on cooling the isotropic and that as long as solidification does not occur the nematic-to-isotropic transition is reversible. This may be attributed to a more planar structure which, though metastable, is stable enough, as a consequence of planar conjugation involving the ester linkage, to sustain a nematic phase. In this orientationally ordered nematic phase the molecules are probably strained at dihedral angles less than 46.4° . On reaching the solidification point by cooling this strain is released and an order-disorder transition takes place. When this occurs the molecules revert to the most stable conformers predicted by the above mentioned ab initio calculations, i.e.; a 46.4° dihedral angle.

CHAPTER 4

THE GLC

EXPERIMENT

CHAPTER 4

THE GLC EXPERIMENT

4.1 Introduction

Thermodynamic data are important and useful for chemical engineers, separation scientists, theoreticians, and thermodynamicists. Gas Liquid Chromatography (GLC) has become an established technique for the determination of reliable thermodynamic data for volatile nonmesomorphic solutes at “infinite dilution” in the mesophases and isotropic phases of liquid crystals [22-34].

In Henry’s law region, infinite dilution solute activity coefficients from GLC studies were confirmed to be in agreement with those obtained from static methods to better than 1% [36]. An example is

given in Table 4.1 in which the GLC data () for n-hexane in a hexadecane solvent are contrasted with those obtained by the static method [53,64]. Indeed, in this region GLC activity coefficients from GLC are preferred because of the speed and ease with which data can be obtained for a wide variety of solutes.

Table 4.1 : Comparison of GLC and Static Specific Retention Volumes, V_g^0 , for n-Hexane in a Hexadecane Solvent [36].

Temperature (°C)	V_g^0 (GLC)	V_g^0 (static)	V_g^0 (static) / V_g^0 (GLC)
20	493.1	492.0	1.0022
40	224.9	226.4	0.9934
60	116.4	115.6	1.006

Such thermodynamic data provide useful information about the effect of solute structure (size, shape, flexibility, polarizability, and polarity) on the solution process in ordered and disordered assemblies of rod-like molecules. They are also used to test statistical theories of binary mixtures and to investigate the effect of potential additives or impurities on nematic phase stability [24]. Such information is necessary since often impurities are intentionally added to nematogens to modify their viscosities and conductivities.

Whenever possible the thermodynamic results obtained for various nonmesomorphic solutes at infinite dilution in the p-cyano-p-n-alkylbenzoate homologous series of liquid crystals were interpreted in the light of an infinite dilution solution model proposed by Chow and Martire.

4.2 Experimental

4.2.1 Chemicals

Six liquid crystals were used in this study. These are the ethyl, n-propyl, n-butyl, n-pentyl, n-hexyl, and n-heptyl members of the p-cyanophenyl-p-n-alkylbenzoate homologous series. The first four are monotropic liquid crystals showing the nematic phase only on the cooling of their isotropic phase. The last two show a nematic phase on melting. These liquid crystals were obtained from Roche Chemicals and their physical properties are given in table 4.2. A purity in excess of 99.5 % (from GLC) and a water content less than 0.03 % (from the Karl Fischer method) are quoted by the manufacturer [38]. The high purity was reflected in the sharp melting and isotropic-to-nematic transition temperatures observed by DSC.

The solutes used, obtained from Fluka, were highly pure and were used as supplied. They fall into five categories namely normal

alkanes(C₆-C₉), branched alkanes, a hexadiene, a cyclic compound, and an aromatic compound. All the solutes were sufficiently volatile at the experimental temperatures used. Further purification was not carried out in this study since a high purity is not necessary. The physical properties of these solutes were obtained from Dreisbach's compilation [38] and are shown in Table 4.3.

Table 4.2 : Some Physical Properties of the Ethyl, n-Propyl, n-Butyl, n-Pentyl, n-Hexyl, n-Heptyl, and n-Octyl Members of p-Cyanophenyl-p-n-alkylbenzoate Homologous Series of Liquid Crystals.

Liquid Crystal	Melting Point (°C)	Clearing Point (°C)	Resistivity ($\Omega.m$)	Bulk Viscosity (mPa.s)	Dielectric constant (ϵ_{11})	Dielectric anisotropy (at 35°C)
P-Cyanophenyl p-ethylbenzoate	75.1	42.6	1×10^6	-----	-----	-----
p-Cyanophenyl-p-n-propylbenzoate	101.6	53.2	1×10^5	-----	-----	-----
p-Cyanophenyl-p-n-butylbenzoate	66.5	42.3	5×10^6	39	34.2	22.7
p-Cyanophenyl-p-n-pentylbenzoate	60.0	56.5	5×10^6	-----	29.0	18.5
p-Cyanophenyl-p-n-hexylbenzoate	44.5	48.0	5×10^6	42	30.6	21.2
p-Cyanophenyl-p-n-heptylbenzoate	43.5	56.5	5×10^6	46	28.5	20.7

Table 4.3 : Melting Points and Molar Masses of the Solutes Studied

Solute No.	Solute	MM(g mol ⁻¹)	Boiling Point (°C)
1	n-Hexane	86.17	68.70
2	n-Heptane	100.21	98.427
3	n-octane	114.20	125.665
4	n-Nonane	128.26	150.798
5	Benzene	78.11	80.10
6	C-1, 4-Hexadiene	82.140	65.00
7	1-Hexene	84.156	63.485
8	Cyclohexane	84.16	80.74
9	3-Methylpentane	86.17	63.28
10	2, 4- Dimethylhexane	114.224	109.103

4.2.2 Preparation of Columns

Since earlier studies show [23,25] that the most suitable support material is one with a moderate surface area, a Johns-Manville 60-80 mesh, acid washed, and DMCS treated Chromosorb W was used. The coating was done by dissolving a known mass of the liquid crystal under study in methylene chloride and placed in a round bottom flask. A preweighed solid support was added to the resulting solution. The flask was attached to a rotatory evaporator to remove the solvent. A water aspirator was used to reduce the pressure inside the flask. To remove any traces of the solvent, the packing material was kept in a vacuum dessicator for 48 hours.

Ashing of the packing was then done for three accurately weighed samples to calculate the weight percent of the liquid phase in the packing materials [39]. Empty copper columns (1.2 m in length and 0.25 in O.D.) were packed with the packing materials with the help of a vacuum pump. The weight of the packing materials was determined

from weight difference of the bottle containing the packing before and after the packing process.

To minimize the bleeding of the stationary phase from the column during the experiments, two columns with identical packings were used, for each of the liquid crystals used; One of the two columns was used for measurements on the isotropic phase of the liquid crystal solvent and the other was used for measurements in the nematic phase.

4.2.3 Apparatus and Procedure

The GC instrument used was a Perkin Elmer model 3920 modified for accurate temperature measurements to ± 0.03 °C and for precise control of inlet carrier gas (helium) pressure.. The column used was coiled to fit inside the GC oven. A thermal Conductivity Detector (TCD) was used as a detection device. Flow rates were measured at the detector outlet using a soap bubble flowmeter then corrected to

average flow rates through the columns. The inlet pressure was measured by a manometer. The gas flow rate used (~ 20 ml/min) gave reasonable elution times for all the solutes under study.

The temperature of the injection port and the thermal conductivity detector were kept at 200 °C and 150 °C respectively throughout the study. A 0-200 mv recorder (model D5217-15) was used to trace sample elution.

The volumes of the injected solute samples were kept below 0.05 μ l using a 10 μ l Hamilton syringe. Symmetrical peaks were obtained for different volumes of the injected solute samples indicating that the infinite dilution concentration (Henry's law region) was reached [40,41].

CHAPTER 5

GLC

RESULTS

CHAPTER 5

GLC RESULTS

5.1 Specific Retention Volume

The solute specific retention volume (V_g^0) is calculated from the peak maximum retention time using air as a reference peak. The specific retention volume expression was derived by Littlewood and co-workers [42]:

$$V_g^0 = \frac{F \cdot t_r}{g_i} \cdot \frac{p_o - p_w}{p_o} \cdot \frac{273.2}{T_r} \cdot J \quad (5.1)$$

where

$$J = \frac{3[(p_i/p_o)^2 - 1]}{2[(p_i/p_o)^3 - 1]}$$

T_f = ambient temperature (K)

p_i = column inlet pressure (absolute)

p_o = column outlet pressure

p_w = saturated vapor pressure of water at T_f

F = carrier gas flow rate($\text{cm}^3/\text{min.}$)

t_r = peak maximum retention time (minutes)

g_l = weight of stationary phase in column (grams)

V_g^o = solute specific retention volume (cm^3 carrier gas/gm. liquid
crystal)

For the six liquid crystals used specific retention volumes were obtained at four temperatures in both the nematic and isotropic phases of the liquid crystal stationary phases used. To ensure that these temperatures are far from the isotropic to nematic transition temperatures of these liquid crystals as reported by the manufacturer [37], all measurements were done at about 5 °C above or below the

transition temperatures. The results listed in Tables (A1 - A11) in Appendix A reflect duplicate experimental runs. The closeness of the duplicate runs and previous experience with such measurements [49,50] indicate that the percent standard deviation in the V_g^0 values is well below 1 %. The results of linear least squares fits of $\ln V_g^0$ versus $10^3/T$ are also reported in Appendix A (Tables A12- A22).

5.2 Solute Activity Coefficients

The infinite dilution solute activity coefficient γ_2^∞ corrected for gas phase nonideality may be calculated from equation (5.2) [42]

$$\ln \gamma_2^\infty = \ln(273.2R/M_1 p_2^\circ V_g^\circ) - (B_{22} p_2^\circ/RT) \quad (5.2)$$

where

M_1 = solvent molar mass

p_2° = saturated vapor pressure of the pure solute (in torr)

B_{22} = second virial coefficient of the pure solute

T= the experimental absolute temperature

The second term on the right hand side of equation (5.2) corrects for the gas phase nonideality of the solute. Under our experimental conditions this term is negligible thus equation (5.2) reduces to:

$$\gamma_2^\infty = \frac{1.704 \times 10^7}{M p_2^\circ V_g^\circ} \quad (5.3)$$

In appendix C we outline how equation (5.3) is reached.

The solute vapor pressures are calculated from the Antoine equation using the constants from Dreisbach's compilation [38]. The infinite dilution solute activity coefficients calculated from equation (5.3) are reported for all the studied systems in Appendix B (Tables B1- B11). Taking into account the errors introduced by all factors in equation (5.3) the percent standard deviation in γ_2^∞ is estimated to be less than 1 % .

5.3 Partial Molar Excess Enthalpies and Entropies

From Thermodynamics:

$$\ln \gamma_2^\infty = \bar{G}^\circ/RT = \bar{H}^\circ/RT - \bar{S}^\circ/R \quad (5.4)$$

where:

\bar{G}° = the infinite dilution solute partial molar excess free energy

\bar{H}° = the infinite dilution solute partial molar excess enthalpy

\bar{S}° = the infinite dilution solute partial molar excess entropy

A linear least square fits of $\ln \gamma_2^\infty$ against $1/T$ gives \bar{H}° and \bar{S}° from the slope and the intercept respectively. The good linear correlation coefficients (all in excess of 0.99) obtained and the small standard deviations for the slopes and the intercepts reflect the quality of the data. Representative examples of $\ln \gamma_2^\infty$ versus $10^3/T$ plots are given for n-alkanes (solutes 1-4) and for benzene, c-1,4-hexadiene, and 1-hexene (solutes 5-7) are shown in Figures 5.1 - 5.12.

5.4 Partial molar Enthalpies and Entropies of Solution

\bar{H}° and \bar{S}° represent the molar values for the hypothetical transfer of a solute from an ideal solution to the actual solution, both being at the same temperature, pressure and composition. If we consider the hypothetical transfer of solute from an ideal gaseous mixture to the actual solution (again both being at the same temperature, pressure and composition), the corresponding quantities become $\Delta\bar{H}_{\text{sol}}$ and $\Delta\bar{S}_{\text{sol}}$, the partial molar enthalpy and entropy of solution, respectively. $\Delta\bar{H}_{\text{sol}}$ and $\Delta\bar{S}_{\text{sol}}$ are related to \bar{H}° and \bar{S}° through [24]

$$\Delta\bar{H}_{\text{sol}} = \bar{H}^\circ - \Delta\bar{H}_{\text{vap}} \quad (5.5)$$

and

$$\Delta\bar{S}_{\text{sol}} = \bar{S}^\circ - \Delta\bar{H}_{\text{vap}}/T \quad (5.6)$$

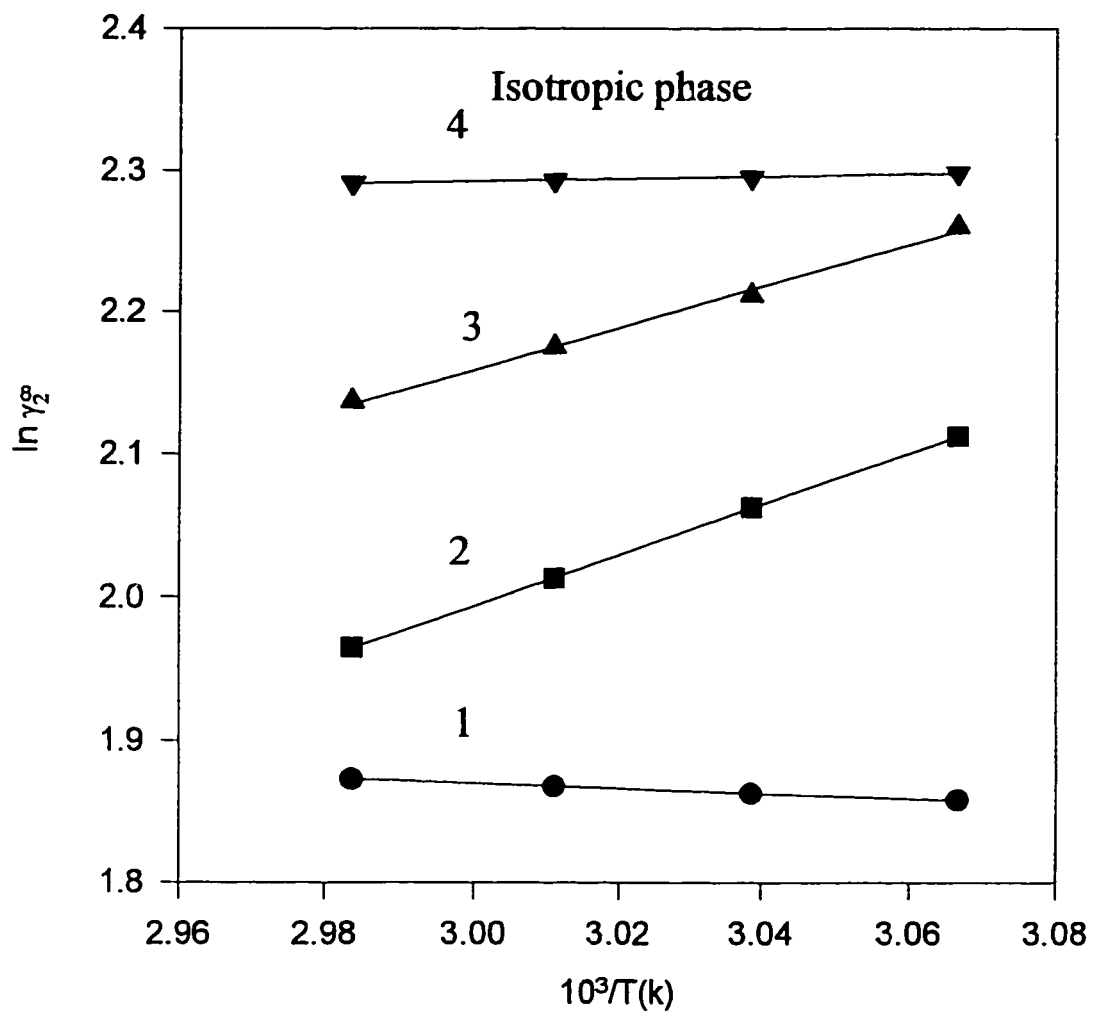


Figure 5.1: $\ln \gamma_2^\circ$ Versus $10^3/T$ for n-alkanes in the Isotropic Phase of p-Cyanophenyl-p-ethylbenzoate. The Numbering of the Solutes Follows that Given in Table 4.3

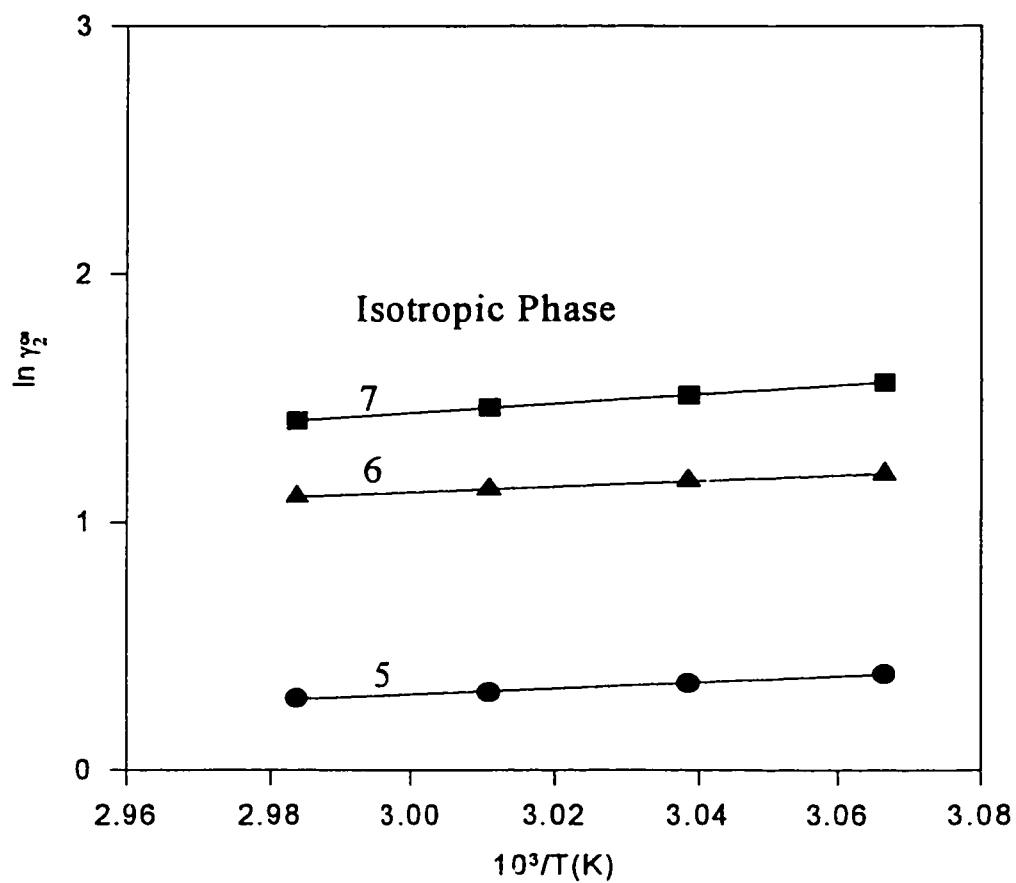


Figure 5.2 $\ln \gamma_2^\circ$ Versus $10^3/T$ for Benzene (5), c-1,4-Hexadiene (6) and 1-Hexene (7) in the Isotropic Phase of p-Cyanophenyl-p-ethylbenzoate.

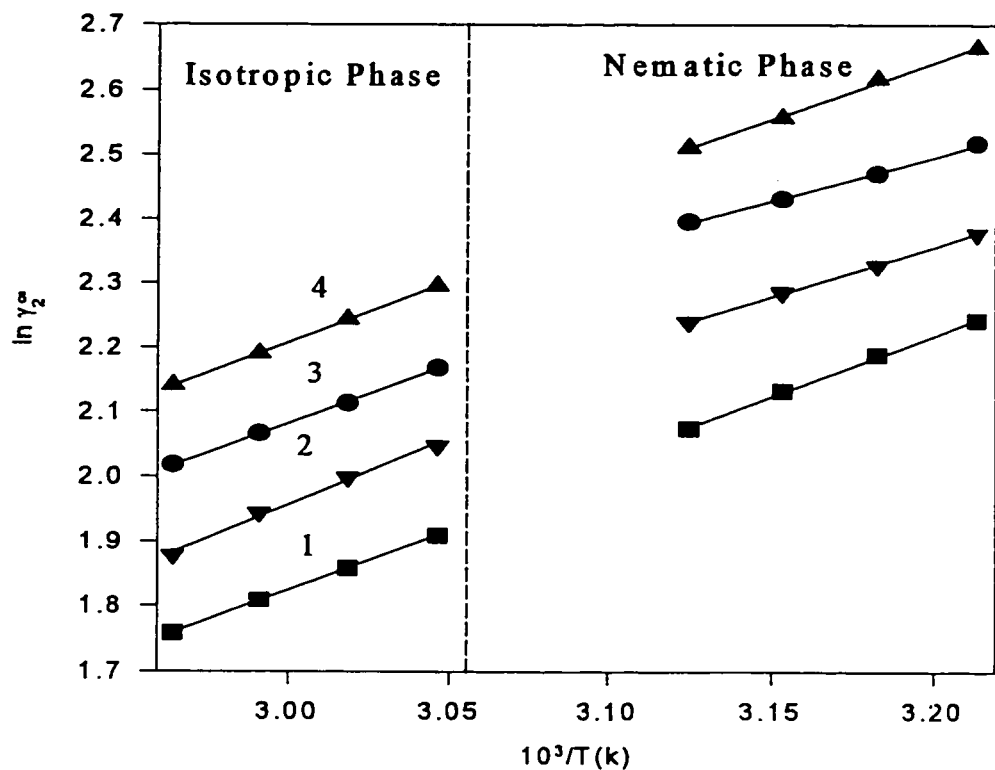


Figure 5.3 : $\ln \gamma_2^\infty$ Versus $10^3/T$ for n-Alkanes in the Isotropic and Nematic Phases of p-Cyanophenyl-p-n-propylbenzoate. The Numbering of the Solutes Follows that Given in Table 4.3. The Dashed Vertical Line is Located at the Isotropic-to-Nematic Transition Temperature.

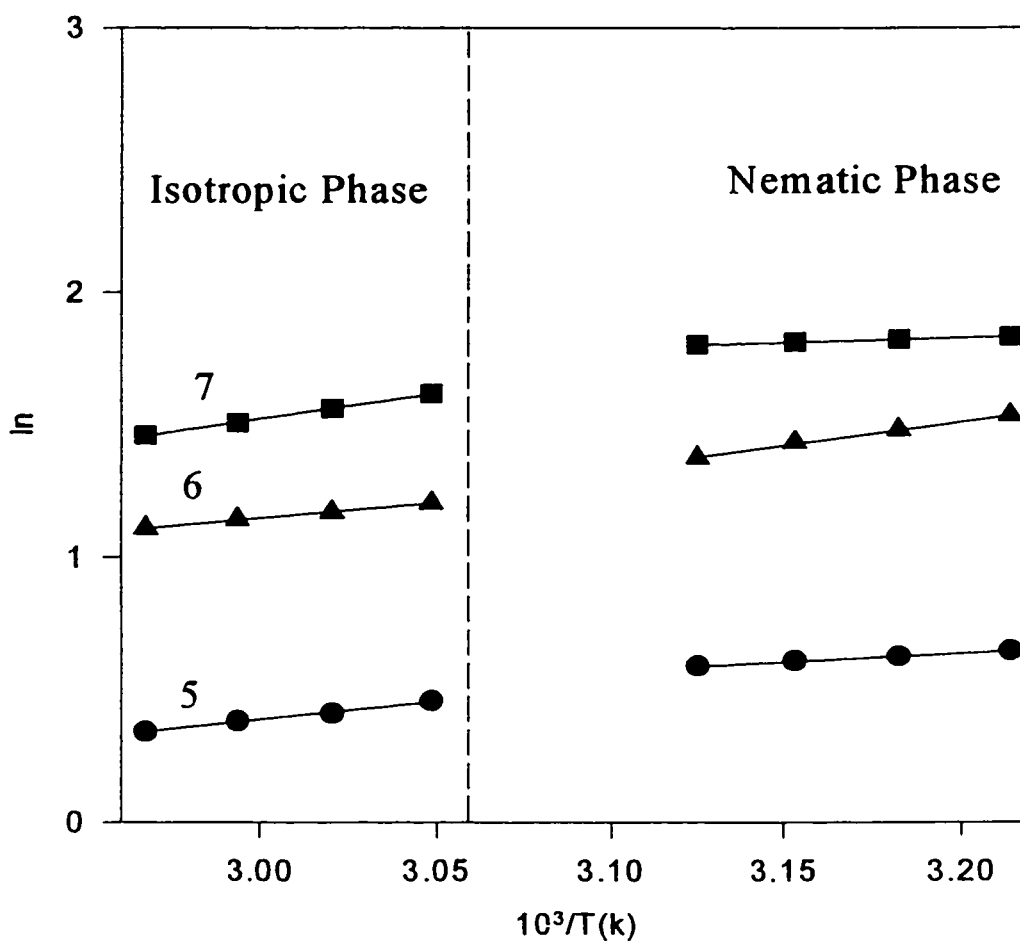


Figure 5.4 : $\ln \gamma_2^\infty$ Versus $10^3/T$ for Benzene (5), c-1,4- Hexadiene (6), and 1- Hexene in the Isotropic and Nematic Phases of Cyanophenyl-p-n-propylbenzoate. The Dashed Vertical Line is Located at the Isotropic-to-Nematic Transition Temperature.

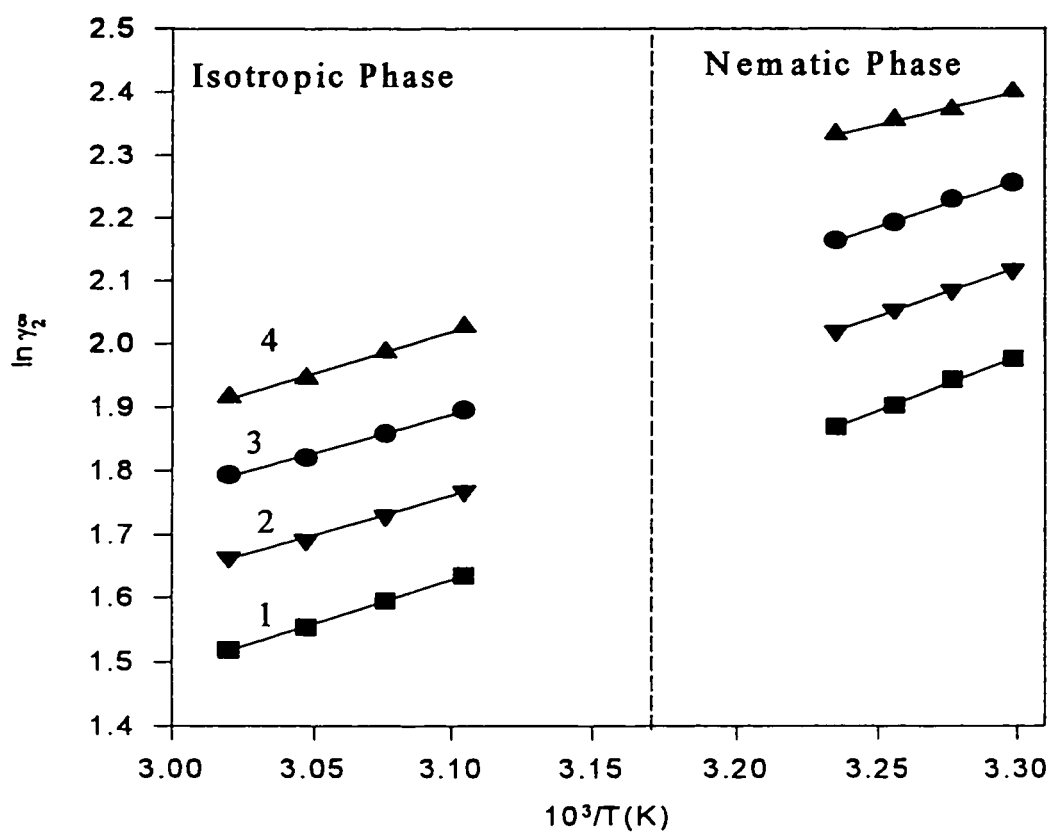


Figure 5.5 : $\ln \gamma_2^0$ Versus $10^3/T$ for n- alkanes in the Isotropic and Nematic Phases of Cyanophenyl-p-n-butylbenzoate. The Numbering of the Solutes Follows that Given in Table 4.3. The Dashed Vertical Line is Located at the Isotropic-to-Nematic Transition Temperature.

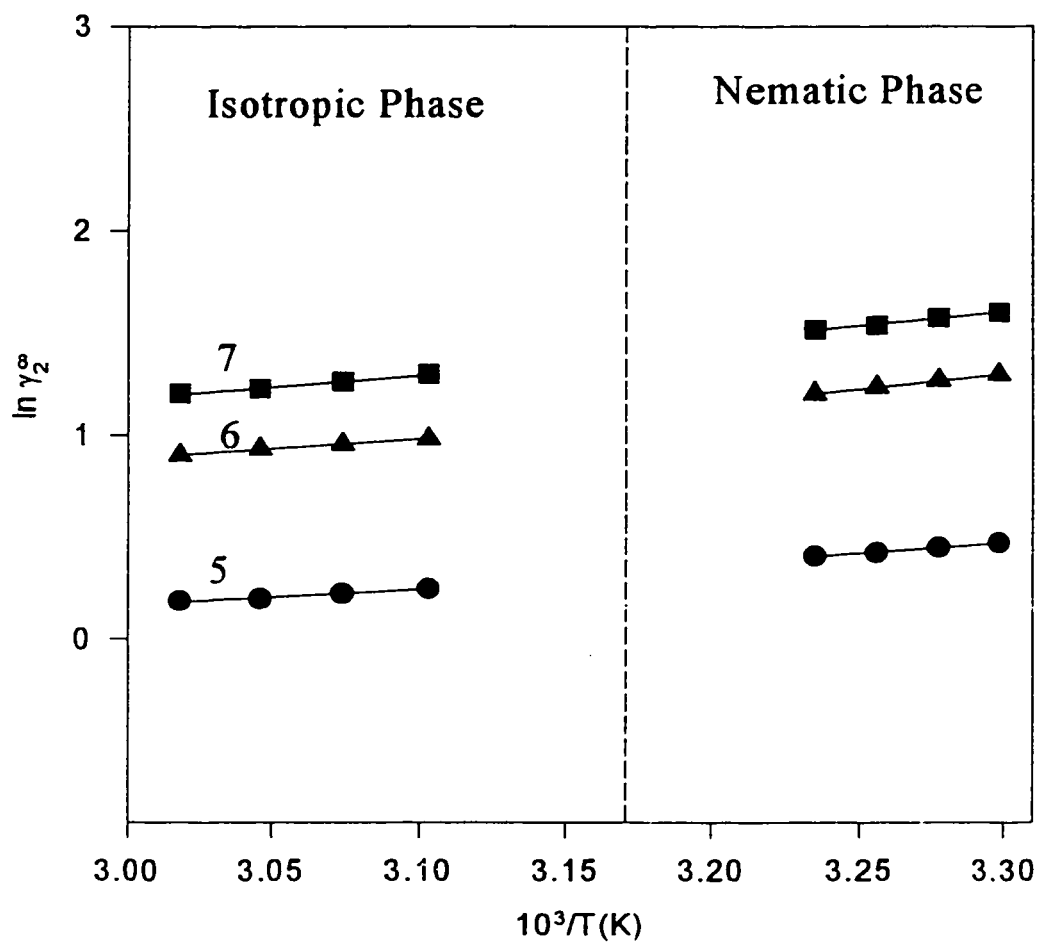


Figure 5.6 : $\ln \gamma_2^\infty$ Versus $10^3/T$ for Benzene (5), c-1,4-Hexadiene (6) and 1-Hexene (7) in the Isotropic and Nematic Phases of p-Cyanophenyl-p-n-butylbenzoate. The Dashed Vertical Line is Located at the Isotropic-to-Nematic Transition Temperature.

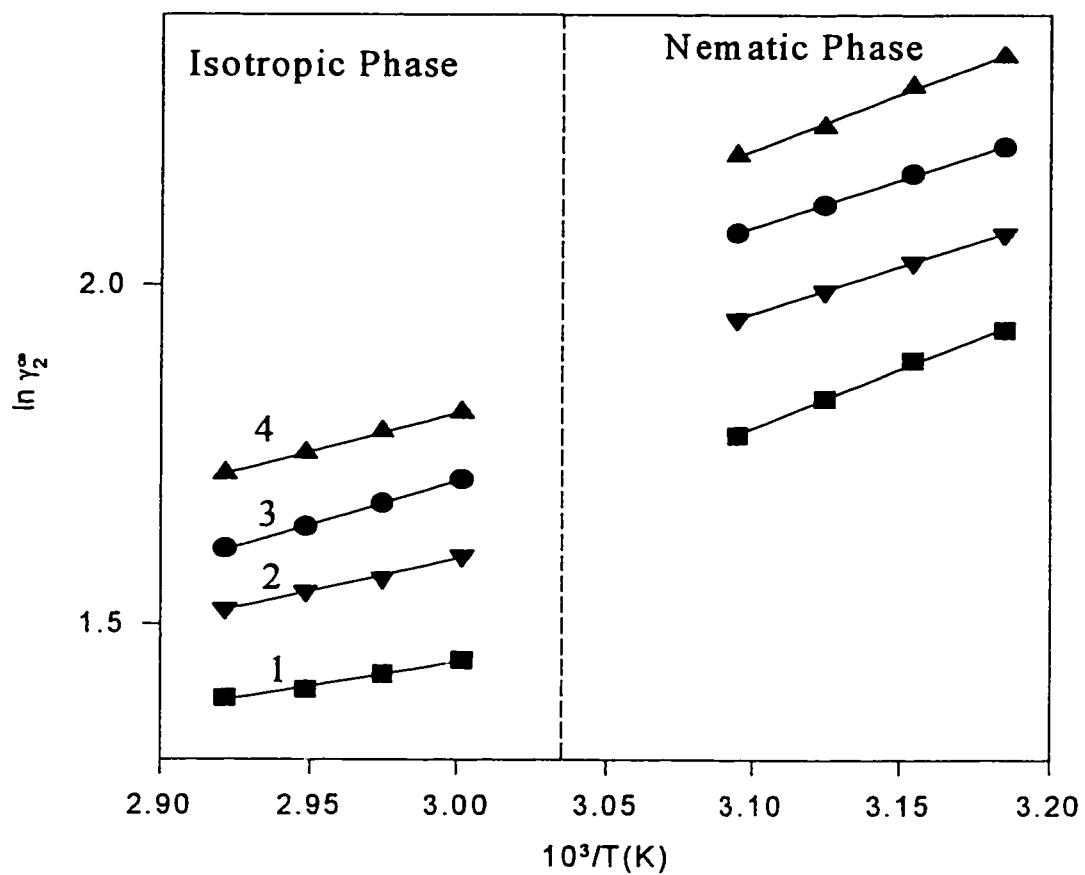


Figure 5.7: $\ln \gamma_2^\infty$ Versus $10^3/T$ for n- alkanes in the Isotropic and Nematic Phases of p-Cyanophenyl-p-n-pentylbenzoate. The Numbering of the Solutes Follows that Given in Tables 4.3. The Dashed Vertical Line is Located at the Isotropic-to-Nematic Transition Temperature.

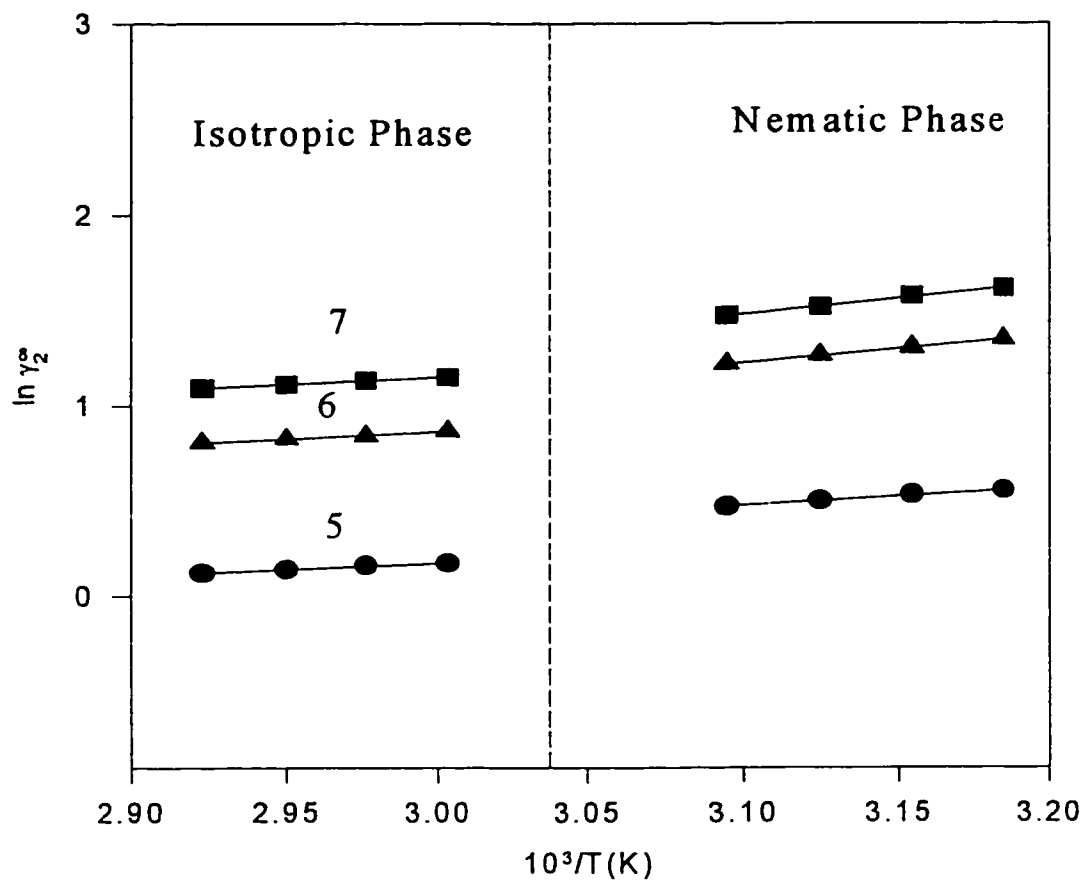


Figure 5.8 : $\ln \gamma_2^\infty$ Versus $10^3/T$ for Benzene (5), c-1,4-Hexadiene (6) and 1-Hexene (7) in the Isotropic and Nematic Phases of p-Cyanophenyl-p-n-pentylbenzoate. The Dashed Vertical Line is Located at the Isotropic-to-Nematic Transition Temperature.

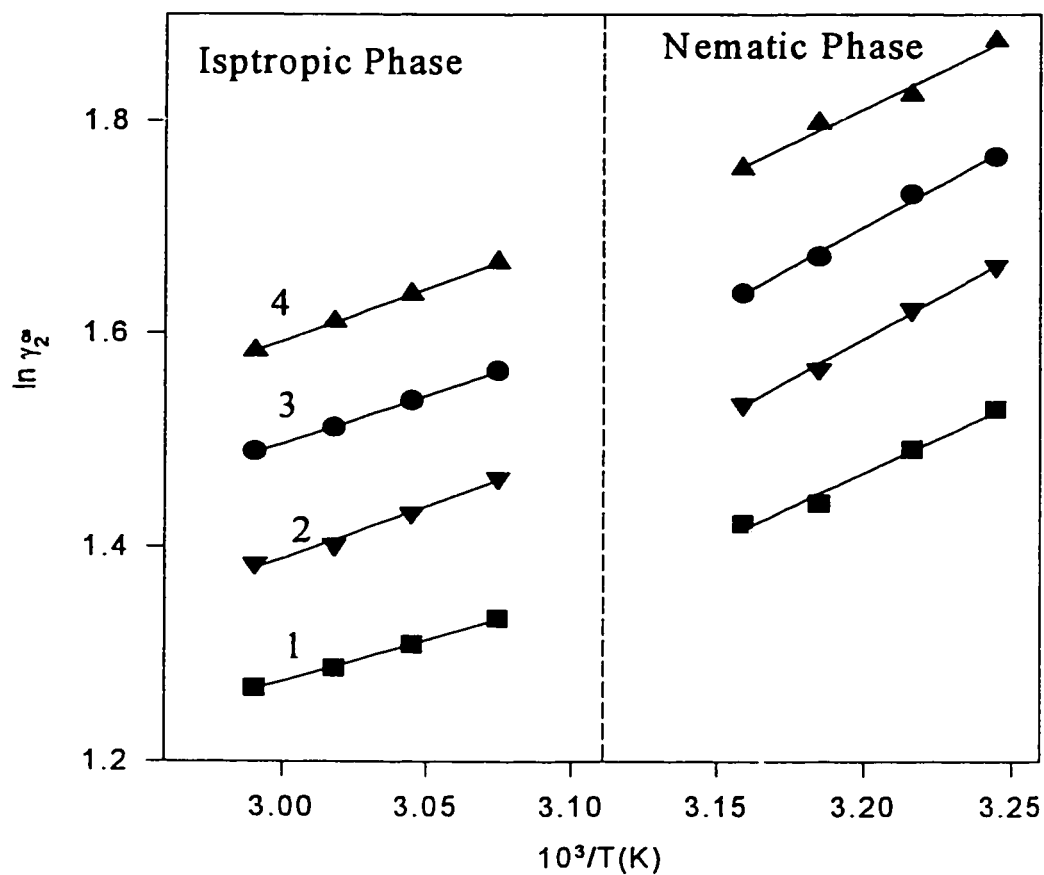


Figure 5.9: $\ln \gamma_2^\infty$ Versus $10^3/T$ for n- alkanes in Isotropic and Nematic Phases of p-Cyanophenyl-p-n-hexylbenzoate. The Numbering of the Solutes Follows That Given In Table 4.3. The Dashed Vertical Line is Located at the Isotropic-to-Nematic Transition Temperature.

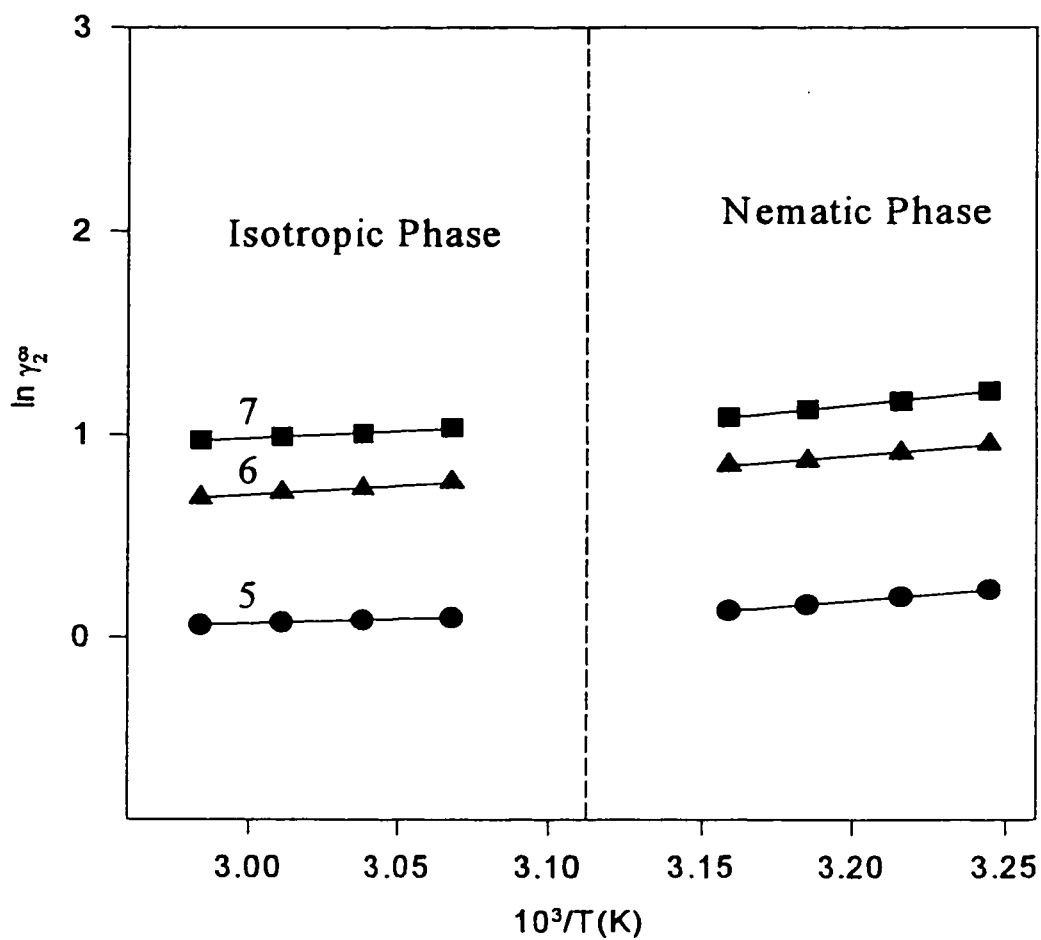


Figure 5.10: $\ln \gamma_2^\infty$ Versus $10^3/T$ for Benzene (5), c-1,4-Hexadiene (6), and 1-Hexene (7) in the Isotropic and Nematic Phases of p-Cyanophenyl-p-n-hexylbenzoate. The Dashed Vertical Line is Located at the Isotropic-to-Nematic Transition Temperature.

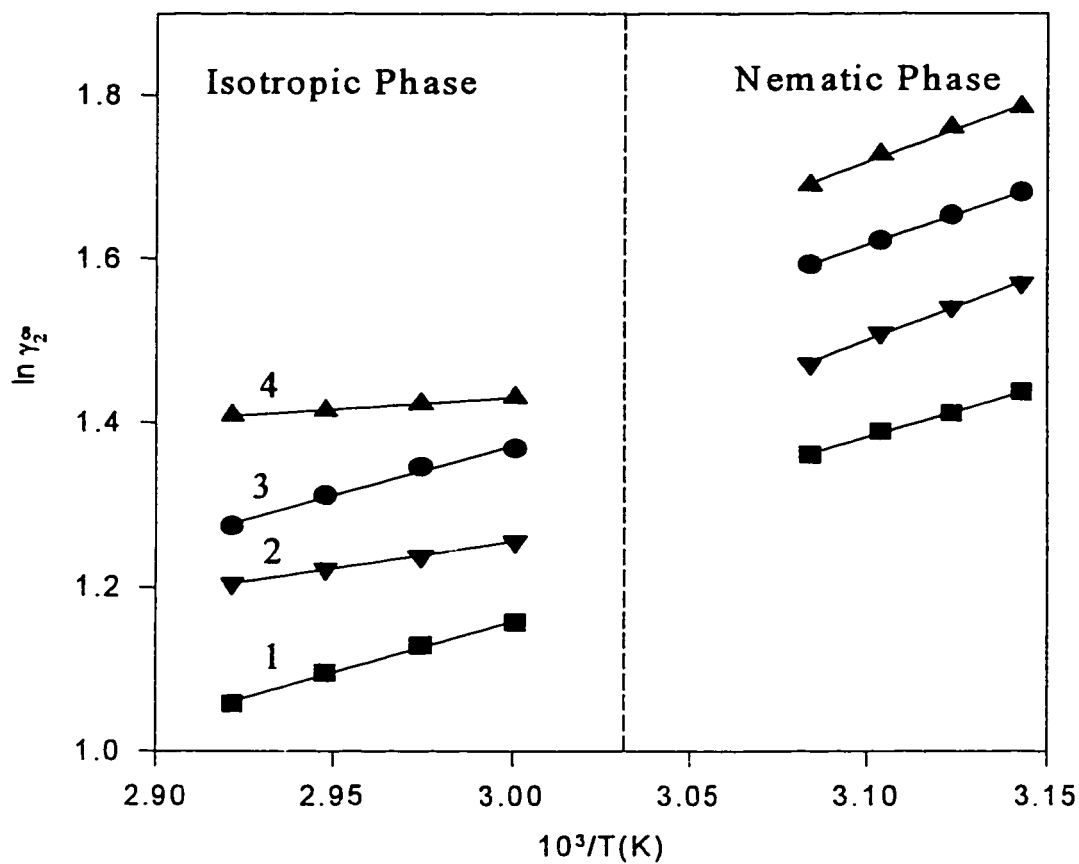


Figure 5.11 : $\ln \gamma_2^\infty$ Versus $10^3/T$ for n- alkanes in the Isotropic and Nematic Phases of p-Cyanophenyl-p-n-heptylbenzoate. The Numbering of the Solutes Follows that Given in Table 4.3. The Dashed Vertical Line is Located at the Isotropic-to-Nematic Transition Temperature.

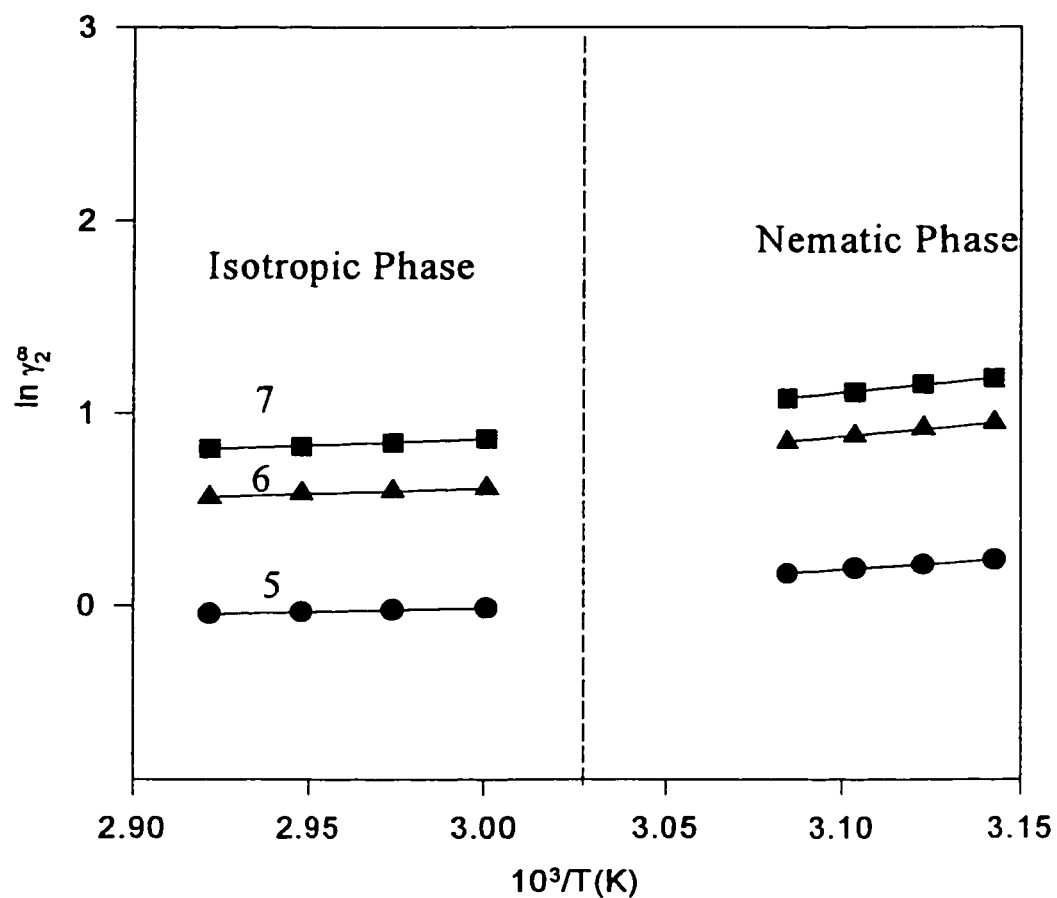


Figure 5.12: $\ln \gamma_2^\infty$ Versus $10^3/T$ for Benzene (5), c-1,4-Hexadiene (6), and 1-Hexene (7) in the Isotropic and Nematic Phases of p-Cyanophenyl-p-n-heptylbenzoate. The Dashed Vertical Line is Located at the Isotropic-to-Nematic Transition Temperature.

where $\Delta \bar{H}_{v,sp}$ is the molar enthalpy of vaporization of the pure solute. \bar{H}° and \bar{S}° contain solute - solute interaction energy (through interchange energy) while $\Delta \bar{H}_{s,oi}$ and $\Delta \bar{S}_{s,oi}$ reflect solvent-solvent and solute-solvent interaction terms only. Values of $\Delta \bar{H}_{s,oi}$ and $\Delta \bar{S}_{s,oi}$ are reported in Tables (5.1 - 5.11) at 60 °C and 40 °C for all solutes in the isotropic and nematic phases of the six liquid crystals studied. The $\Delta \bar{H}_{v,sp}$ values used in the computations were obtained from Dreisbach's compilation [38]. The standard deviation of $\Delta \bar{H}_{s,oi}$ and $\Delta \bar{S}_{s,oi}$ are essentially those for \bar{H}° and \bar{S}° (given in Tables 5.1-5.11) because $\Delta \bar{H}_{v,sp}$ is known to within a few cal/mol.

Table 5.1 : Thermodynamic Data for Solutes in Isotropic p- Cyanophenyl
p-ethylbenzoate.

Solute	$\bar{H}^\circ /(\text{kJ/mol})$	$\bar{S}^\circ /(\text{J/ mol K})$	$\Delta\bar{H}_{\text{sol}}$ (60.0°C)	$-\Delta\bar{S}_{\text{sol}}$ (60.0 °C)
1	-1.52 ± 0.03	-20.09 ± 0.09	30.92	68.17
2	14.82 ± 0.06	27.89 ± 0.18	19.54	131.05
3	12.20 ± 0.53	18.66 ± 11.59	29.20	142.93
4	0.73 ± 0.06	-16.86 ± 0.18	43.64	116.33
5	10.02 ± 0.67	27.53 ± 2.04	21.87	123.26
6	9.36 ± 0.28	18.78 ± 0.84	20.47	108.32
7	15.34 ± 0.08	34.05 ± 0.25	13.27	119.93
8	12.75 ± 0.68	25.89 ± 2.06	18.49	119.66
9	13.17 ± 0.77	24.45 ± 2.31	15.10	109.31
10	13.37 ± 0.16	21.84 ± 0.50	22.52	129.58

Table 5.2: Thermodynamic Data for Solutes in the Isotropic Phase of p-Cyanophenyl-p-n-propylbenzoate.

Solute	\bar{H}° /(kJ/mol)	\bar{S}° /(J/mol K)	$\Delta\bar{H}_{\text{sol}}$ (60.0°C)	$-\Delta\bar{S}_{\text{sol}}$ (60.0 °C)
1	15.31 ± 0.08	30.70 ± 0.25	14.10	118.96
2	17.23 ± 0.10	35.36 ± 3.01	17.14	138.52
3	15.28 ± 0.34	28.49 ± 1.03	26.12	152.76
4	15.90 ± 0.14	29.28 ± 0.43	28.48	162.47
5	11.56 ± 0.56	31.49 ± 1.67	20.33	127.22
6	9.51 ± 0.28	19.04 ± 0.83	20.32	108.59
7	16.26 ± 0.43	36.18 ± 1.30	12.35	122.05
8	15.21 ± 0.77	33.61 ± 2.32	16.02	127.38
9	16.53 ± 0.32	34.22 ± 0.96	11.74	119.08
10	17.25 ± 1.04	33.87 ± 3.13	18.64	141.62

Table 5.3 : Thermodynamic Data for Solutes in the Nematic phase of p-Cyanophenyl-p-n-propylbenzoate.

Solute	\bar{H}° /(kJ/mol)	\bar{S}° /(J/ mol K)	$\Delta\bar{H}_{sol}$ (40.0°C)	$-\Delta\bar{S}_{sol}$ (40.0 °C)
1	15.74 ± 0.43	31.92 ± 1.36	14.93	129.85
2	12.83 ± 0.20	21.47 ± 0.65	22.92	135.66
3	11.35 ± 0.30	15.54 ± 0.96	31.47	152.26
4	14.56 ± 0.58	24.62 ± 1.83	31.50	171.70
5	5.29 ± 0.16	11.64 ± 0.49	27.72	117.05
6	14.72 ± 0.46	34.57 ± 1.46	16.33	133.73
7	2.92 ± 0.09	-5.85 ± 0.28	26.89	89.35
8	9.22 ± 0.63	13.91 ± 1.99	23.14	117.27
9	13.67 ± 0.40	25.15 ± 1.28	15.78	119.19
10	11.45 ± 0.49	14.57 ± 1.56	25.73	133.28

Table 5.4 : Thermodynamic Data for Solutes in the Isotropic Phase of p-Cyanophenyl-p-n-butylbenzoate.

Solute	\bar{H}° /(kJ/mol)	\bar{S}° /(J/ mol K)	$\Delta\bar{H}_{sol}$ (60.0°C)	$-\Delta\bar{S}_{sol}$ (60.0 °C)
1	11.50 ± 0.17	22.11 ± 0.525	17.904	110.37
2	10.39 ± 0.44	17.56 ± 1.36	23.98	120.71
3	10.21 ± 0.46	15.94 ± 1.42	31.19	140.21
4	11.02 ± 0.51	17.38 ± 1.56	33.35	150.57
5	6.13 ± 0.58	17.15 ± 1.77	25.76	112.87
6	7.99 ± 0.46	16.77 ± 1.41	21.84	106.32
7	9.20 ± 0.39	17.95 ± 1.18	19.41	103.82
8	11.20 ± 0.09	24.17 ± 0.28	20.03	117.94
9	13.53 ± 0.04	28.32 ± 0.13	14.74	113.18
10	16.28 ± 0.59	33.98 ± 0.98	19.61	141.73

Table 5.5 : Thermodynamic Data for Solutes in the Nematic Phase of p-Cyanophenyl-p-n-butylbenzoate.

Solute	\bar{H}° /(kJ/mol)	\bar{S}° /(J/mol K)	$\Delta\bar{H}_{\text{tot}}$ (40.0°C)	$-\Delta\bar{S}_{\text{tot}}$ (40.0 °C)
1	13.97 ± 0.40	29.64 ± 1.30	16.70	127.57
2	12.67 ± 0.28	24.19 ± 0.90	23.09	138.38
3	12.25 ± 0.58	21.64 ± 1.90	30.56	158.36
4	8.53 ± 0.58	8.19 ± 1.89	37.53	155.27
5	8.65 ± 0.54	24.63 ± 1.75	24.36	130.04
6	12.20 ± 0.27	24.13 ± 0.90	23.09	138.38
7	11.26 ± 0.92	23.88 ± 3.00	18.55	119.08
8	13.29 ± 0.09	30.09 ± 0.28	19.08	133.45
9	10.96 ± 0.17	19.65 ± 0.57	18.49	113.70
10	16.72 ± 0.07	35.16 ± 0.24	20.46	153.87

Table 5.6 : Thermodynamic Data for Solutes in the Isotropic Phase of p-Cyanophenyl-p- n-pentylbenzoate.

Solute	\bar{H}° /(kJ/mol)	\bar{S}° /(J/ mol K)	$\Delta\bar{H}_{sol}$ (60.0°C)	$-\Delta\bar{S}_{sol}$ (60.0 °C)
1	5.98 ±0.48	5.92 ±1.44	23.42	94.18
2	8.04 ± 0.54	10.84 ± 1.60	26.33	114.00
3	10.56 ±0.12	17.46 ± 0.37	30.84	141.73
4	9.47 ± 0.20	13.36 ±0.60	34.90	146.54
5	5.37 ± 0.34	14.55 ± 1.00	26.52	110.28
6	6.34 ±0.43	11.74 ± 1.27	23.50	101.28
7	6.00 ± 0.11	8.34 ± 0.32	22.61	94.21
8	12.01 ± 0.10	26.75 ± 0.32	19.23	120.52
9	11.75 ± 0.08	23.16 ± 0.25	16.52	108.02
10	9.03 ± 0.22	12.46 ± 0.64	26.86	120.21

Table 5.7 : Thermodynamic Data for Solutes in the Nematic Phase of p-Cyanophenyl-p-n-pentylbenzoate.

Solute	\bar{H}° /(kJ/mol)	\bar{S}° /(J/mol K)	$\Delta\bar{H}_{\text{sol}}$ (40.0°C)	$-\Delta\bar{S}_{\text{sol}}$ (40.0 °C)
1	14.61 ± 0.53	30.41 ± 1.65	16.06	128.34
2	11.72 ± 0.09	20.04 ± 0.27	24.04	134.23
3	11.89 ± 0.29	19.52 ± 0.92	30.93	156.24
4	13.90 ± 0.66	24.80 ± 2.09	32.16	171.88
5	7.77 ± 0.34	20.18 ± 1.08	25.24	125.60
6	11.80 ± 0.09	26.42 ± 0.46	19.25	125.58
7	13.61 ± 0.72	29.91 ± 2.25	16.20	125.11
8	12.60 ± 0.29	26.58 ± 0.90	16.26	119.70
9	13.19 ± 0.44	25.66 ± 1.39	16.26	119.70
10	16.90 ± 0.31	34.21 ± 0.96	20.27	152.92

Table 5.8 : Thermodynamic Data for Solutes in the Isotropic Phase of p-Cyanophenyl-p-n-hexylbenzoate.

Solute	\bar{H}° /(kJ/mol)	\bar{S}° /(J/ mol K)	$\Delta\bar{H}_{\text{sol}}$ (60.0°C)	$-\Delta\bar{S}_{\text{sol}}$ (60.0 °C)
1	6.42 ± 0.18	8.62 ± 0.55	22.98	96.88
2	8.07 ± 0.63	12.62 ± 1.92	26.29	115.77
3	7.49 ± 0.14	9.97 ± 0.42	33.91	134.24
4	8.282 ± 0.07	11.55 ± 0.20	36.09	144.74
5	3.41 ± 0.04	9.69 ± 0.13	28.48	105.41
6	7.49 ± 0.37	16.66 ± 1.11	22.34	106.21
7	5.95 ± 0.56	9.68 ± 1.69	22.66	95.552
8	9.10 ± 0.30	19.59 ± 0.90	22.14	113.36
9	9.45 ± 0.14	18.05 ± 0.42	18.82	102.89
10	10.92 ± 0.11	20.09 ± 0.34	24.97	127.83

Table 5.9 : Thermodynamic Data for Solutes in the Nematic Phase of p-Cyanophenyl-p-n-hexylbenzoate.

Solute	\bar{H}° /(kJ/mol)	\bar{S}° /(J/ mol K)	$\Delta\bar{H}_{sol}$ (40.0°C)	$-\Delta\bar{S}_{sol}$ (40.0 °C)
1	10.82 ± 1.02	22.42 ± 3.26	19.84	120.34
2	12.87 ± 0.59	27.93 ± 1.88	22.88	142.12
3	12.84 ± 0.78	26.93 ± 2.48	29.98	163.65
4	11.09 ± 1.07	20.42 ± 3.42	34.96	167.49
5	10.15 ± 0.18	31.01 ± 0.58	22.86	136.42
6	10.05 ± 0.79	24.74 ± 2.53	21.00	123.90
7	12.53 ± 0.37	30.57 ± 1.19	17.28	125.76
8	15.12 ± 0.41	38.79 ± 1.32	17.24	142.15
9	13.07 ± 0.26	29.53 ± 0.83	16.38	123.58
10	17.06 ± 0.92	39.40 ± 12.96	20.12	158.10

Table 5.10 : Thermodynamic Data for Solutes in the Isotropic Phase of p-Cyanophenyl-p-n-heptylbenzoate.

Solute	\bar{H}° /(kJ/mol)	\bar{S}° /(J/ mol K)	$\Delta\bar{H}_{sol}$ (60.0°C)	$-\Delta\bar{S}_{sol}$ (60.0 °C)
1	10.46 ± 0.50	21.78 ± 1.46	18.94	110.01
2	5.30 ± 0.09	5.46 ± 0.27	29.07	108.62
3	10.07 ± 0.78	18.80 ± 2.31	31.33	143.07
4	2.37 ± 0.06	-4.78 ± 0.19	42.00	128.41
5	3.03 ± 0.20	9.22 ± 0.58	28.86	104.94
6	4.84 ± 0.41	9.47 ± 1.21	25.00	99.02
7	5.42 ± 0.34	9.07 ± 1.15	23.19	94.94
8	6.35 ± 0.34	12.40 ± 1.02	24.89	106.17
9	7.43 ± 0.23	12.94 ± 0.68	20.84	97.80
10	9.20 ± 0.85	15.838 ± 2.514	26.70	123.58

Table 5.11 : Thermodynamic Data for Solutes in the Nematic Phase of p-Cyanophenyl-p-n-heptylbenzoate.

Solute	\bar{H}° /(kJ/mol)	\bar{S}° /(J/ mol K)	$\Delta\bar{H}_{sol}$ (40.0°C)	$-\Delta\bar{S}_{sol}$ (40.0 °C)
1	10.81 ± 0.32	22.01 ± 1.01	19.86	119.94
2	13.93 ± 0.56	30.71 ± 1.74	21.83	144.90
3	12.60 ± 0.17	26.61 ± 0.54	30.216	162.33
4	13.62 ± 0.88	27.93 ± 2.73	32.44	175.00
5	9.99 ± 0.56	29.44 ± 1.76	23.02	134.85
6	14.40 ± 0.57	37.34 ± 1.78	16.65	136.50
7	15.01 ± 0.62	37.37 ± 1.94	14.80	132.56
8	15.48 ± 0.23	38.94 ± 0.72	16.89	142.30
9	15.66 ± 0.30	36.95 ± 0.95	13.79	131.00
10	17.60 ± 0.85	40.26 ± 2.66	19.58	158.99

5.6 Odd-Even Effect

One of the objectives of our study was the examination of the effect that the tail length of the liquid crystal molecule may have on the value of the infinite dilution solute activity coefficient. Since liquid crystals of different tail lengths would have different isotropic-to-nematic transition temperatures, an extrapolation of the data in each of the nematic and isotropic phases of different liquid crystals to a common reference hypothetical transition temperature is needed. For our homologous series we found that a 50 °C is suitable for our analysis since we verified that the same trends would be obtained anywhere between 40 °C and 60 °C. The extrapolation of data in the nematic and isotropic for all the systems studied to 50 °C allowed the evaluation of γ_N° and γ_I° respectively for all the solutes. The \cdot notation is reserved for extrapolated γ_2^∞ values. In Figure 5.13 the variation of γ_N° and γ_I° with the number of carbon atoms in the tail of the liquid crystal molecules is given for n-hexane, n-heptane, n-

octane, and n-nonane (solutes 1-4), and in Figures 5.14 and 5.15 give the same information for the remaining solutes. Figures 5.13 and 5.14 show that γ_N^* and γ_I^* values for all solutes exhibit an odd-even effect with respect to the number of carbon atoms on the alkyl tails of the liquid crystal molecules. This odd-even effect tends to be less drastic as the tail length increases. In addition these figures reflect differences between γ_N^* and γ_I^* for the same solute/solvent system and the variation of γ_N^* and γ_I^* for different solutes in the same solvent with solute structure.

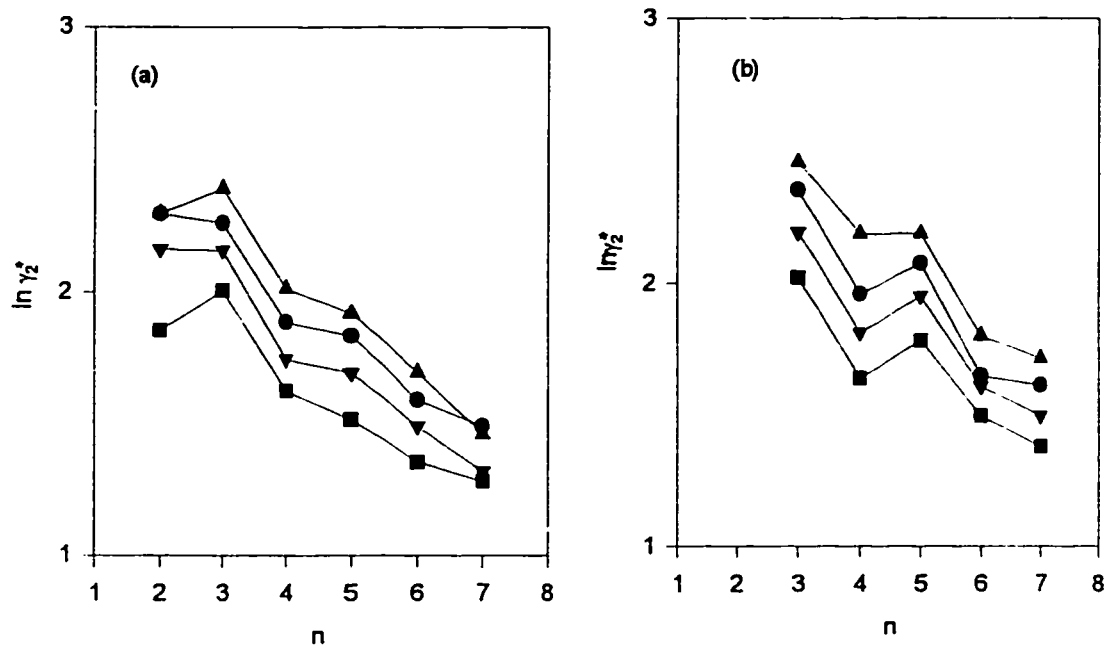


Figure 5.13 : Reduced Activity Coefficients for n-Alkanes (solutes 1-4) vs. n (the number of Carbon Atoms on the Tails of the Liquid Crystals) in (a) the Isotropic Phase and (b) the Nematic Phase.

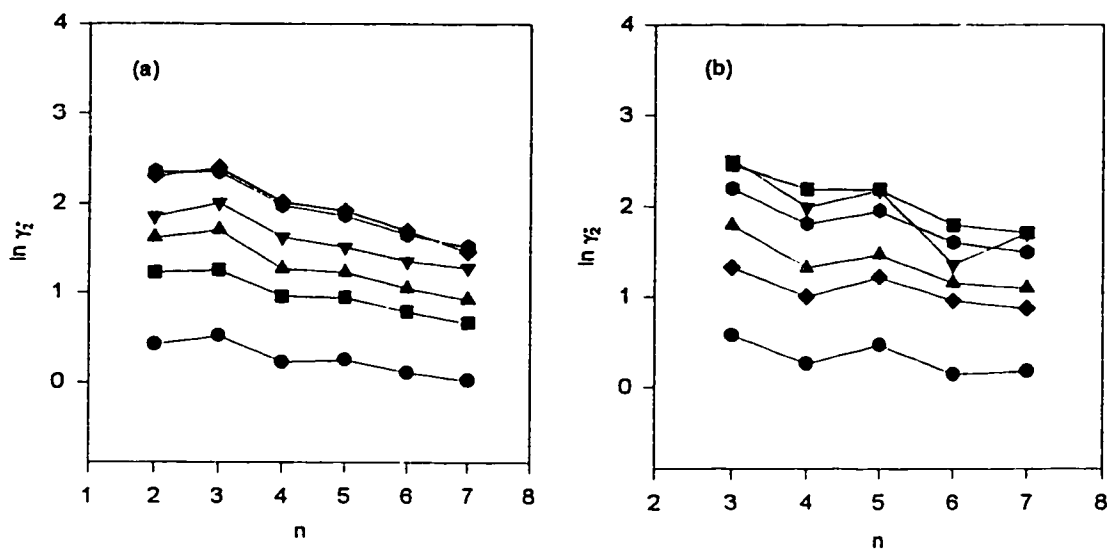


Figure 5.14 : Reduced Activity Coefficients for Solutes (5-10) vs. n (the Number of Carbon Atoms on the Tails of the Liquid Crystals) in (a) the Isotropic Phase and (b) the Nematic Phase.

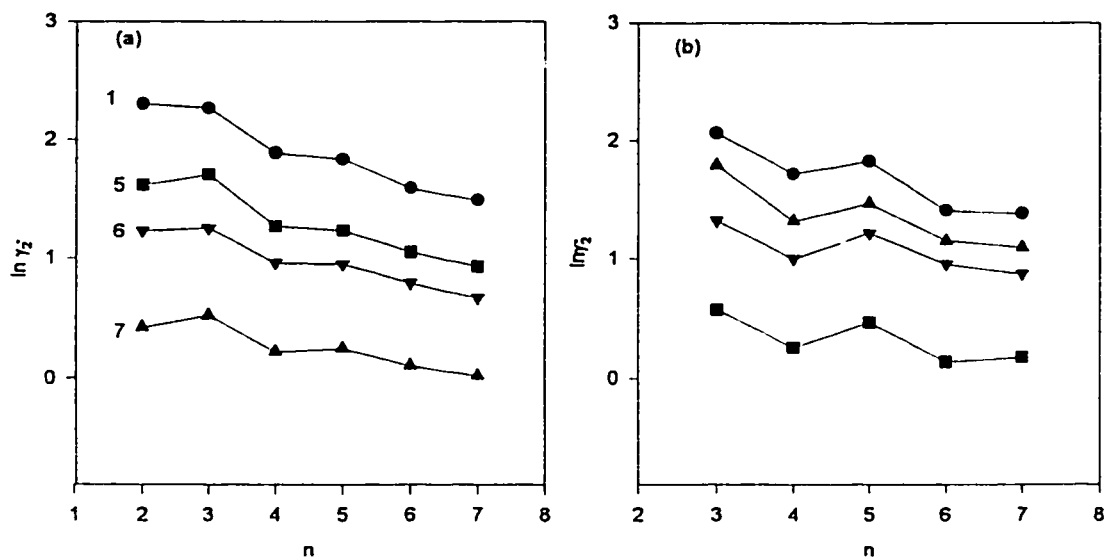


Figure 5.15 : Reduced Activity Coefficients for n-Hexane, 1-Hexene, c-1,4-Hexadiene, and Benzene (solutes 1,5-7) vs. n (the Number of Carbon Atoms on the Tails of the Liquid Crystal) in (a) the Isotropic Phase and (b) the Nematic Phase.

CHAPTER 6

INTERPRETATION OF

GLC

DATA

CHAPTER 6

INTERPRETATION OF GLC DATA

6.1 Chow And Martire Statistical Model

As mentioned in the introduction (chapter 1) simple conventional nonmesomorphic liquids possess short range positional order only whereas the nematic and isotropic phases of liquid crystals possess in addition long range and short range orientational orders respectively. All these forms of order are believed to originate from repulsive interactions which in the case of nematogens are anisotropic or shape dependent [10,30,49].

The Flory [55] and Sanchez-Lambe [56] theories of solution attribute excess thermodynamic solution quantities to combinatorial, free volume and contact interaction contributions. To understand

solutions of polymers in normal liquids Flory [57] used a lattice model. Polymers, treated as inflexible rods of length-to-breadth ratio (m), and monomeric solvent particles were placed on a simple cubic lattice. The solute rod was placed at an angle ψ to the preferred direction by dividing it into sub rods of length $m \sin \psi$ oriented parallel to the preferred direction and joined laterally at their ends.

DiMarzio [58] developed a counting procedure for approximating the configurational partition function for a system of hard rods of length-to-breadth ratio m on a simple cubic lattice. With each rod allowed to point in only one of the three mutually orthogonal axis directions. (by hard rods we mean that the only interaction between rods is the infinite repulsion that prevents their overlapping). Cotter and Martire [59] extended this approach to a face-centered cubic lattice of inflexible rods with repulsive and attractive interactions, treating the attractions in the quasichemical or Bethe-Guggenheim approximation. More recently, Alben has considered hard rods, using a modification of the DiMarzio method in which the density of rods on the lattice

and the orientational order parameters are determined as a function of temperature and pressure. He has also applied this approach to a van der Waal's model and two-component mixtures of hard rods and plates.

Peterson , Martire and Cotter [60] extended the DiMarzio-Alben model to two component mixtures of hard rods of different length to breadth ratio (m) on a simple cubic lattice, in an effort to gain insight into the role of molecular size and shape in determining the behavior of solutions of nonmesomorphic solutes in nematic solvents.

For infinite dilute solutions Chow and Martire [24-26] proposed a statistical model with the basic assumption that the product of $p \bar{V}^e$ (where P is the pressure and \bar{V}^e is the solute partial molar excess volume) is negligible.

Thus from thermodynamics:

$$\bar{G}^{\circ} = \bar{A}^{\circ} + p\bar{V}^{\circ} \approx \bar{A}^{\circ} = RT \ln\left(\frac{Q_i}{Q_a}\right) \quad (6.1)$$

$$\bar{H}^{\circ} = \bar{U}^{\circ} + p\bar{V}^{\circ} = \bar{U}^{\circ} = RT^2 \frac{\delta}{dT} \ln\left(\frac{Q_i}{Q_a}\right) \quad (6.2)$$

where, \bar{G}° , \bar{A}° , \bar{H}° and \bar{U}° are the solute partial molar excess Gibbs, Helmholtz, enthalpy and internal energy functions respectively. Q_i and Q_a refer to the solute molecular partition functions in the ideal and actual solutions respectively. In view of its infinite dilution, the solute is assumed to perturb the local solvent structure only. Thus the long-range order (if it exists) and the molecular energy states (on the average) of the solvent are considered unchanged. Also the solute molecular partition function (Q) is assumed to be separable into translational, rotational, vibrational and electronic parts Q^t , Q^r , and Q^e respectively. The translational part (Q^t) consists of kinetic and potential energy components (Q^k and Q^p) while the vibrational part

involves contributions from high frequency vibrational modes (Q^v) and low frequency internal rotational modes (Q^r). Thus,

$$Q = Q^t Q^v Q^r Q^e = (Q^k \times Q^p) \cdot (Q^{v'} \times Q^e) \cdot Q^r \cdot Q^e \quad (6.3)$$

Assuming that Q^k , $Q^{v'}$, and Q^e are independent of the solute's environment, and substituting for the Q^i and Q^a values, the model arrives at the following expressions

$$\frac{\bar{G}^\circ}{RT} = \ln \left[\left(\frac{Q_i^p}{Q_i^a} \right) \cdot \left(\frac{Q_i^r}{Q_i^a} \right) \cdot \left(\frac{Q_i^e}{Q_i^a} \right) \right] \quad (6.4)$$

$$\bar{H}^\circ \approx RT^2 \frac{\delta}{\delta T} \ln \left[\left(\frac{Q_i^p}{Q_i^a} \right) \cdot \left(\frac{Q_i^r}{Q_i^a} \right) \cdot \left(\frac{Q_i^e}{Q_i^a} \right) \right] \quad (6.5)$$

Remembering that

$$\frac{\overline{G}^\circ}{RT} = \ln \gamma_2^\infty$$

equation 6.4 may be written as

$$\gamma_2^\infty \approx \left(\frac{Q_i^p}{Q_i^g}\right) \cdot \left(\frac{Q_i^r}{Q_i^g}\right) \cdot \left(\frac{Q_i^c}{Q_i^g}\right) = \gamma^p \gamma^r \gamma^c \quad (6.6)$$

where γ^p, γ^r and γ^c are the potential energy, rotational and conformational contributions to the solute activity coefficient.

Equation 6.5 may be written as

$$\overline{H}^\circ \approx (\overline{H}^\circ)^p + (\overline{H}^\circ)^r + (\overline{H}^\circ)^c \quad (6.7)$$

and

$$\Delta \overline{H}_{\text{sol}} \approx (\overline{H}^\circ)^p + (\overline{H}^\circ)^r + (\overline{H}^\circ)^c - \Delta \overline{H}_{\text{vap}} \quad (6.8)$$

Using two quantum-mechanical treatments, Martire [51] showed that

Q_i^r/Q_i^g or γ^r is greater than unity if the rotation of the solute

molecule in the actual solution is restricted (e.g., due to the aligned nematic environment) relative to such motion in an ideal solution. Thus, increasing the rod-like character of the solute makes it rotationally less favored for solution in a nematic phase and leads to a higher γ^r values. Both treatments suggest that $(\overline{H}^e)^r \approx 0$, indicating the near equality of the solute rotational energy in the actual and ideal solutions, i.e., γ^r is largely entropic in origin.

Similar conclusions were reached for Q_i^o/Q_i^c or γ^c and $(\overline{H}^e)^c$ using a rotational isomeric model [51]. γ^c was found to be greater than unity for solutes conformationally restricted in the actual solution relative to the ideal solution. Also γ^c was found to be only slightly dependent on temperature, thus $(\overline{H}^e)^c$ is small, i.e., γ^c is also largely entropic in origin.

Since both $(\overline{H}^e)^r$ and $(\overline{H}^e)^c$ are small and equation 6.8 can be written as

$$\Delta \bar{H}_{\text{sol}} \approx (\bar{H}^{\circ})^p - \Delta \bar{H}_{\text{vap}} \quad (6.9)$$

Unlike the situation in ideal solutions, the solute-solvent interaction energy in actual solutions does not necessarily equal the mean of the solute-solute and solvent-solvent interaction energies, and may be anisotropic in nature. Thus the Q_i^p/Q_i^p or γ^p value depends on the strength and anisotropy of the solute-solvent interactions and may be greater or less than unity.

Considering solution properties arising from the potential energy contribution, we can write

$$RT \ln \gamma^p = (\Delta H_{\text{sol}})^p - T(\Delta S_{\text{sol}})^p \quad (6.10)$$

At a particular temperature T , equation (6.10) may be written as

$$\ln \gamma^p = k_1(\Delta \bar{H}_{\text{sol}})^p - k_2(\Delta \bar{S}_{\text{sol}})^p \quad (6.11)$$

where k_1 and k_2 are constants. It has been shown [51] that the plots of $\ln \gamma^p$ vs. $(\Delta \bar{H}_{sol})^p$ for a series of solutes in the same solvent are quite linear, indicating the dominance of enthalpy trend over the entropy trend. On this basis, one may assume that $(\Delta \bar{H}_{sol})^p$ values for solutions of a series of solutes in a given solvent provides a relative measure of γ^p values of these solutes. Since from equation (6.9)

$$\Delta \bar{H}_{sol} \approx (\Delta \bar{H}_{sol})^p \quad (6.12)$$

then the experimentally available $\Delta \bar{H}_{sol}$ values may be used as a relative measure of γ^p values.

In conventional liquid solutions deviations from ideality are assumed to be due to ‘structural’ (rotational plus conformational), energetic and combinatorial contributions. In solutions of nonmesomorphic solutes in liquid crystalline solvents the structural contribution depends on orientational order and is coupled to the energetic contribution. Our GLC results for infinitely dilute solutions of

nonmesomorphic solutes in liquid crystals were, to a limited extent, explainable by the Chow and Martire model.

In previous studies [27, 30-32], branched alkanes, alkenes, aromatics etc., were studied and the results were rationalized on the basis of the above mentioned model. Many results were explained on the basis of competing entropy and enthalpy effects. In this study we focus on a few solutes and we do not have a homologous series of similar solutes except for the four alkanes (n-hexane, n-heptane, n-octane, and n-nonane) This study is concerned with the effect of the solvent structure on the activity coefficient and, for the same solvent, the effect of increased unsaturation on the activity coefficients of the six liquid crystals.

In fact an analysis of our results in a manner similar to previous studies is extremely complex if not impossible due to the use (in our study) of six liquid crystal systems while earlier studies focused on one liquid crystal at a time. For some of our solute/solvent systems we agreed with trends from earlier studies while for other

solute/solvent systems our results are opposite to those previously obtained. No satisfactory solution is available at this point in time due to the complexity of the problem. Further complexity arises from the difference between our liquid crystals and those used in earlier studies. The cyanophenyl-p-n-alkylbenzoate homologous series have an ester group linkage between two central benzene rings which is absent in the previously studied liquid crystals.

6.2 Discussion

6.2.1 General Comparison

For all the solutes studied in all the liquid crystals studied the γ_2^∞ in both the isotropic and nematic phases are greater than zero (except for benzene in the isotropic phase of the heptyl member of the liquid crystals studied) indicating a positive deviation from Raoult's law. The partial molar excess enthalpies and excess entropies, for most of

the solutes, in the isotropic and the nematic phases are positive. Nonmesomorphic solutes are therefore generally incompatible with both phases of these liquid crystals. In the following section we will discuss the general trends for n-alkanes in all the liquid crystals studied.

In both the nematic and the isotropic phases for the liquid crystal series n-alkanes had positive excess enthalpies and entropies and a positive deviation from Raoult's law.

Comparing the results for the isotropic (I) and nematic (N) phases we note, in general, the following trends:

$$(1). (\Delta \bar{H}_{\text{sol}})_i < (\Delta \bar{H}_{\text{sol}})_n$$

$$(2). (\Delta \bar{S}_{\text{sol}})_i < (\Delta \bar{S}_{\text{sol}})_n$$

$$(3). (\gamma_2^\infty)_i < (\gamma_2^\infty)_n$$

Judging from the relative small ΔH_{NI} 's, solvent-solvent interactions in the nematic phase appear to be only slightly stronger than those in the isotropic phase. Thus, trend (1) is most likely due to effectively stronger solute-solvent interactions in the isotropic phase. Trend (2) is less straightforward. Rotational and conformational restrictions tend to reduce solute entropy in the nematic phase. On the other hand, effectively weaker solute-solvent interactions in the nematic phase tend to increase solute (translational) entropy. The experimental results indicate that the second effect prevails. Trend (3) indicates that the solute solubility is greater in the isotropic phase because its more favorable enthalpy.

Turning now to the well-defined trends in the nematic phase, we find that the increase in $\Delta \bar{S}_{sol}$, $\Delta \bar{H}_{sol}$ and γ_2^∞ with increasing solute chain length (L_2) may be explained as follows [29]. As L_2 increases, the

combinatorial contribution decreases, leading to less positive $\Delta\bar{S}_{sol}$, the rotational and conformational entropy losses increase, leading to more negative and larger $\Delta\bar{S}_{sol}$, and the overall strength of solute-solvent attractive interactions increases, leading to larger $\Delta\bar{H}_s$ values.

The trend of γ_2^∞ indicates that the enthalpy of solution increases less rapidly with increasing L_2 than do the combined entropy of solution effect as shown in equation 6.13

$$RT \left[\frac{\partial \ln \gamma_2^\infty}{\partial L_2} \right]_T = \left[\frac{\partial (\bar{H}^\circ - T\bar{S}^\circ)}{\partial L_2} \right]_2 = \left[\frac{\partial (T|\Delta\bar{S}| - |\Delta\bar{H}|)}{\partial L_2} \right] > 0 \quad (6.13)$$

Thus the trend of increasing γ_2^∞ values with increasing solute chain lengths reflects the dominance of entropy factor.

In the isotropic phase, a similar trend is observed but rotational and conformational effects are smaller compared to those exhibited in the ordered nematic phase.

If we compare the effect of introducing double bonds to the six member carbon atom solutes, γ_2^∞ decrease with increasing unsaturation (n-hexane > 1-hexene > c-1,4-hexadiene > benzene). This trend (shown in Figure 5.15) is attributed to the increase in polarizability even though rotational and conformational entropy losses upon solvation are smaller in the less orientationally ordered isotropic phase. The rigidity of cyclohexane is slightly less than that of benzene while its polarizability is comparable to that for hexane, we would expect cyclohexane to have γ_2^∞ values similar to those of hexane or slightly higher. The increased compatibility of cyclohexane with liquid crystalline phases relative to hexane is probably due to its smaller size.

6.2.2 Odd-even effect

The odd-even effect is the term used for the alternation in the values of a thermodynamic or other quantity (ΔH_m , ΔH_{NI} , γ_2^∞ , T_{NI} , etc.) with

the number (odd and even) of carbon atoms in an alkane or molecules with alkyl tails. All solutes studied show an odd even effect for their γ_2^∞ values in the six liquid crystals studied as shown in Figures 5.13 and 5.14. This trend is not strange since earlier studies [31, 33] for different homologous series show a similar trend. This trend is explained as follows: consider the nematic phase (actually existing or assumed by extrapolation) of a liquid crystalline solvent molecule with an even number of carbon atom. At the same temperature (50 °C in our case) this phase is less ordered (i.e., has a lower order parameter) than the nematic phases of solvent molecules with alkyl tails that are longer or shorter by one methyl group. This is evidenced in the alternation of the nematic-to-isotropic transition temperatures, as discussed in chapter 2, which is accounted for on the basis of the anisotropy of the polarizability of these molecules. A solute molecule is more compatible (has lower γ_N° value) with the less ordered nematic phase due to a liquid crystalline solvent molecule with an even number of carbon atoms (n) than with nematic phases due to solvent molecules with alkyl tails of length n+1 and n-1. As a result

the odd-even effect exhibited in the γ_2^∞ values is opposite to that observed for enthalpies and entropies of melting and for the isotropic-to-nematic transition temperatures. As the effect of the tail on the ordering of the solvent molecules levels out with increasing tail length so does the odd-even effect of γ_2^∞ values levels out with increasing tail length.

CHAPTER 7

SUMMARY AND

CONCLUSIONS

CHAPTER 7

SUMMARY AND CONCLUSIONS

Six members of the p-cyanophenyl-p-n-alkylbenzoate liquid crystal homologous series (alkyl = ethyl, n-propyl, n-butyl, n-pentyl, n-hexyl and n-heptyl) were investigated by DSC, ESR and GLC.

The DSC and ESR studies were mainly concerned with the thermodynamic properties and structures of the pure liquid crystals. The GLC study examined the thermodynamics of solution of nonmesomorphic solutes at infinite dilution in these liquid crystals.

The DSC measurements verified that the last two liquid crystals (with n-hexyl and n-heptyl tails) in the above mentioned series are conventional liquid crystals showing a crystal-to-nematic transition and a nematic-to-isotropic transition on heating, and an isotropic-to-nematic transition and a nematic-to-crystal transition on cooling. It

also showed that the first four liquid crystals (with ethyl, n-propyl, n-butyl and n-pentyl tails) are monotropic i.e. they only show a crystal-to-isotropic transition on heating and an isotropic-to-nematic transition on cooling. Additionally for the monotropic liquid crystals it has been shown that after an initial heating cycle to obtain the crystal-to-isotropic phase transition reversibility back and forth across the nematic-to-isotropic transition is achieved and persists as long as the solidification of the liquid crystal does not occur. Finally DSC measurements on bulk liquid crystals and liquid crystals coated on the GLC support (60/80 mesh AW/DMCS chromosorb W) gave very similar transition temperatures and enthalpy of transition values. These two findings made the GLC experiment possible. Finally the transition temperatures and enthalpies of transition of the liquid crystals studied showed an odd-even effect with respect to the number of carbon atoms on the alkyl tails which corroborates findings of previous studies and which is explained on the basis of the overall polarizability of the liquid crystal molecule.

ESR studies, using PDT as a probe, confirmed the transition temperatures obtained by other methods as well as the above mentioned reversibility in the isotropic-nematic region. In addition a sudden discontinuity in the a and g -factor values on solidification of the nematic phase suggest structural changes in the liquid crystal molecules during solidification. STO-3G calculations on the *p*-cyanophenyl-*p*-ethylbenzoate shed light on these probable structural changes showing a presence of two stable conformers having dihedral angles of about 46° and 40° between the planes of the cyano portion and the benzoate portion of the molecule at their linkage at the ester oxygen and an unstable conformer with a dihedral angle of 0° .

Using GLC, infinite dilution activity coefficients were measured for ten nonmesomorphic solutes at four temperatures in each of the nematic and isotropic phases of the *p*-cyanophenyl-*p*-*n*-alkylbenzoate homologous series of liquid crystals. The solutes studied included *n*-hexane, 3-methylpentane, 1-hexene, *c*-1,4-hexadiene and benzene;

All having six carbon atoms but of varying structures, polarizability and unsaturation. From the dependence of the infinite dilution activity coefficients on temperatures partial molar excess enthalpies, entropies, enthalpies of solution and entropies of solution were obtained and qualitatively interpreted in the light of a statistical thermodynamic model forwarded by Chow and Martire.

A more detailed interpretation was not possible due to the absence of a better theoretical model. However, the study indicates that solute size, shape, flexibility, and polarizability influence solution behavior.

Extrapolated values of the infinite dilution activity coefficients from the isotropic and nematic phases to a reference temperature allowed a comprehensive examination of the effects of both solutes and solvents structures on the solution process. These 'reduced' activity coefficient exhibited an odd-even effect with respect to the number of carbon atoms on the alkyl tails of the liquid crystal solvents. This effect was opposite to that observed for the transition temperatures

and enthalpies of transition of the liquid crystals studied and was rationalized on the basis of solute structures.

Finally those activity coefficients have analytical implications for the separation of solutes on the basis of their structures. Additionally combined with entropies of transitions of the pure liquid crystals they provide information on the ability of a solute to disrupt nematic order and bring about a two-phase region. Such information is much needed by those working on liquid crystal displays (LCD) because they intentionally add solute impurities to nematogens to modify their viscosities and conductivities.

APPENDIX

A

Table A-1 : Solute Specific Retention Volumes (cm³/g) in the Isotropic Phase of p-Cyanophenyl p-ethylbenzoate.

Solute No.	62.00°C	58.98°C	55.95°C	52.96°C
1	17.03	18.93	21.09	23.51
2	41.91	44.83	47.94	51.39
3	93.41	102.38	112.66	122.79
4	209.44	241.73	279.62	324.04
5	120.92	131.42	141.12	151.85
6	32.73	35.21	37.73	40.77
7	22.78	23.87	25.09	26.37
8	37.77	40.11	42.55	45.85
9	15.52	16.47	17.46	18.29
10	48.68	52.54	56.58	61.26

Table A-2 : Solute Specific Retention Volumes (cm³/g) in the Isotropic Phase of P-Cyanophenyl-p-n-propylbenzoate.

Solute No.	63.91°C	60.94°C	57.94°C	54.91°C
1	16.81	17.63	18.56	19.56
2	39.90	41.75	44.34	47.54
3	91.09	98.28	106.88	115.51
4	208.70	228.43	250.30	276.08
5	102.01	108.75	117.36	125.13
6	29.03	31.07	33.47	35.87
7	19.38	20.35	21.24	22.18
8	36.16	38.02	39.92	42.69
9	13.93	14.58	15.16	15.87
10	47.16	49.46	52.78	56.75

Table A-3 : Solute Specific Retention Volumes (cm³/g) in the Nematic Phase of p-Cyanophenyl-p-n-propylbenzoate.

Solute No.	46.88°C	43.99°C	41.08°C	38.02°C
1	22.30	23.41	24.71	26.37
2	54.94	59.29	64.50	70.30
3	134.46	149.04	165.22	184.10
4	340.08	379.63	419.88	476.10
5	148.21	162.73	179.96	199.92
6	40.26	42.36	45.16	48.23
7	24.30	26.66	29.40	32.64
8	44.04	48.06	52.10	56.60
9	17.63	18.75	19.85	21.06
10	58.76	64.00	70.49	77.18

Table A-4 : Solute Specific Retention Volumes (cm³/g) in the Isotropic Phase of p-Cyanophenyl-p-n-butylbenzoate.

Solute No.	58.00°C	55.01°C	51.98°C	48.98°C
1	24.96	26.68	28.466	30.45
2	59.38	64.86	70.47	76.65
3	140.80	156.27	172.51	190.80
4	332.66	374.40	418.57	469.76
5	141.56	155.86	169.95	186.09
6	42.02	45.08	49.04	53.24
7	29.15	31.40	33.62	36.10
8	52.589	56.27	60.52	65.06
9	21.06	22.21	23.49	24.87
10	72.25	77.82	82.74	89.01

Table A-5 : Solute Specific Retention Volumes (cm³/g) in the Nematic Phase of p-Cyanophenyl-p-n-butylbenzoate.

Solute No.	35.98°C	34.00°C	32.02°C	30.03°C
1	39.39	41.24	42.99	45.18
2	104.83	110.90	118.08	125.63
3	276.60	297.82	319.05	346.10
4	709.01	778.44	862.70	946.55
5	263.31	281.94	299.65	319.32
6	69.09	72.57	76.38	80.44
7	46.14	48.82	50.82	53.77
8	82.50	86.69	91.20	95.89
9	31.02	32.51	34.22	36.02
10	120.18	126.71	133.61	141.03

Table A-6 : Solute Specific Retention Volumes (cm³/g) in the Isotropic Phase of p-Cyanophenyl-p-n-pentylbenzoate.

Solute No.	69.09°C	65.97°C	63.00°C	59.97°C
1	24.96	26.68	28.46	30.45
2	59.38	64.86	70.47	76.65
3	140.80	156.27	172.51	190.80
4	332.66	374.40	418.57	469.76
5	141.56	155.86	169.95	186.08
6	42.02	45.09	49.04	53.24
7	29.15	31.40	33.62	36.10
8	52.59	56.27	60.52	65.06
9	21.06	22.21	23.49	24.87
10	72.25	77.82	82.74	89.01

Table A-7 : Solute Specific Retention Volumes (cm^3/g) in the Nematic Phase of p-Cyanophenyl-p-n-pentylbenzoate.

Solute No.	49.97°C	46.90°C	43.88°C	40.87°C
1	39.39	41.24	42.99	45.18
2	104.83	110.90	118.08	125.63
3	276.60	297.82	319.05	346.10
4	709.01	778.44	862.70	946.56
5	263.31	281.94	299.66	319.32
6	69.10	72.57	76.38	80.44
7	46.15	48.82	50.82	53.77
8	82.50	86.69	91.20	95.89
9	31.02	32.51	34.22	36.01
10	120.18	126.71	133.61	141.04

Table A-8: Solute Specific Retention Volumes (cm³/g) in the Isotropic Phase of p-Cyanophenyl-p-n-hexylbenzoate.

Solute No.	61.98°C	58.98°C	56.00°C	52.81°C
1	25.47	27.63	29.91	32.62
2	61.29	67.49	73.50	80.77
3	146.05	162.40	180.35	202.46
4	347.92	390.75	440.41	501.74
5	124.41	136.73	150.48	167.30
6	40.57	43.75	47.52	51.52
7	28.79	31.22	33.90	36.69
8	53.52	57.854	62.32	67.52
9	22.33	23.87	25.53	27.42
10	77.78	84.48	91.68	100.62

Table A-9 Solute Specific Retention Volumes (cm³/g) in
Nematic p-Cyanophenyl-p-n-hexylbenzoate.

Solute No.	43.44°C	40.84°C	37.80°C	34.97°C
1	42.00	45.48	48.62	52.20
2	111.21	120.45	130.34	141.78
3	292.25	320.79	352.38	392.05
4	752.88	832.56	963.33	1073.74
5	231.85	249.96	272.05	295.18
6	66.78	72.21	78.20	83.74
7	48.59	51.38	55.22	58.48
8	89.20	93.74	100.68	106.76
9	34.70	36.52	38.96	41.48
10	131.55	142.00	152.18	162.52

Table A-10 : Solute Specific Retention Volumes (cm^3/g) in the Isotropic Phase of p-Cyanophenyl-p-n-heptylbenzoate.

Solute No.	69.12°C	66.10°C	63.07°C	60.12°C
1	23.92	25.36	27.02	28.97
2	54.01	59.20	65.15	71.54
3	129.10	140.63	154.02	170.69
4	285.12	324.87	371.07	423.46
5	103.34	113.53	124.39	136.78
6	34.93	37.70	41.137	44.75
7	25.81	27.99	30.18	32.57
8	47.90	51.96	56.11	61.09
9	20.28	21.80	23.35	25.04
10	67.82	73.54	80.93	87.22

Table A-11 Solute Specific Retention Volumes (cm^3/g) in the Nematic Phase of p-Cyanophenyl-p-n-heptylbenzoate.

Solute No.	54.91°C	49.06°C	47.06°C	45.06°C
1	32.27	33.74	35.48	37.21
2	82.18	86.03	90.66	95.70
3	203.59	217.37	231.61	247.56
4	512.31	548.40	589.99	640.18
5	159.28	167.18	177.30	187.07
6	48.12	50.06	51.92	54.36
7	35.74	37.10	38.25	39.87
8	65.17	67.65	70.55	73.34
9	26.58	27.55	28.42	29.44
10	96.79	100.66	105.20	110.83

Table A-12 : Linear Least Squares Fits of $\ln V_g^*$ vs. $1/T$ in the Isotropic Phase of p-Cyanophenyl-p-ethylbenzoate

Solute No.	slope	Slope	Intercept
1	0.9999	3.895 ± 0.002	-8.785 ± 0.007
2	0.9999	2.458 ± 0.008	-3.597 ± 0.023
3	0.9997	3.317 ± 0.058	-5.358 ± 0.174
4	0.9999	5.270 ± 0.002	-10.380 ± 0.006
5	0.9992	2.731 ± 0.077	-3.351 ± 0.233
6	0.9998	2.636 ± 0.035	-4.377 ± 0.106
7	0.9999	1.766 ± 0.012	-2.145 ± 0.038
8	0.9986	2.321 ± 0.086	-3.296 ± 0.269
9	0.9981	1.996 ± 0.089	-3.212 ± 0.269
10	0.9999	2.765 ± 0.022	-4.366 ± 0.066

Table A-13 : Linear Least Squares Fits of $\ln V_g^\circ$ vs. $1/T$ in the Isotropic Phase of p-Cyanophenyl-p-n-propylbenzoate.

Solute No.	Correlation Coefficient	Slope	Intercept
1	0.9999	1.866 ± 0.013	-2.714 ± 0.039
2	0.9967	2.159 ± 0.125	-2.725 ± 0.375
3	0.9998	2.935 ± 0.039	-4.196 ± 0.118
4	0.9999	3.432 ± 0.022	-4.840 ± 0.065
5	0.9978	2.018 ± 0.095	-2.402 ± 0.286
6	0.9998	2.613 ± 0.032	-4.385 ± 0.097
7	0.9993	2.539 ± 0.066	-2.909 ± 0.199
8	0.9991	1.649 ± 0.049	-1.927 ± 0.147
9	0.9995	1.587 ± 0.037	-2.074 ± 0.111
10	0.9969	2.288 ± 0.129	-2.940 ± 0.390

Table A-14 : Linear Least Squares Fits of $\ln V_g^*$ vs. $1/T$ in the Nematic Phase of p-Cyanophenyl-p-n-propylbenzoate.

Solute No.	Correlation Coefficient	Slope	Intercept
1	0.9999	1.880 ± 0.056	-2.772 ± 0.177
2	0.9999	2.780 ± 0.025	-4.681 ± 0.081
3	0.9999	3.530 ± 0.029	-6.128 ± 0.093
4	0.9996	3.749 ± 0.072	-5.884 ± 0.229
5	0.9994	2.812 ± 0.071	-4.996 ± 0.225
6	0.9992	2.049 ± 0.58	-2.711 ± 0.184
7	0.9999	3.316 ± 0.013	-7.172 ± 0.041
8	0.9999	3.370 ± 0.020	-5.533 ± 0.063
9	0.9995	1.992 ± 0.044	-3.353 ± 0.142
10	0.9997	3.086 ± 0.056	-5.570 ± 0.178

Table A-15 : Linear Least Squares Fits of $\ln V_g^*$ vs. $1/T$ in the Isotropic Phase of p-Cyanophenyl-p-n-butylbenzoate.

Solut No.	Correlation Coefficient	Slope	Intercept
1	0.9999	2.344 ± 0.008	-3.861 ± 0.026
2	0.9997	3.012 ± 0.048	-5.008 ± 0.149
3	0.9998	3.584 ± 0.050	-5.874 ± 0.152
4	0.9998	4.068 ± 0.054	-6.473 ± 0.165
5	0.9996	3.217 ± 0.066	-4.758 ± 0.202
6	0.9996	2.815 ± 0.058	-4.764 ± 0.179
7	0.9997	2.520 ± 0.044	-4.234 ± 0.133
8	0.9999	2.523 ± 0.013	-3.657 ± 0.040
9	0.9999	1.968 ± 0.085	-2.894 ± 0.026
10	0.9992	2.437 ± 0.069	-3.076 ± 0.211

Table A-16 : Linear Least Squares Fits of $\ln V_g^{\circ}$ vs. $1/T$ in the Nematic Phase of p-Cyanophenyl-p-n butylbenzoate.

Solut No.	Correlation Coefficient	Slope	Intercept
1	0.9999	2.139 ± 0.048	-3.244 ± 0.159
2	0.9998	2.860 ± 0.036	-4.601 ± 0.119
3	0.9996	3.502 ± 0.072	-5.705 ± 0.237
4	0.9998	4.579 ± 0.067	-8.250 ± 0.219
5	0.9996	3.021 ± 0.061	-4.196 ± 0.201
6	0.9999	2.397 ± 0.010	-3.518 ± 0.033
7	0.9979	2.356 ± 0.110	-3.789 ± 0.360
8	0.9999	2.371 ± 0.008	-3.256 ± 0.025
9	0.9999	2.359 ± 0.023	-4.196 ± 0.076
10	0.9999	2.518 ± 0.056	-3.355 ± 0.018

Table A-17 : Linear Least Squares Fits of $\ln V_g^\circ$ vs. $1/T$ in the Isotropic Phase of p-Cyanophenyl-p-n pentylbenzoate.

Solut No.	Correlation coefficient	Slope	Intercept
1	0.9999	2.969 ± 0.055	-5.689 ± 0.164
2	0.9996	3.239 ± 0.062	-5.652 ± 0.183
3	0.9999	3.470 ± 0.010	-5.474 ± 0.029
4	0.9999	4.161 ± 0.031	-6.676 ± 0.091
5	0.9999	2.382 ± 0.044	-3.213 ± 0.131
6	0.9997	2.977 ± 0.049	-5.259 ± 0.145
7	0.9999	2.867 ± 0.016	-5.277 ± 0.048
8	0.9998	3.263 ± 0.016	-4.933 ± 0.048
9	0.9999	2.145 ± 0.009	-3.405 ± 0.026
10	0.9999	3.251 ± 0.023	-5.488 ± 0.068

Table A-18 : Linear Least Squares Fits of $\ln V_g^\circ$ vs. $1/T$ in the Nematic Phase of p-Cyanophenyl p-n-pentylbenzoate.

Solute No.	Correlation Coefficient	Slope	Intercept
1	0.9996	3.801 ± 0.067	-5.826 ± 0.210
2	0.9999	2.898 ± 0.014	-4.852 ± 0.044
3	0.9999	3.444 ± 0.040	-5.634 ± 0.125
4	0.9999	2.006 ± 0.079	-2.972 ± 0.247
5	0.9998	3.058 ± 0.045	-4.515 ± 0.141
6	0.9999	2.389 ± 0.019	-3.707 ± 0.061
7	0.9981	2.020 ± 0.087	-2.892 ± 0.274
8	0.9998	2.394 ± 0.036	-3.486 ± 0.114
9	0.9994	2.039 ± 0.050	-3.310 ± 0.156
10	0.9997	2.412 ± 0.043	-3.205 ± 0.134

Table A-19 : Linear Least Squares Fits of $\ln V_g^\circ$ vs. $1/T$ in the Isotropic Phase of p-Cyanophenyl p-n-hexylbenzoate.

Solut No.	Correlation Coefficient	Slope	Intercept
1	0.9999	2.940 ± 0.019	-5.536 ± 0.056
2	0.9995	3.270 ± 0.072	-5.638 ± 0.217
3	0.9999	3.886 ± 0.012	-6.611 ± 0.035
4	0.9999	4.362 ± 0.013	-7.166 ± 0.040
5	0.9999	3.526 ± 0.009	-5.698 ± 0.028
6	0.9998	2.861 ± 0.042	-4.833 ± 0.128
7	0.9995	2.898 ± 0.063	-5.284 ± 0.193
8	0.9999	2.762 ± 0.032	-4.259 ± 0.100
9	0.9999	2.445 ± 0.014	-4.188 ± 0.042
10	0.9999	3.059 ± 0.016	-4.775 ± 0.049

Table A-20 : Linear Least Squares Fits of $\ln V_g^\circ$ vs. $1/T$ in the Nematic Phase of p-Cyanophenyl-p-n-hexylbenzoate.

Solute No.	Correlation Coefficient	Slope	Intercept
1	0.9999	2.487 ± 0.120	-4.114 ± 0.383
2	0.9994	2.796 ± 0.070	-4.117 ± 0.223
3	0.9992	3.378 ± 0.096	-4.992 ± 0.307
4	0.9991	4.201 ± 0.126	-6.649 ± 0.404
5	0.9999	2.804 ± 0.021	-3.410 ± 0.067
6	0.9988	2.626 ± 0.091	-4.090 ± 0.292
7	0.9996	2.176 ± 0.042	-2.991 ± 0.135
8	0.9994	2.119 ± 0.051	-2.204 ± 0.162
9	0.9997	2.078 ± 0.035	-3.018 ± 0.113
10	0.9981	2.434 ± 0.106	-2.803 ± 0.340

Table A-21 : Linear Least Squares Fits of $\ln V_g^*$ vs. $1/T$ in the Isotropic Phase of p-Cyanophenyl p-n-heptylbenzoate.

Solute No.	Correlation coefficient	Slope	Intercept
1	0.9999	2.429 ± 0.063	-3.924 ± 0.186
2	0.9999	3.568 ± 0.012	-6.437 ± 0.036
3	0.9992	3.528 ± 0.100	-5.452 ± 0.296
4	0.9999	5.013 ± 0.001	-8.994 ± 0.002
5	0.9999	3.543 ± 0.023	-5.714 ± 0.068
6	0.9997	3.156 ± 0.051	-5.669 ± 0.153
7	0.9998	2.937 ± 0.044	-5.330 ± 0.130
8	0.9998	3.064 ± 0.043	-5.083 ± 0.127
9	0.9999	2.665 ± 0.026	-4.776 ± 0.076
10	0.9990	3.231 ± 0.100	-5.222 ± 0.296

Table A-22 : Linear Least Squares Fits of $\ln V_g^{\circ}$ vs. $1/T$ in the Nematic Phase of p-Cyanophenyl-p-n-heptylbenzoate.

Solute	Correlation Coefficient	Slope	Intercept
1	0.9999	2.453 ± 0.042	-4.092 ± 0.131
2	0.9993	2.619 ± 0.069	-3.670 ± 0.215
3	0.9999	3.342 ± 0.017	-4.990 ± 0.052
4	0.9992	3.812 ± 0.107	-5.522 ± 0.335
5	0.9994	2.781 ± 0.072	-3.507 ± 0.222
6	0.9990	2.069 ± 0.066	-2.509 ± 0.206
7	0.9985	1.844 ± 0.071	-2.113 ± 0.222
8	0.9998	2.036 ± 0.032	-2.105 ± 0.099
9	0.9996	1.733 ± 0.033	-2.063 ± 0.103
10	0.9981	2.315 ± 0.103	-2.572 ± 0.321

APPENDIX

B

Table B-1 : Corrected Solute Activity Coefficient, γ_2^∞ , in the Isotropic Phase of p-Cyanophenyl-p-ethylbenzoate.

Solute No.	62.00°C	58.98°C	55.95°C	52.95°C
1	6.50	6.47	6.44	6.40
2	7.13	7.48	7.87	8.27
3	8.47	8.80	9.13	9.58
4	9.89	9.90	9.93	9.96
5	1.34	1.37	1.42	1.47
6	3.01	3.10	3.21	3.30
7	4.09	4.30	4.52	4.76
8	4.31	4.50	4.72	4.88
9	5.99	6.22	6.47	6.83
10	8.78	9.17	9.60	10.03

Table B-2 : Corrected solute Activity Coefficients, γ_2^∞ , in the
 Isotropic Phase of p-Cyanophenyl-p-n-
 propylbenzoate.

Solut No.	63.91°C	60.94°C	60.94°C	54.91°C
1	5.87	6.16	6.48	6.82
2	6.61	7.06	7.46	7.83
3	7.59	7.98	8.35	8.83
4	8.59	9.03	9.53	10.03
5	1.40	1.46	1.51	1.58
6	3.02	3.11	3.20	3.31
7	4.28	4.48	4.74	5.02
8	3.99	4.20	4.44	4.63
9	5.945	6.25	6.62	6.98
10	7.98	8.54	9.01	9.46

Table B-3 : Corrected Solute Activity Coefficients, γ_2^∞ , in the Nematic Phase of p-Cyanophenyl-p-n-propylbenzoate.

Solute No.	46.88°C	44.00°C	41.09°C	38.02°C
1	7.96	8.43	8.91	9.4151
2	9.40	9.83	10.26	10.7898
3	10.98	11.38	11.84	12.40
4	12.33	12.90	13.69	14.37
5	1.80	1.84	1.87	1.91
6	3.94	4.18	4.38	4.627
7	6.05	6.12	6.17	6.24
8	6.04	6.18	6.39	6.66
9	8.28	8.63	9.07	9.58
10	12.81	13.34	13.79	14.50

Table B-4 : Corrected Solute Activity Coefficients, γ_2^∞ , in the
 Isotropic Phase of p-Cyanophenyl-p- n
 butylbenzoate.

Solute No.	58.00°C	55.01°C	51.98°C	48.98°C
1	4.56	4.73	4.93	5.13
2	5.28	5.43	5.64	5.86
3	6.01	6.17	6.41	6.66
4	6.79	6.99	7.29	7.58
5	1.18	1.20	1.23	1.26
6	2.41	2.50	2.55	2.62
7	3.27	3.36	3.47	3.59
8	3.20	3.32	3.45	3.58
9	4.51	4.72	4.95	5.18
10	6.23	6.53	6.953	7.34

Table B-5 : Corrected Solute Activity Coefficients, γ_2^∞ , in the Nematic Phase of p-Cyanophenyl-p-n butylbenzoate.

Solut No.	35.98°C	34.00°C	32.02°C	30.03°C
1	6.49	6.71	6.98	7.21
2	7.54	7.80	8.04	8.31
3	8.70	8.96	9.30	9.54
4	10.30	10.54	10.71	11.02
5	1.50	1.52	1.56	1.60
6	3.33	3.43	3.54	3.65
7	4.53	4.63	4.81	4.92
8	4.72	4.87	5.04	5.22
9	6.68	6.88	7.06	7.26
10	9.73	10.14	10.58	11.05

Table B-6 : Corrected Solute Activity Coefficients, γ_2^∞ , in the Isotropic Phase of p-Cyanophenyl-p-n-pentylbenzoate.

Solute No.	69.09°C	65.97°C	63.00°C	59.97°C
1	4.02	4.07	4.16	4.25
2	4.58	4.71	4.80	4.96
3	5.01	5.18	5.35	5.55
4	5.59	5.76	5.95	6.12
5	1.14	1.17	1.19	1.20
6	2.26	2.30	2.34	2.41
7	3.02	3.09	3.14	3.20
8	2.72	2.84	2.94	3.06
9	3.83	3.98	4.13	4.29
10	5.34	5.50	5.64	5.83

Table B-7 : Corrected Solute Activity Coefficients, γ_2^∞ , in the Nematic Phase of p-Cyanophenyl-p-n-pentylbenzoate.

Solute No.	49.97°C	46.90°C	43.88°C	40.87°C
1	5.92	6.24	6.61	6.92
2	7.03	7.33	7.65	7.98
3	7.98	8.32	8.72	9.06
4	8.95	9.34	9.91	10.37
5	1.59	1.64	1.69	1.73
6	3.37	3.52	3.67	3.83
7	4.35	4.54	4.82	5.02
8	4.44	4.64	4.88	5.08
9	6.21	6.47	6.79	7.15
10	8.81	9.40	9.98	10.58

Table B-8 : Corrected Solute Activity Coefficients, γ_2^∞ , in the Isotropic Phase of p-Cyanophenyl-p-n-hexylbenzoate.

Solute No.	61.98°C	58.98°C	56.00°C	52.80°C
1	3.56	3.62	3.70	3.80
2	3.99	4.06	4.19	4.33
3	4.43	4.54	4.65	4.78
4	4.87	5.01	5.14	5.30
5	1.06	1.07	1.09	1.10
6	1.99	2.04	2.08	2.15
7	2.65	2.69	2.73	2.81
8	2.49	2.55	2.63	2.72
9	3.40	3.51	3.61	3.75
10	4.50	4.66	4.84	5.02

Table B-9 : Corrected Solute Activity Coefficients, γ_2^∞ , in the Nematic Phase of p-Cyanophenyl-p-n-hexylbenzoate.

Solute No.	43.44°C	40.84°C	37.80°C	34.97°C
1	4.14	4.22	4.44	4.61
2	4.64	4.79	5.07	5.28
3	5.14	5.33	5.65	5.85
4	5.79	6.04	6.20	6.52
5	1.14	1.17	1.22	1.26
6	2.34	2.39	2.48	2.59
7	2.96	3.08	3.21	3.37
8	2.94	3.10	3.26	3.44
9	4.11	4.29	4.51	4.70
10	5.74	5.98	6.41	6.83

Table B-10 : Corrected Solute Activity Coefficients, γ_2^∞ , in
the Isotropic Phase of p-Cyanophenyl-p-n-
heptylbenzoate.

Solute No.	69.12°C	66.10°C	63.08°C	60.12°C
1	2.88	2.99	3.10	3.18
2	3.34	3.39	3.465	3.51
3	3.57	3.71	3.84	3.93
4	4.09	4.12	4.15	4.18
5	0.96	0.97	0.98	0.99
6	1.75	1.79	1.81	1.83
7	2.26	2.29	2.33	2.38
8	2.09	2.13	2.18	2.22
9	2.87	2.93	3.01	3.08
10	3.77	3.89	3.97	4.13

Table B-11 : Corrected Solute Activity Coefficients, γ_2^∞ , in
the Nematic Phase of p-Cyanophenyl-p-n-
heptylbenzoate.

Solute No.	51.11°C	49.06°C	47.06°C	45.06°C
1	3.90	4.010	4.10	4.21
2	4.36	4.52	4.67	4.81
3	4.92	5.06	5.22	5.37
4	5.42	5.62	5.81	5.96
5	1.18	1.21	1.24	1.27
6	2.34	2.42	2.51	2.58
7	2.93	3.03	3.15	3.25
8	2.88	2.99	3.09	3.21
9	3.92	4.05	4.22	4.37
10	5.36	5.62	5.86	6.07

Table B-12 : Linear Least Squares Fits for $\ln \gamma_2^{\infty}$ vs. $1/T$ in the Isotropic Phase of p-Cyanophenyl p-ethylbenzoate.

Solute No.	Correlation Coefficient	slope	Intercept
1	-0.9996	-0.182 ± 0.003	2.416 ± 0.011
2	0.9999	1.783 ± 0.007	-3.355 ± 0.022
3	0.9981	1.467 ± 0.063	-2.245 ± 0.191
4	0.9933	0.088 ± 0.007	2.028 ± 0.022
5	0.9955	1.205 ± 0.081	-3.311 ± 0.244
6	0.9991	1.126 ± 0.033	-2.258 ± 0.101
7	0.9999	1.844 ± 0.010	-4.096 ± 0.030
8	0.9972	1.534 ± 0.082	-3.114 ± 0.248
9	0.9966	1.584 ± 0.092	-2.941 ± 0.279
10	0.9998	1.608 ± 0.020	-2.626 ± 0.060

Table B-13 : Linear Least Squares Fits for $\ln \gamma_2^{\infty}$ vs. $1/T$ in the Isotropic Phase of p-Cyanophenyl-p-n-propylbenzoate.

Solute No.	Correlation Coefficient	Slope	Intercept
1	0.9999	1.841 ± 0.100	-3.6927 ± 0.032
2	0.9966	$2.072. \pm 0.012$	-4.2534 ± 0.361
3	0.9995	$1.838. \pm 0.041$	-3.4270 ± 0.123
4	0.9999	$1.912. \pm 0.017$	-3.5217 ± 0.052
5	0.9977	$1.391. \pm 0.067$	-3.7876 ± 0.200
6	0.9992	$1.144. \pm 0.033$	-2.2899 ± 0.099
7	0.9993	$1.956. \pm 0.052$	-4.3513 ± 0.156
8	0.9975	$1.830. \pm 0.092$	-4.0423 ± 0.278
9	0.9996	1.988 ± 0.038	-4.1155 ± 0.115
10	0.9964	2.075 ± 0.125	-4.0742 ± 0.377

Table B-14 : Linear Least Squares Fits for $\ln \gamma_2^\infty$ vs. $1/T$ in the Nematic Phase of p-Cyanophenyl-p-n-propylbenzoate

Solute No.	Correlation Coefficient	slope	Intercept
1	0.9993	1.893 ± 0.052	-3.8392 ± 0.164
2	0.9997	1.543 ± 0.025	-2.5821 ± 0.078
3	0.9993	1.365 ± 0.037	-1.8698 ± 0.116
4	0.9984	1.751 ± 0.069	-2.9617 ± 0.220
5	0.9991	0.636 ± 0.0187	-1.3996 ± 0.059
6	0.9990	1.771 ± 0.055	-4.1583 ± 0.175
7	0.9991	0.351 ± 0.010	0.7032 ± 0.033
8	0.9954	1.109 ± 0.075	-1.6729 ± 0.239
9	0.9991	1.644 ± 0.049	-3.0245 ± 0.155
10	0.9981	1.377 ± 0.059	-1.7524 ± 0.188

Table B-15 : Linear Least Squares Fits for $\ln \gamma_2^\infty$ vs. $1/T$ in the Isotropic Phase of p-Cyanophenyl-p-n-butylbenzoate.

Solute No.	Correlation Coefficient	Slope	Intercept
1	0.9998	1.383 ± 0.021	2.6596 ± 0.063
2	0.9982	1.249 ± 0.054	2.1117 ± 0.164
3	0.9979	1.228 ± 0.056	1.9177 ± 0.170
4	0.9979	1.325 ± 0.061	2.0903 ± 0.187
5	0.9912	0.737 ± 0.070	2.0624 ± 0.213
6	0.9967	0.961 ± 0.055	2.0176 ± 0.170
7	0.9982	1.107 ± 0.046	2.1586 ± 0.142
8	0.9999	1.348 ± 0.011	2.9073 ± 0.033
9	0.9999	1.627 ± 0.005	3.406 ± 0.016
10	0.9987	1.958 ± 0.071	4.0875 ± 0.218

Table B-16 : Linear Least Squares Fits for $\ln \gamma_2^\infty$ vs. $1/T$ in the Nematic Phase of p-Cyanophenyl-p-n-butylbenzoate.

Solute No.	Correlation Coefficient	Slope	Intercept
1	0.9992	1.680 ± 0.048	-3.5648 ± 0.156
2	0.9995	1.524 ± 0.033	-2.9097 ± 0.108
3	0.9978	1.474 ± 0.070	-2.6033 ± 0.229
4	0.9954	1.026 ± 0.070	-0.9855 ± 0.228
5	0.9962	1.040 ± 0.064	-2.9623 ± 0.211
6	0.9999	1.468 ± 0.007	-3.5462 ± 0.024
7	0.9934	1.355 ± 0.110	-2.8729 ± 0.361
8	0.9999	1.598 ± 0.010	-3.6195 ± 0.034
9	0.9997	1.318 ± 0.021	-2.3637 ± 0.068
10	0.9999	2.010 ± 0.009	-4.2290 ± 0.029

Table B-17: Linear Least Squares Fits for $\ln \gamma_2^\infty$ vs. $1/T$ in the Isotropic Phase of p-Cyanophenyl-p-n-pentylbenzoate.

Solute No.	Correlation Coefficient	Slope	Intercept
1	0.9935	0.719 ± 0.058	-0.7126 ± 0.173
2	0.9955	0.967 ± 0.065	-1.3036 ± 0.200
3	0.9999	1.270 ± 0.015	-2.1006 ± 0.044
4	0.9995	1.139 ± 0.025	-1.6063 ± 0.073
5	0.9961	0.646 ± 0.040	-1.7504 ± 0.120
6	0.9955	0.762 ± 0.051	-1.411 ± 0.153
7	0.9997	0.722 ± 0.013	-1.0026 ± 0.038
8	0.9999	1.444 ± 0.013	-3.2175 ± 0.039
9	0.9999	1.413 ± 0.010	-2.7860 ± 0.030
10	0.9994	1.086 ± 0.026	-1.4992 ± 0.077

Table B-18 : Linear Least Squares Fits for $\ln \gamma_2^\infty$ vs. $1/T$ in the Nematic Phase of p-Cyanophenyl-p-n-pentylbenzoate.

Solute No.	Correlation Coefficient	slope	Intercept
1	0.9987	1.757 ± 0.063	-3.6577 ± 0.199
2	0.9999	1.409 ± 0.010	-2.4104 ± 0.033
3	0.9994	1.430 ± 0.035	-2.3479 ± 0.111
4	0.9977	1.671 ± 0.079	-2.9831 ± 0.251
5	0.9980	0.935 ± 0.041	-2.4279 ± 0.130
6	0.9998	1.420 ± 0.018	-3.1773 ± 0.055
7	0.9973	1.637 ± 0.086	-3.5979 ± 0.270
8	0.9995	1.515 ± 0.034	-3.1971 ± 0.109
9	0.9989	1.586 ± 0.053	-3.0860 ± 0.168
10	0.9997	2.033 ± 0.037	-4.1145 ± 0.115

Table B-19 : Linear Least Squares Fits for $\ln \gamma_2^\infty$ vs. $1/T$ in the Isotropic Phase of p-Cyanophenyl-p-n-hexylbenzoate.

Solute No.	Correlation Coefficient	Slope	Intercept
1	0.9992	0.773 ± 0.022	-1.0374 ± 0.066
2	0.9939	0.971 ± 0.076	-1.5175 ± 0.230
3	0.9997	0.900 ± 0.017	-1.1994 ± 0.050
4	0.9999	0.996 ± 0.007	-1.3892 ± 0.024
5	0.9998	0.410 ± 0.005	-1.1651 ± 0.015
6	0.9976	0.901 ± 0.0441	-2.0036 ± 0.133
7	0.9913	0.715 ± 0.067	-1.1641 ± 0.203
8	0.9989	1.094 ± 0.036	-2.3563 ± 0.108
9	0.9998	1.137 ± 0.017	-2.1689 ± 0.051
10	0.9999	1.314 ± 0.013	-2.4161 ± 0.040

Table B-20 : Linear Least Squares Fits for $\ln \gamma_2^\infty$ vs. $1/T$ in the Nematic Phase of p- Cyanophenyl-p-n hexylbenzoate.

solute No.	Correlation coefficient	Slope	Intercept
1	0.9913	1.302 ± 0.122	-2.6961 ± 0.392
2	0.9979	1.548 ± 0.071	-3.3595 ± 0.226
3	0.9964	1.544 ± 0.093	-3.2398 ± 0.299
4	0.9908	1.334 ± 0.129	-2.4566 ± 0.411
5	0.9997	1.221 ± 0.022	-3.7293 ± 0.069
6	0.9939	1.209 ± 0.095	-2.9758 ± 0.304
7	0.9991	1.507 ± 0.045	-3.676 ± 0.143
8	0.9993	1.819 ± 0.050	-4.6660 ± 0.158
9	0.9996	1.572 ± 0.031	-3.5525 ± 0.100
10	0.9971	2.052 ± 0.111	-4.7385 ± 1.559

Table B-21 : Linear Least Squares Fits for $\ln \gamma_2^\infty$ vs. $1/T$ in the Isotropic Phase of p-Cyanophenyl-p-n-heptylbenzoate.

Solute No.	Correlation Coefficient	Slope	Intercept
1	0.9978	1.258 ± 0.060	-2.6159 ± 0.176
2	0.9997	0.637 ± 0.011	-0.6574 ± 0.032
3	0.9941	1.211 ± 0.094	-2.2613 ± 0.278
4	0.9993	0.285 ± 0.007	0.5748 ± 0.022
5	0.9959	0.365 ± 0.024	-1.1084 ± 0.070
6	0.9929	0.582 ± 0.049	-1.1389 ± 0.146
7	0.9949	0.651 ± 0.047	-1.0905 ± 0.138
8	0.9971	0.763 ± 0.041	-1.4915 ± 0.122
9	0.9990	0.893 ± 0.028	-1.5564 ± 0.082
10	0.9916	1.106 ± 0.102	-1.9050 ± 0.270

Table B-22 : Linear Least Squares Fits for $\ln \gamma_2^\infty$ vs. $1/T$ in the Nematic Phase of p-Cyanophenyl-p-n-heptylbenzoate.

Solute No.	Correlation Coefficient	Slope	Intercept
1	0.9991	1.300 ± 0.039	-2.6473 ± 0.121
2	0.9984	1.676 ± 0.067	-3.6938 ± 0.209
3	0.9998	1.515 ± 0.021	-3.0805 ± 0.065
4	0.9959	1.638 ± 0.106	-3.3589 ± 0.387
5	0.9968	1.202 ± 0.068	-3.5415 ± 0.211
6	0.9984	1.732 ± 0.069	-4.4917 ± 0.214
7	0.9983	1.806 ± 0.075	-4.4951 ± 0.233
8	0.9998	1.861 ± 1.231	-4.6841 ± 0.087
9	0.9996	1.884 ± 0.037	-4.4448 ± 0.114
10	0.9977	2.117 ± 0.103	-4.8456 ± 0.320

APPENDIX

C

C.1 The retention Equation in Gas Liquid Chromatography

At constant temperature and pressure the solute in glc is distributed between two phases: a stationary liquid phase (L) and a mobile gas phase (M). When the solute free energy is minimum, equilibrium occurs (i.e. the chemical potential in one phase is equal to that in the other phase) [43]

$$\mu_L = \mu_M \quad (C.1)$$

where

$$\mu_i = \mu_i^\circ + RT \ln a_i \quad (C.2)$$

a_i is the solute activity in the i th phase and μ_i° is the solute chemical potential at unit activity. Making the approximation that the activities can be replaced by concentrations gives:

$$\mu_L^\circ + RT \ln C_L = \mu_M^\circ + RT \ln C_M \quad (\text{C.3})$$

which on rearrangement yields

$$\frac{C_L}{C_M} = \text{EXP}\left(\frac{\Delta u^\circ}{RT}\right) = K_R \quad (\text{C.4})$$

Where K_R is the partition coefficient which is assumed to be invariant with the amount of solute and phase extent in the system, and

$$\Delta \mu^\circ = \mu_M^\circ - \mu_L^\circ.$$

C.2 Linear Ideal Chromatography

When the solute is dissolved in the stationary phase, it is assumed to be immobile, movement occurs only when the solute vaporizes and is carried down the column by the mobile phase. The linear rate of travel

is therefore equal to the average carrier velocity \bar{u} multiplied by the fraction of time the solute spends in the mobile phase

$$\text{Rate of Travel} = \bar{u} \left(\frac{C_M V_M}{C_M V_M + C_L V_L} \right) \quad (\text{C.5})$$

Where V_M and V_L are the mobile and stationary phase volumes.

Arrangement of the above equation leads to

$$\text{Rate of Travel} = \bar{u} \left(1 + \frac{C_L V_L}{C_M V_M} \right)^{-1} \quad (\text{C.6})$$

where

$$K_R = \frac{C_L}{C_M}$$

Thus

$$\text{Rate} = \bar{u} \left(1 + K_R \frac{V_L}{V_M}\right)^{-1} \quad (\text{C.7})$$

Alternatively, the solute rate of travel is given by:

$$\text{Rate of Travel} = \frac{\text{column length (L)}}{\text{retention time (t)}_R} \quad (\text{C.8})$$

$$\bar{u} \left(1 + K_R \frac{V_L}{V_M}\right)^{-1} = \frac{L}{t_R} \quad (\text{C.9})$$

Then

$$t_R = \frac{L}{\bar{u}} \left(1 + K_R \frac{V_L}{V_M}\right) \quad (\text{C.10})$$

The above equation was first deduced by Synge [44] and is applicable to all chromatographic techniques.

In order to convert the observed retention times to gas volumes of the mobile phase, flow rate inside the column must be known. Generally, it is measured at the column's outlet, usually after the detector. The

measured flow rate F must be therefore corrected to a flow rate F_c that takes the prevailing conditions in the column into account.

$$F_c = F \left(\frac{273.15}{T} \right) \cdot \left(\frac{p_o - p_w}{p_o} \right) \quad (\text{C.11})$$

p_o = outlet pressure

p_w = water-vapor pressure at room temperature

T = room temperature

The “ raw “ dead (V_A) and retention (V_R) volumes are now given by:

$$V_A = t_r F_c \quad (\text{C.12})$$

$$V_R = t_r F_c \quad (\text{C.13})$$

and equation C.11 becomes

$$V_R = V_A \left(1 + K_R \frac{V_L}{V_M} \right) \quad (\text{C.14})$$

The adjusted retention volume is defined as:

$$V_R' = V_R - V_A = F_c (t_R - t_A) \quad (\text{C.15})$$

In order for a mobile phase to flow through a column, a pressure gradient must exist. This necessitates the introduction of a gas compressibility correction factor (recognized by Martin and James in 1952) [45].

Consider a carrier gas flowing through a packed column of uniform cross section A at a pressure p and velocity u . The volume throughout must be constant everywhere within the column so that:

$$puA = p_o u_o A = \overline{p\mu A} \quad (\text{C.16})$$

Where \bar{p} , p_o , \bar{u} , and u_o are the average and outlet pressures and velocities, respectively. The velocity at any point is therefore given by:

$$u = \frac{p_o u_o}{p} \quad (C.17)$$

The velocity can be also be related to the pressure gradient dp within a length dx along the column, the column specific permeability coefficient K porosity ϵ and the gas viscosity η through Darcy's law

$$u = -\frac{K dp}{\epsilon \eta} dx \quad (C.18)$$

Rearranging, substituting for u from equation C.18, and multiplying through by p , gives

$$dx = \left(-\frac{K}{\epsilon\eta u_o p_o}\right) p dp \quad (C.19)$$

$$p dx = \left(-\frac{K}{\epsilon\eta u_o p_o}\right) p^2 dp \quad (C.20)$$

The average value of a continuous function $F(x)$ is

$$F(X) = \frac{\int F(X) dX}{\int dX} \quad (C.21)$$

so that

$$\bar{p} = \frac{\int (-K/\epsilon\eta u_o p_o) P^2 dp}{\int (-K/\epsilon\eta u_o p_o) p^2 dp} \quad (C.22)$$

integrating over the column pressure gradient which is bounded by the inlet (p_i) and outlet (p_o) pressures, gives

$$\frac{\bar{p}}{p_o} = \frac{2}{3} \left[\frac{p_i^3 - p_o^3}{p_i^2 - p_o^2} \right] \quad (\text{C.23})$$

dividing by p_o followed by rearrangement gives the derived ratio

$$\frac{p_o}{\bar{p}} = \frac{3 [(p_i/p_o)^2 - 1]}{2 [(p_i/p_o)^3 - 1]} \quad (\text{C.24})$$

which is usually denoted by the letter j

V_R and V_A in equation C.14 are corrected for pressure drop across the column by multiplying them by j to give :

$$V_R j = V_A j \left(1 + K_R \frac{V_L}{V_M} \right) \quad (\text{C.25})$$

Writing $V_R \cdot j = V_R^o$ and $V_A \cdot j = V_M$ gives

$$V_R^\circ = V_M \left(1 + K_R \frac{V_L}{V_M} \right) \quad (\text{C.26})$$

where V_R° is the corrected retention volume and V_M is the corrected mobile phase volume. Comparing equation C.25 and equation C.26 and remembering (see C.15) that $jV'_R = j(V_R - V_A) = V_R^\circ - V_M$ gives

$$V_N = jV'_R = V_R^\circ - V_M = K_R V_L \quad (\text{C.27})$$

The specific retention volume V_g° is obtained by dividing V_N by the mass of the stationary phase, w_L , and by converting the data to 0°C (273.15 K) :

$$V_g^\circ = \frac{V_N}{w_L} \left(\frac{273.15}{T} \right) \quad (\text{C.28})$$

C.3 Relating v_g° (K_R) to Activity Coefficient (γ_2°)

The pressure is related to the activity coefficient through the equation

$$p_2 = \gamma_2^\infty \cdot p_2^\circ \cdot x_2 \quad (\text{C.29})$$

where p_2 is the total pressure, p_2° is the solute partial pressure and x_2 is the solute mole fraction in the liquid phase. Substituting the value of p_2 from the ideal gas equation leads to:

$$\frac{n_2^v \cdot R \cdot (273.15)}{V} = \gamma_2^\infty \cdot p_2^\circ \cdot x_2 \quad (\text{C.30})$$

where n_2^v , R and V are the solute mole fraction in the vapor phase, the gas constant and the total volume respectively. Replacing n_2^v / V by c , the solute concentration in the vapor phase gives

$$c \cdot R \cdot (273.15) = \gamma_2^\infty \cdot p_2^\circ \cdot x_2 \quad (\text{C.31})$$

The solute mole fraction x_2 is given by

$$x_2 = \frac{n_2}{n_2 + n_1} \quad (\text{C.32})$$

where n_1 and n_2 are the numbers of moles of solvent and solute respectively in the liquid phase. At infinite dilution however, equation C.32 is reduces to :

$$x_2 = \frac{n_2}{n_1} \quad (\text{C.33})$$

Replacing n_2/n_1 by $\frac{m_2^l M_1}{M_2 m_1}$ where m_2^l and m_1 are respectively, the solute and solvent masses in the liquid phase and M_2 and M_1 are the solute and solvent molar masses respectively, and substituting in C.31 gives this by m_2/m_1 and substitution in equation C.31

$$c.R.(273.15) = \gamma_2^\infty \cdot p_2^\circ \cdot \frac{(m_2^i / M_2) M_1}{m_1} \quad (C.34)$$

The solute concentration q in the liquid phase is

$$q = \frac{n_2^i}{m_1} = \frac{m_2^i / M_2}{m_1} \quad (C.35)$$

Replacing $\frac{m_2^i / M_2}{m_1}$ by q in C.34 and rearranging give

$$R.(273.15) = \gamma_2^\infty \cdot p_2^\circ \cdot \frac{q \cdot M_1}{c} \quad (C.36)$$

replacing q/c by V_g^0 yeilds the final equation:

$$\gamma_2^\infty = \frac{R \cdot (273.15)}{P_2^\circ M_1 V_g^0} \quad (C.37)$$

REFERENCES

REFERENCES

1. A. P. Young, "Melting and Vector Coulomb Gas in Two Dimensions", Phys. Rev. B 19, 1855 (1979).
2. B. I. Halperin and D. R. Nelson, "Theory of Two Dimensional Melting", Phys. Rev. Lett., 41, 121 and, 519 (E) (1978).
3. Nelson and B. I. Halperin, "Dislocation Mediated Melting in Two Dimensions", Phys. Rev. B 19, 2457 (1979).
4. R. J. Birgeneau and J. D. Litster, "Bond Orientational Order Model for Smectic B Liquid Crystals", J. Phys. (Paris) Lett. 39, L399 (1978).
5. Iam Choon Khoo and Francesco Simoni, "Physics of Liquid Crystalline Materials", Gordon and Breach, Amestrdam, (1991).
6. H. Stegemeyer, Macmillan India Ltd. , "Liquid Crystals", Germany (1994).
7. "Webester's Third New International Dictionary", vol. 11, p.1464, Merriam Co (Philippines).

8. Peter. W. Atkins, "Physical Chemistry", Richard Clay, Bungay, Suffolk (1990).
9. T. Daniels, "Thermal Analysis", Anchor Press, London, (1973).
10. G. R. Luckhurst and G. W. Gray, "The Molecular Physics of Liquid Crystals", Academic Press, London, (1979).
11. Julian F. Johnson and Roger S. Porter "Liquid Crystals and Ordered Fluids" vol 2, New York, USA, 1974.
 - (a) J. R. Flick, A. S. Marshall, and S. E. B. Petrie, p. 97.
 - (b) Mary E. Neubert, Leo T. Carlino, Richard D'Sidocky and D. E. Fishel, p. 293.
 - (c) Y. Hsu and D. Dolphin, p.461.
 - (d) Zack G. Gardlund, Ralph J. and George W. Smith, p.541.
 - (e) W. Gray, K. J. Harrison and J. A. Nash, p. 617.
12. Carel F. Polnaszek and Jack H. Freed, J. Phys. Chem. 79 (21),2283 (1975).
13. Hemminga, M. A., Chem. Phys. 6, 87 (1974).
14. G. A. Oweimreen, M. A. Morsy and J. S. Hwang, Appl. Magn. Reson.,9, 61 (1995).

15. G. A. Oweimreen, M. A. Morsy, and J. S. Hwang, *Mol. Cryst. Liq. Cryst.*, 265, 197 (1995).
16. M. A. Morsy, *Doctoral Dissertation*, KFUPM, Dhahran, Saudi Arabia, (1993).
17. Hwang J. S., M. A. Morsy and G. A. Oweimreen, *J. Phys. Chem.*, 98, 9056 (1994).
18. Naeem, A., Freed J. H., *J. Phys. Chem.* 93, 6539 (1989).
19. Shutt, W. E., Gelerinter, E., Fryburg, G. C., Sheley, C. F. J. *Chem. Phys.* 59, 143 (1973).
20. Morsy, G. A. Oweimreen and J. S. Hwang, *J. Phys. Chem.* Accepted February 12, (1996).
21. Gendell, J., Freed J. H., and Fraenckel G. K., *J. Chem. Phys.* 37, 2832 (1962).
22. L. C. Chow D. E. Martire, *Mol. Cryst. Liq. Cryst.*, 14, 1201 (1971).
23. L. C. Chow and D. E. Martire, *J. Phys. Chem.*, 73, 1127 (1969).
24. L. C. Chow and D. E. Martire, *J. Phys. Chem.*, 75, 2005 (1971).

25. J. M. Schnur and D. E. Martire, *Anal. Chem.*, 43, 1201 (1971).
26. J. M. Schnur and D. E. Martire, *Mol. Cryst. Liq. Cryst.*, 26, 213 (1974).
27. G. A. Oweimreen, and D. E. Martire, *J. Chem. Phys.* 72(4), 2500, (1980).
28. G. A. Janini and D. E. Martire, *J. Chem. Soc., Faraday Trans. 2*, 70, 837 (1974).
29. G. A. Oweimreen, G. C. Lin, and D. E. Martire, *J. Phys. Chem.* 63, No. 16, 2111 (1979).
30. G. A. Oweimreen, G. C. Lin, and D. E. Martire, *J. Phys. Chem.* 83, 2111 (1979).
31. G. A. Oweimreen, *Journal of Solution Chemistry*, 11, No. 2, 105 (1982).
32. G. A. Oweimreen, *Doctoral Dissertation*, Georgetown University, Washington, D. C., (1977).
33. G. A. Oweimreen, and A. I. Shihab, *J. Chem. Eng. Data*, 39, 266 (1994).

34. Samir Ghodbane and Daniel E. Martire, *J. Phys., Chem.* 91, 6410(1987).
35. Samir Ghodbane, Ghassan A. Oweimreen and Daniel E. Martire, *J. Chromatogr.* 556, 317 (1991).
36. R. J. Laub, J. H. Purnell and P. S. Williams, *J. Chromatogr.* 155, 233 (1978).
37. Hoffman-La Roche Inc. , *Liquid Crystals : Ester Component*, RO-CE (1420, 1430, 1500, 1530, 1510, and 1540) Nov. (1983).
38. R. R. Dreisbach, *Adv. Chem Ser.* No. 15 (1955); No. 22 (1959).
39. D. E. Martire and P. Riedl, *J. Phys. Chem.*, 72, 3478 (1968).
40. J. R. Conder, *J. Chromatogr.*, 39,273 (1969).
41. H. L. Liao and D. E. Martire, *Anal. Chem.*, 44, 498 (1972).
42. A. B. Littlewood, C. S. G. Phillips and D. T. Price, *J. Chem. Soc.*,1480 (1974).
43. Richard J. Laub and Robert L. Pecksok, “*Physicochemical Applications of Gas Chromatography*”, Jhon Wiley & Sons , Canada (1978).

44. A. J. P. Martin and R. L. M. Synge, *Biochem. J.*, 35, 1358 (1941).
45. A. J. P. Martin and A. T. James, *Biochem. J.* 50, 679 (1952).
46. Reynaldo C. Castells and Cecilla B. Castells *J. Sol. Chem.*, 24(3), 285,(1995).
47. F. Dowell and D. E. Martire, *J. Chem. Phys.* 69(6), 2332 (1978).
48. F. Dowell, *J. Chem. Phys.* 69(9), 4012(1978).
49. D. E. Martire, G. A. Oweimreen, G. J. Agren, S. G. Ryan, and H. T. Peterson, *J. Chem. Phys.*, 64, 1456 (1976).
50. D. E. Martire, "The Molecular Physics of Liquid Crystals" G. R. Luckhurst and G. W. Gray, ED, Academic Press, London, 1979, Chapter 11.
51. D. E. Martire, *Mol. Cryst. Liq. Crystal.*, 28, 63 (1974).
52. G. A. Oweimreen, A. K. Shihab, K. Halhouli, and S. F. Sikander, *Mol. Cryst.* 138, 327 (1986).
53. A. B. Cruickshank, B. W. Gainey, and C. L. Young, in *Gas Chromatography* 1968, C. L. A. Harbourn, Ed., Institute of Petroleum, London, 1969, p. 76.

54. Gaussian 92/DFT, Revision G. 3, J. Frisch, G. W. Trucks, H. B. Schlegel, P.M. W. Gill, B.G. Johnson, M. W. Wong, J. B. Foresman, M.A. Rabb, M. J. S. Binkley, C. Gonzalez, R. L. Martin, D. J. Fox, D. J. Defrees, J. Barker, J. J. P. Stewart, and J. A. Pople, Gaussian, Inc., Pittsburgh PA, 1993.
55. P. J. Flory, R.A. Orwoll, and A. Vrij, *J. Am Chem. Soc.* 86, 3507, 3515 (1964).
56. I. Sanchez and R. H. Lacombe, *J. Phys. Chem.* 80, 2352 (1972).
57. P. J. Flory, *Proc. R. Soc. A.* 234, 73 (1956).
58. E. A. DiMarzio, *J. Chem. Phys.* 35, 658 (1961).
59. M. A. Cotter and D. E. Martire, *Mol. Cryst. Liq. Cryst.* 7, 295 (1969).
60. Henry T. Peterson, Daniel E. Martire and Wolfgang Lindner, *J. Phys. Chem.* 76 (4), 596 (1972).
61. D. E. Martire, P. A. Blasco, P. F. Carone, L. C. Chow, and H. Vieini, *J. Phys. Chem.* 72 (10), 3489 (1968).
62. W. Gray and A. Mosley *J. Chem. Soc. Perkin II* 97 (1976).

63. Arls Doelman, Annie R. Gregges, and Edward M. Daxrall, *Anal. Chem.* 4 (1), 1 (1977).
64. M. L. McGlashan and A. G. Williamson, *Trans. Faraday Soc.*, 57, 558 (1961).
65. M. A. Morsy personal communications.